

Università degli Studi di Napoli

Federico II

Facoltà di Ingegneria

Tesi di Dottorato di Ricerca

in

Ingegneria Elettrica

XIX ciclo

# **Novel FACTS controllers for power system stability enhancement**

Antonio Griffo

Tutor: Davide Lauria

Coordinatore: Guido Carpinelli

November 2006



---

# Contents

---

<b>Contents</b>	<b>i</b>
<b>1 Stability of Electric Power Systems: definitions and dynamic phenomena</b>	<b>5</b>
1.1 Power system stability . . . . .	5
1.2 Mathematical definitions . . . . .	8
1.3 Stability criteria . . . . .	9
1.3.1 Lyapunov's linearization method . . . . .	10
1.4 Dynamical phenomena in power systems . . . . .	14
1.5 Rotor angle stability . . . . .	15
1.5.1 Small signal stability . . . . .	17
1.5.2 Transient stability . . . . .	18
1.6 Voltage stability . . . . .	19
1.7 Synchronism oscillations . . . . .	20
<b>2 Power system modelling</b>	<b>21</b>
2.1 Synchronous generator . . . . .	21
2.1.1 Mechanical equations . . . . .	22
2.1.2 Electrical equations . . . . .	23
2.1.3 Generator-network interface equations . . . . .	26
2.1.4 Torsional dynamics . . . . .	27
2.2 Generator's controllers . . . . .	28
2.2.1 Turbine governor . . . . .	28
2.2.2 Automatic Voltage Regulator . . . . .	29
2.2.3 Power System Stabilizer . . . . .	30
2.3 Transmission network and loads . . . . .	30

2.3.1	Load flow equations . . . . .	31
2.3.2	Load modelling . . . . .	31
<b>3</b>	<b>Flexible AC Transmission Systems</b>	<b>35</b>
3.1	FACTS role in modern power systems . . . . .	35
3.2	Active and reactive power flow control through shunt and series compensators . . . . .	37
3.3	Static compensator (STATCOM) . . . . .	39
3.4	Static synchronous series compensator (SSSC) . . . . .	42
3.5	Shunt and series reactive compensation and stability region . . . .	45
3.6	FACTS devices with active power compensation capabilities . . . .	48
3.7	Conclusion . . . . .	49
<b>4</b>	<b>Phasor dynamics influence on electric power system performances</b>	<b>51</b>
4.1	Introduction . . . . .	51
4.2	Time-varying phasors and their dynamics . . . . .	53
4.3	Three-phase to rectangular reference transformation . . . . .	58
4.4	Comparison of transmission line modellings . . . . .	59
4.5	Numerical results . . . . .	61
4.5.1	SMIB test system . . . . .	61
4.5.2	4-machine test system . . . . .	65
4.6	Subsynchronous oscillations phenomena . . . . .	66
4.7	Conclusion . . . . .	71
<b>5</b>	<b>Lyapunov's theory</b>	<b>77</b>
5.1	Lyapunov's direct method . . . . .	77
5.2	Direct methods for power system stability analysis . . . . .	80
5.2.1	SMIB system . . . . .	81
5.2.2	Lyapunov function for structure preserving models . . . . .	82
5.3	Transfer conductances and the extended invariance principle . . . .	84
5.3.1	Extended invariance principle . . . . .	84
5.4	A new extended Lyapunov function . . . . .	86
5.4.1	SMIB system . . . . .	88
5.5	Lyapunov functions and control systems . . . . .	89
5.5.1	Control Lyapunov function . . . . .	89

5.5.2	Extended control Lyapunov function . . . . .	91
5.5.3	Numerical applications: SMIB system with series compen- sator . . . . .	94
5.5.4	Numerical applications: 2nd benchmark system for subsyn- chronous resonance . . . . .	94
5.6	Adaptive equilibrium point estimation . . . . .	96
5.6.1	Numerical applications: interarea oscillations damping in multimachine power system . . . . .	98
5.7	Conclusion . . . . .	99
<b>6</b>	<b>Two-leg three-phase inverter control for STATCOM and SSSC applications</b>	<b>103</b>
6.1	Introduction . . . . .	104
6.2	Converter Topology, STATCOM Operation and Control . . . . .	105
6.2.1	Converter equations . . . . .	108
6.2.2	Variable Structure Control . . . . .	110
6.3	Converter Topology, SSSC Operation and Control . . . . .	112
6.4	Numerical Simulations . . . . .	115
6.4.1	STATCOM . . . . .	115
6.4.2	SSSC . . . . .	119
6.5	Converter control for active power exchange . . . . .	123
6.6	Conclusion . . . . .	127
	<b>Bibliography</b>	<b>131</b>
	<b>A Test systems' data</b>	<b>151</b>
	<b>B Derivation of expression for matrix <math>\Omega</math> in eq. (6.27)</b>	<b>153</b>
	<b>C FACTS circuits and controllers data</b>	<b>155</b>
	<b>List of Symbols and Abbreviations</b>	<b>157</b>
	<b>List of Figures</b>	<b>158</b>
	<b>List of Tables</b>	<b>163</b>



---

# Acknowledgements

---

This thesis is a result of my doctoral studies at the Department of Electrical Engineering at the Università degli Studi di Napoli "Federico II" where I have worked for the last three years. At the conclusion of this period I would like to spend a few words to thank my supervisor Davide Lauria for his encouragement, constant support, and help. His guidance throughout the work was an invaluable resource. I would also like to acknowledge the help and the valuable advice of Professor Guido Carpinelli.





---

# Introduction

---

Electric power systems are among the most complex outcomes of engineering, being the result of the interconnection of a huge number of different devices. Safe and reliable operation of such systems is mainly the result of real-time action of several control devices, which ensures proper operation of the whole system both in steady-state and after an equilibrium condition is perturbed by sudden contingencies. Guaranteeing proper operation of electric power systems is therefore the problem of maintaining system's stability.

Although many power systems were firstly devised several years ago, they are still continuously growing in complexity and extension.

Many analysis and control tools share with electric power systems the same long history of research and practical application. Despite this long tradition, the continuous evolution in technologies has strongly affected power systems. In recent years the progress in semiconductor technologies have led to the commercial availability of devices capable of very high power handling, leading to the concept of Flexible Alternating Current Transmission Systems (FACTS). Based on power electronics converters FACTS devices are capable of rapid regulation of various network quantities, therefore being serious candidates for future power system control.

As in all control problems, a deep understanding of power system operation and a sound mathematical description of its behaviour are both required in deriving control laws for stability enhancement.

The present thesis addresses the problems of deriving control laws for FACTS devices which can enhance power system stability, making use of a mathematical description of the transmission network which takes into account usually neglected fast transients. Once these control laws are derived the problem of

their tracking by an actual converter is addressed, by proposing a novel topology for power electronic converters useful for FACTS applications.

The thesis is structured as follows:

Description of dynamic phenomena in power system and main definitions related to system's stability are presented in Chapter 1;

Classical modelling for power system stability analysis is the subject of Chapter 2 in which models of main power system components are described;

Chapter 3 gives a brief introduction to FACTS devices structure and operation, as well as to their capabilities in providing wider stability margins;

Chapter 4 introduces the network modelling which will be used in subsequent derivations, and illustrates some results which highlight the relevance of an accurate modelling of usually neglected fast network transients;

Main results of Lyapunov's stability theory are briefly introduced in Chapter 5 along with the concept of Control Lyapunov Function and its usage in deriving stabilising control laws;

A novel topology for FACTS devices is proposed in Chapter 6 which is proven to be easily employable in designing FACTS devices for reactive power compensation, as well as active power exchange, if a suitable storage device is available.

## Chapter 1

---

# Stability of Electric Power Systems: definitions and dynamic phenomena

---

### Summary

*Safe operation of electric power system is largely related to its stability which depends of the ability in making all generators supplying the network rotate synchronously despite faults and other contingencies. Stability of general dynamical systems and more specific definitions for power systems are introduced in the chapter. Dynamical phenomena in power systems along with main causes of instability and their underlying phenomena are briefly described.*

### 1.1 Power system stability

Electric power systems are constituted by the interconnection of a huge number of different components. They can therefore be considered among the most complex systems to be planned and safely operated. This complexity arises as a consequence of the large amount of devices contemporaneously in operation, each one with its own internal dynamics, that however interact with each other, giving rise to a complex collective behaviour. The wide geographic extension of electric power systems that can span entire countries and even continents, adds

even greater complexity to issues connected to their analysis and control.

During their operation power systems undergo a large number of disturbances, some of them occurring continually, such as modifications in load demands, while others are less common but nonetheless can potentially be very dangerous, such as faults and structural changes like tripping of circuit breaker. From a practical viewpoint such disturbances are usually classified as either small or large, respectively, depending on the effects they have on system behaviour. Just like any other dynamical system, the most basic requirement related to power system secure operation is therefore its stability.

Although several mathematical definitions have been proposed for generic dynamical systems, and most of them can be usefully applied to power systems too, the need for more practical definitions have led joint IEEE/CIGRE Task Forces to propose commonly agreed definitions [1, 2]. Quoting from [2]:

*"Power system stability is the ability of an electric power system, for a given initial operating condition, to regain a state of operating equilibrium after being subjected to a physical disturbance, with most system variables bounded so that practically the entire system remains intact."*

Under very general assumptions the dynamics of power systems can be described by a switched set of coupled algebraic and ordinary differential equations\* of the form [6]:

$$\dot{\mathbf{x}} = \mathbf{f}_i(\mathbf{x}, \mathbf{y}, t) \quad (1.1)$$

$$\mathbf{0} = \mathbf{g}_i(\mathbf{x}, \mathbf{y}, t) \quad i \in \{e_1 \dots e_k\} \quad (1.2)$$

The index  $i$  spans over a discrete set of possible events that make the system change its intrinsic dynamics, at specified time instants. State variables  $\mathbf{x}$  are not allowed to change instantaneously following an event, while algebraic variables  $\mathbf{y}$ , which are defined by (1.2) as implicit function of the state variables  $\mathbf{x}$ , can undergo discontinuities. Systems of this kind fall into the wide category of hybrid systems, i.e. systems in which continuous dynamics coexists with discrete events. A more detailed description of such hybrid systems along with a more formal

---

\*Some attempts have recently been made to describe propagation of disturbances in power systems as wave propagation phenomena hence described by partial differential equations [3, 4, 5].

mathematical framework suitable for their application to the description of power systems is presented in [7, 8, 9]. Examples of discrete events that can trigger a structural change in system's dynamics are faults, tripping or reclosure of a transmission line, load shedding and under load tap changer action.

Due to the explicit dependence on time of right-hand sides of eqs. (1.1-1.2) the system is said to be non-autonomous.

In the foregoing discussion it is assumed that the hypotheses of the implicit function theorem are satisfied. In particular the Jacobian of  $\mathbf{g}$  with respect to  $\mathbf{y}$  is supposed to verify:

$$\det \left( \frac{\partial \mathbf{g}(\mathbf{x}, \mathbf{y})}{\partial \mathbf{y}} \right) \neq 0 \quad (1.3)$$

which guarantees that there exist a function  $\mathbf{h}(\mathbf{x})$  such that the algebraic variables can be expressed as  $\mathbf{y} = \mathbf{h}(\mathbf{x})$ , therefore the differential-algebraic equations (DAE) (1.1)-(1.2) can be replaced by:

$$\dot{\mathbf{x}} = \mathbf{f}(\mathbf{x}, \mathbf{h}(\mathbf{x})) \quad (1.4)$$

A typical power system stability study considers the system to be in a pre-disturbance steady state, mathematically described by [10]:

$$\mathbf{x} = \mathbf{x}_{prefault}^* \quad (1.5)$$

$$\mathbf{0} = \mathbf{f}_{prefault}(\mathbf{x}, \mathbf{y}, t) \quad (1.6)$$

$$\mathbf{0} = \mathbf{g}_{prefault}(\mathbf{x}, \mathbf{y}, t) \quad \forall t < t_{fault} \quad (1.7)$$

where  $\mathbf{x}_{prefault}^*$  is the pre-fault equilibrium point, and  $t_{fault}$  is the time instant when fault happens. During the fault, most often a short circuit at some network location, system's dynamics are described by:

$$\dot{\mathbf{x}} = \mathbf{f}_{fault}(\mathbf{x}, \mathbf{y}, t) \quad (1.8)$$

$$\mathbf{0} = \mathbf{g}_{fault}(\mathbf{x}, \mathbf{y}, t) \quad \forall t_{fault} \leq t < t_{fault} + t_{cl} \quad (1.9)$$

where  $t_{cl}$  is the fault clearing time. Studying system's stability is thus the question of whether post-fault state variables reach a new acceptable equilibrium point or not. The post-fault equilibrium point  $\mathbf{x}_{postfault}^*$  can either be the same as pre-fault equilibrium or differ from it. Analogously, post-fault dynamics can either be the same as pre-fault dynamics, in which case  $\mathbf{f}_{postfault}(\mathbf{x}) = \mathbf{f}_{prefault}(\mathbf{x})$  or differ from it, i.e.  $\mathbf{f}_{postfault}(\mathbf{x}) \neq \mathbf{f}_{prefault}(\mathbf{x})$ , depending on the event of structural changes following the intervention of protective equipment, like line tripping or

load shedding. The aforementioned definition from [2] does not explicitly mention equilibrium points in order to allow for the possibility that satisfactory operation can also be attained while some state variables remain on a limit cycle, thus never reaching a true equilibrium point, but still remaining limited within an acceptable region. This possibility is however not commonly encountered in actual power system operation, since small parameter variations can either transform stable limit cycles into unstable ones or into stable equilibrium points.

## 1.2 Mathematical definitions

For a given dynamical system described by the set of first order ordinary differential equations  $\dot{\mathbf{x}} = \mathbf{f}(\mathbf{x})$ , the following definition holds:

**Equilibrium point:** *If:*

$$\mathbf{x}(t_0) = \mathbf{x}^* \Rightarrow \mathbf{x}(t) = \mathbf{x}^* \quad \forall t \geq t_0 \quad (1.10)$$

*than the state  $\mathbf{x}^*$  is said to be an **equilibrium point***

which means that the system is in an equilibrium state if once  $\mathbf{x}(t)$  is equal to  $\mathbf{x}^*$  it remains  $\mathbf{x}(t) = \mathbf{x}^*$  for all subsequent time. From this condition it follows that:

$$\mathbf{x}^* \text{ is an equilibrium point} \Leftrightarrow \mathbf{f}(\mathbf{x}^*) = \mathbf{0} \quad (1.11)$$

The definitions of stability for an equilibrium point of the generic system  $\dot{\mathbf{x}} = \mathbf{f}(\mathbf{x})$  can be formalised using the classical definition by Lyapunov [11, 12, 13]:

**Stability:** *The equilibrium point  $\mathbf{x} = \mathbf{0}$  is said to be **stable** if:*

$$\forall \varepsilon > 0, \quad \forall t_0 > 0, \quad \exists \delta(t_0, \varepsilon) :$$

$$\|\mathbf{x}_0\| < \delta(t_0, \varepsilon) \Rightarrow \|\mathbf{x}(t)\| < \varepsilon \quad \forall t \geq t_0 \quad (1.12)$$

Roughly stated, the definition implies that trajectories initiating sufficiently close to the equilibrium point will eventually remain in its neighbourhood. If  $\delta(t_0, \varepsilon)$  can be chose independent of  $t_0$  uniform stability holds according to the following definition:

**Uniform stability:** *The equilibrium point  $\mathbf{x} = \mathbf{0}$  is said to be **uniformly stable** if:*

$$\forall \varepsilon > 0, \quad \forall t_0 > 0, \quad \exists \delta(\varepsilon) :$$

$$\|\mathbf{x}_0\| < \delta(\varepsilon) \Rightarrow \|\mathbf{x}(t)\| < \varepsilon \quad \forall t \geq t_0 \quad (1.13)$$

**Instability:** *The equilibrium point  $\mathbf{x} = \mathbf{0}$  is said to be **unstable** if it is not stable*

The following definition of asymptotic stability entails the convergence of system's trajectories towards the equilibrium point:

**Asymptotic Stability:** *The equilibrium point  $\mathbf{x} = \mathbf{0}$  is said to be **asymptotically stable** if, in addition to being stable:*

$$\forall t_0 > 0, \quad \exists \delta(t_0) :$$

$$\|\mathbf{x}_0\| < \delta(t_0) \Rightarrow \lim_{t \rightarrow \infty} \|\mathbf{x}(t)\| = 0 \quad (1.14)$$

Therefore in the case of asymptotic stability, systems trajectories initiating sufficiently close to the equilibrium point will eventually converge to it.

All definitions have been given with respect to the equilibrium point  $\mathbf{x} = \mathbf{0}$ . Equilibria others than the origin can be analogously analysed after a suitable coordinate transformation which translates the origin into the equilibrium point of interest [11].

### 1.3 Stability criteria

Stability analysis of nonlinear systems is largely based on the use of the two stability criteria firstly introduced by A. M. Lyapunov in the late 19th century [14]. The first of them relates the local stability of the equilibrium point of a nonlinear system to the much more easily tractable stability of its linear approximation. The second method of Lyapunov, also known as the Lyapunov's direct method, is based on the use of an energy function. Since it will be used in subsequent analysis in the present thesis its statement is deferred to a later chapter.

### 1.3.1 Lyapunov's linearization method

It is well known that for the linear system:

$$\begin{aligned}\dot{\mathbf{x}} &= \mathbf{A}\mathbf{x}, \quad \mathbf{A} \in \mathbb{R}^{n \times n} \\ \mathbf{x}(0) &= \mathbf{x}_0\end{aligned}\tag{1.15}$$

the time evolution of state variables, in case  $\mathbf{A}$  has distinct eigenvalues is given by:

$$\mathbf{x}(t) = \sum_{i=1}^n \phi_i \psi_i \mathbf{x}_0 e^{\lambda_i t}\tag{1.16}$$

where:

- $\lambda_i$  is the (possibly complex)  $i$ -th eigenvalue of the state matrix  $\mathbf{A}$
- $\phi_i$  is the right eigenvector of the state matrix  $\mathbf{A}$  corresponding to the  $i$ -th eigenvalue  $\lambda_i$
- $\psi_i$  is the left eigenvector of the state matrix  $\mathbf{A}$  corresponding to the  $i$ -th eigenvalue  $\lambda_i$

From eq. (1.16) it is easily derived that the origin is:

**stable** if none of the eigenvalues has positive real parts;

**asymptotically stable** if all eigenvalues have negative real parts;

**unstable** if at least one eigenvalue has positive real part;

The Lyapunov's first method is a straightforward extension of this criterion to general nonlinear systems, based on the fact that, assuming  $\mathbf{f}(\mathbf{x})$  continuously differentiable:

$$\Delta \dot{\mathbf{x}} = \left( \frac{\partial \mathbf{f}}{\partial \mathbf{x}} \right)_{\mathbf{x}=\mathbf{x}^*} \Delta \mathbf{x} + \mathbf{f}_{h.o.t.}(\Delta \mathbf{x}), \quad \Delta \mathbf{x} = \mathbf{x} - \mathbf{x}^*\tag{1.17}$$

where  $\mathbf{f}_{h.o.t.}$  denotes higher order terms. The system:

$$\Delta \dot{\mathbf{x}} = \mathbf{J} \Delta \mathbf{x}, \quad \mathbf{J} = \left( \frac{\partial \mathbf{f}}{\partial \mathbf{x}} \right)_{\mathbf{x}=\mathbf{x}^*}\tag{1.18}$$

is called the **linearization** of the original nonlinear system. The relationship between the actual nonlinear system and its linearization is summarised in the following:



**Theorem** *Lyapunov's linearization method*

- If all eigenvalues of  $\mathbf{J}$  have negative real parts than the equilibrium point  $\mathbf{x}^*$  of the actual nonlinear system is asymptotically stable
- If at least one eigenvalue of  $\mathbf{J}$  has positive real part than the equilibrium point  $\mathbf{x}^*$  of the actual nonlinear system is unstable
- If there exists at least one eigenvalue of  $\mathbf{J}$  with zero real part, than, from first order analysis, nothing can be said on stability of the equilibrium point  $\mathbf{x}^*$  of the actual nonlinear system

Differently from the linear case, nonlinear systems with eigenvalues on the imaginary  $j\omega$  axis can either be stable, even asymptotically, or unstable. In this case analysis of higher order terms, which affect the so called center manifold, is necessary to draw conclusions about the stability of the equilibrium point [12, 13].

The following examples are presented in order to illustrate some of the concepts introduced so far. The system analysed will be later recognised as the most basic power system, given by the interconnection of a single machine to a constant voltage network.

**Example 1.1**

Let consider the system of first order switched differential equations given by:

$$\begin{cases} \dot{x}_1 = 376.99x_2 \\ \dot{x}_2 = \frac{1}{7}[0.9 - 1.351 \sin x_1] \end{cases} \quad t < t_f$$

$$\begin{cases} \dot{x}_1 = 376.99x_2 \\ \dot{x}_2 = \frac{1}{7}[0.9] \end{cases} \quad t_f \leq t \leq t_{cl} \quad (1.19)$$

$$\begin{cases} \dot{x}_1 = 376.99x_2 \\ \dot{x}_2 = \frac{1}{7}[0.9 - 1.1024 \sin x_1] \end{cases} \quad t > t_{cl}$$

whose equilibrium points are given by:

$$\mathbf{x}_s = \begin{cases} x_1^* = \arcsin(0.9/1.3510) + 2k\pi, & k \in \mathbb{Z} \\ x_2^* = 0 \end{cases} \quad t < t_f$$

$$\mathbf{x}_s = \begin{cases} x_1^* = \arcsin(0.9/1.1024) + 2k\pi, & k \in \mathbb{Z} \\ x_2^* = 0 \end{cases} \quad t > t_{cl} \quad (1.20)$$

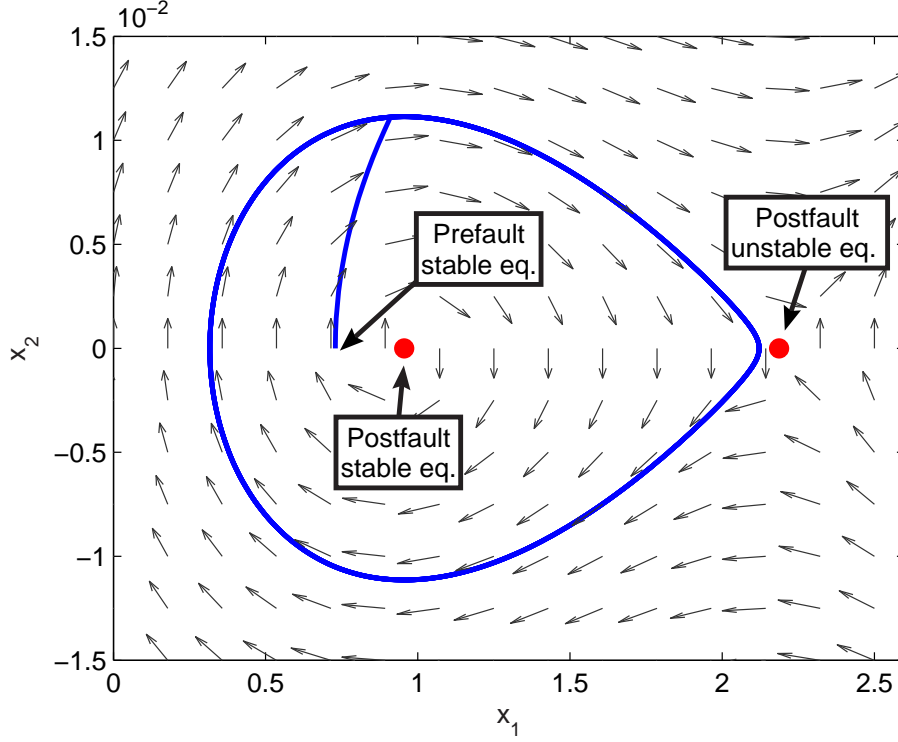


Figure 1.1: Phase plane portrait of the system in example 1

and:

$$\begin{aligned} \mathbf{x}_u = \begin{cases} x_1^* = \pi - \arcsin(0.9/1.351) + 2k\pi, & k \in \mathbb{Z} \\ x_2^* = 0 \end{cases} & t < t_f \\ \mathbf{x}_u = \begin{cases} x_1^* = \pi - \arcsin(0.9/1.1024) + 2k\pi, & k \in \mathbb{Z} \\ x_2^* = 0 \end{cases} & t > t_{cl} \end{aligned} \quad (1.21)$$

For  $t \in [t_f, t_{cl}]$  no equilibria exist. In order to study whether the system will maintain an acceptable operation in postfault condition, i.e. for  $t > t_{cl}$ , the stability of postfault equilibria should be analysed. Evaluating the Jacobian matrix in the equilibrium points given in (1.20) yields:

$$\mathbf{J}_s = \begin{bmatrix} 0 & 376.99 \\ -0.0909 & 0 \end{bmatrix} \quad (1.22)$$

while  $\mathbf{J}$  evaluated in (1.21) yields:

$$\mathbf{J}_u = \begin{bmatrix} 0 & 376.99 \\ 0.0909 & 0 \end{bmatrix} \quad (1.23)$$

The eigenvalues of  $\mathbf{J}_s$  are obtained as:

$$\begin{aligned}\lambda_{1,2-s} &= \pm 5.8539j, \quad \text{if } \mathbf{x} = \mathbf{x}_s \\ \lambda_{1,2-u} &= \pm 5.8539, \quad \text{if } \mathbf{x} = \mathbf{x}_u\end{aligned}\tag{1.24}$$

It can be concluded that the equilibrium point  $\mathbf{x}_u$  is unstable since the corresponding Jacobian has one negative and one positive eigenvalue. Unstable equilibria of this kind are called *saddle*. On the other hand, the eigenvalues of  $\mathbf{J}_s$  are purely imaginary, therefore nothing can be concluded on the nature of the corresponding equilibria from linearized analysis. From the phase portrait in Fig. 1.1 it can be deduced that the postfault equilibrium  $\mathbf{x}_s$  is stable, although not asymptotically. Arrows show the direction of the vector field  $\mathbf{f}(\mathbf{x})$ , while the blue line shows a trajectory of the system's state passing near the boundary of the stability region of the postfault equilibrium. This stability (or attraction) region, which is the set of initial conditions where stable trajectories depart from, is practically encircled by the blue line, which provides a good estimate of its boundary.  $\square$

The lack of damping in the system in Ex. 1, which is due to the absence of dissipation in the underlying physical phenomenon, causes that all trajectories initiating sufficiently close to the equilibrium point will remain in its vicinity, continually swinging around it. The effect of damping to the system of Ex. 1 is illustrated in the following:

### Example 1.2

Let consider the system whose postfault dynamics are given by:

$$\begin{aligned}\dot{x}_1 &= 376.99x_2 \\ \dot{x}_2 &= \frac{1}{7} \left[ 0.9 - 1.1024 \sin x_1 - 10x_2 \right]\end{aligned}\tag{1.25}$$

The addition of a damping term in the Eq. (1.25) makes the equilibrium point asymptotically stable. The Jacobian matrix and its eigenvalues are indeed given by:

$$\mathbf{J} = \begin{bmatrix} 0 & 376.99 \\ -0.0909 & 1.4286 \end{bmatrix} \Rightarrow \lambda_{1,2} = -0.7143 \pm 5.8102j\tag{1.26}$$

thus all eigenvalues are in the left complex half plane. As it is evident from the phase portrait in Fig. 1.2, although the boundary of the stability region in the direction of the faulted trajectory is not greatly altered by the addition of damping, the trajectory in red now settles down to the stable equilibrium, in a practically finite time.  $\square$

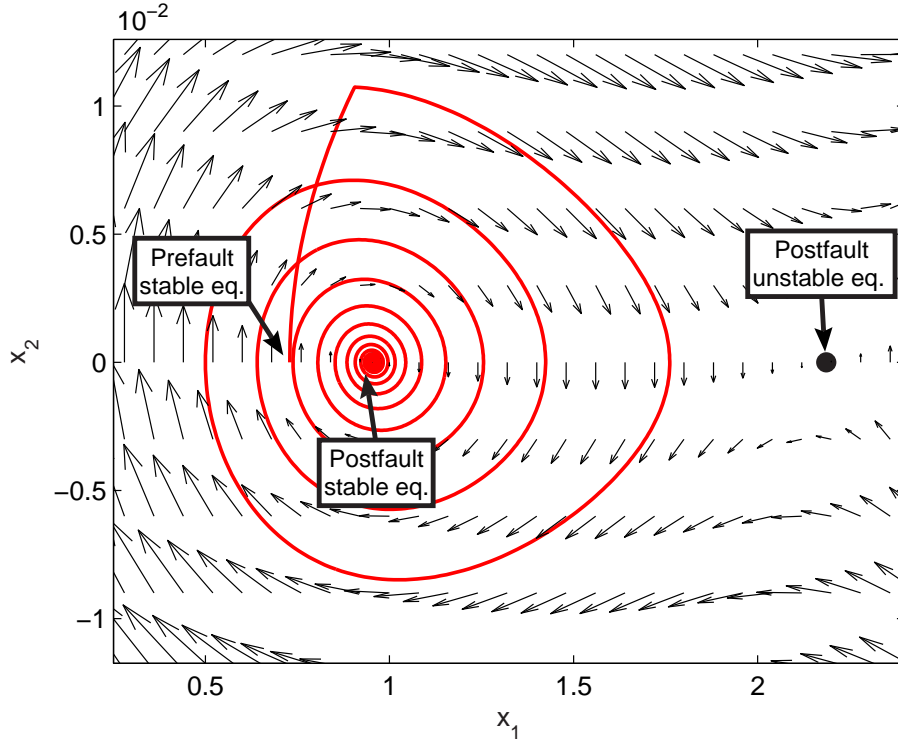


Figure 1.2: Phase plane portrait of the system in example 2

## 1.4 Dynamical phenomena in power systems

Due to the large amount of different devices contemporaneously acting in electric power systems, they are affected by several complex dynamical phenomena. In order to better understand the causes of each phenomenon and make the system working properly, it is of great importance to analyse the range of dynamics which have a role in system's behaviour. A classification of dynamical phenomena could therefore result very useful for analysis purposes. The need for classification arises from the necessity to divide such a complex problem as system stability into sub-problems, utilising simplifying assumptions with the aim of rendering each sub-problem more amenable to mathematical and/or numerical analysis. Simplifications, on the other hand, should be carefully made in order to maintain a sufficient degree of approximation in system's response [2, 15]. Figure 1.3 depicts a schematic drawing which illustrates a commonly used time-scale decomposition of dynamical phenomena in power systems [16, 17]. A first rough classification can be made separating slow from fast phenomena, since very fast transients such

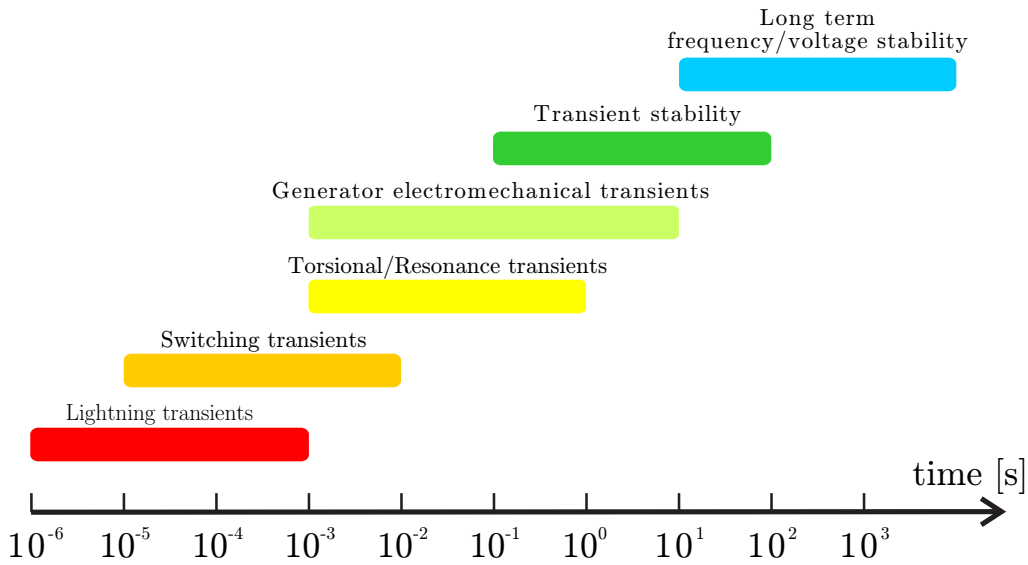


Figure 1.3: A schematic drawing illustrating time-scale of dynamical phenomena in power systems

as those due to lightning or switching of circuit breakers die out very quickly, i.e. in the order of  $10^{-4}s$  compared to slow phenomena such as load restoration or secondary/tertiary regulation involved in voltage or frequency stability evaluation which require study periods spanning several minutes or even hours.

A word of caution is necessary, because although classifications may result very useful, many phenomena are so intertwined that in some situations it is difficult to attribute the cause of a particular failure to a single phenomenon.

The main causes of instability and their underlying phenomena are briefly summarised in the following sections.

## 1.5 Rotor angle stability

Dynamic phenomena related to rotor angle stability, which is the main subject of the present thesis, are typically confined in a time frame ranging from tenth of seconds to few tens of seconds. Torsional transients in generators turbine shafts, which are associated with time constants in the subsynchronous range, i.e. tens of millisecond, could also give rise to instability phenomena which should be taken into account in several practical situations.

A properly working power system is operated in such a way as to constantly

maintain a balance between the power produced in generators and that absorbed by the loads. In current power systems electric power is being produced, almost totally, in conventional power plants where either a thermal or an hydraulic source of energy is transformed into electric energy by means of synchronous generators. Although this situation might change in future due to the constant increase in the amount of distributed generation which is based on the use of alternative energy sources, i.e. wind, sun, fuel cells and so on, which are coupled to the transmission network through power electronics based converters [18, 19, 20], the synchronous generator will remain the main tool for energy conversion for a long time to come.

The ability of all synchronous machines, interconnected through the transmission network, to maintain a synchronous operation is referred to as *rotor angle stability*. Steady state operation is therefore characterised, for each synchronous generator, by a state of equilibrium between the mechanical torque applied by the prime mover through the turbine shaft and the electric torque due to the loading of the generator. If an unbalance arises as a consequence of a disturbance, the state of equilibrium is perturbed and some generators rotors may accelerate while others may decelerate. The behaviour of the system after the perturbation largely depends upon the amplitude of the disturbance. Actual systems must operate in an equilibrium in which they should be able to withstand at least small disturbances. This is possible due to the nature of power-angle relationship for a synchronous generator, which states that the electric power and hence electric torque increases sinusoidally as the angle with respect to the rest of the system increases. Due to the nonlinear nature of the power-angle relationship, a large perturbation and hence a large displacement of a machine angle against the rest of the system, will eventually result in a decrease in the electrical power injected into the network which will lead to a further unbalance between mechanical torque and electrical torque and thus produce an increase in angular separation.

A classical classification of rotor angle related stability analysis is roughly based on the magnitude of the disturbance. It is customary in power system analysis to separate the study of *transient stability* which is mainly related to large disturbances, from that of *small signal stability*.

### 1.5.1 Small signal stability

In most practical situations the disturbances, such as load changes, are sufficiently small such that the system can be linearized around the operating point. The stability of the system and the control actions to improve stability are therefore studied by means of the tools of linear analysis such as eigenvalues, eigenvectors and their associated oscillatory modes. Small disturbances in practical power systems usually result in oscillations of rotor angles of some generators against others. Instability arises if oscillation magnitude constantly increases in time up to the separation of the system. Instability due to small disturbances could also result in non oscillatory increase of separation of rotor angles of synchronous generators. However, in large actual power systems this kind of unstable separation is not commonly encountered due to the large amount of controllers and protections employed, in particular the widespread introduction of fast acting automatic voltage regulators almost eliminated the problem [15, 2].

The main problem commonly analysed in the framework of small signal stability is that related to the so called *interarea oscillations* which are oscillations of rotor angles of generators belonging to one area against rotor angles of generators in other areas. The problem is often that of insufficient damping of these oscillations, which are a result of the increasingly stressed conditions in which power systems are operated. Interarea oscillations usually appear as poorly damped periodic oscillations with frequency in the range  $0.1 \div 2\text{Hz}$ . They are usually present in systems with heavy power transfer over weak transmission links. Since they are related to intrinsic oscillation mode of the system cannot be eliminated, but controllers can be tuned to increase their damping and/or shift their frequency. Several utilities worldwide experienced cases of interarea oscillations [21, 22]. A great amount of research has been devoted to the study of interarea oscillations in the Western system coordinating council in USA [23], in the North-South Brazilian interconnection [24], in the Scandinavian NORDEL system and in the UCTE interconnected European system [25].

Linear analysis is the method best suited to the study of small signal stability. Linearization of the differential/algebraic system of equations representing the power system:

$$\dot{\mathbf{x}} = \mathbf{f}(\mathbf{x}, \mathbf{y}) \quad (1.27)$$

$$\mathbf{0} = \mathbf{g}(\mathbf{x}, \mathbf{y}) \quad (1.28)$$

results in the following:

$$\begin{bmatrix} \Delta \dot{\mathbf{x}} \\ \mathbf{0} \end{bmatrix} = \begin{bmatrix} \frac{\partial \mathbf{f}}{\partial \mathbf{x}} & \frac{\partial \mathbf{f}}{\partial \mathbf{y}} \\ \frac{\partial \mathbf{g}}{\partial \mathbf{x}} & \frac{\partial \mathbf{g}}{\partial \mathbf{y}} \end{bmatrix} \cdot \begin{bmatrix} \Delta \mathbf{x} \\ \Delta \mathbf{y} \end{bmatrix} \quad (1.29)$$

Assuming that  $\partial \mathbf{g} / \partial \mathbf{x}$  is nonsingular,  $\Delta \mathbf{y}$  can be eliminated from (1.29) yielding:

$$\Delta \dot{\mathbf{x}} = \left[ \frac{\partial \mathbf{f}}{\partial \mathbf{x}} - \frac{\partial \mathbf{f}}{\partial \mathbf{y}} \left( \frac{\partial \mathbf{g}}{\partial \mathbf{y}} \right)^{-1} \frac{\partial \mathbf{g}}{\partial \mathbf{x}} \right] \Delta \mathbf{x} \quad (1.30)$$

The matrix:

$$\mathbf{J} = \left[ \frac{\partial \mathbf{f}}{\partial \mathbf{x}} - \frac{\partial \mathbf{f}}{\partial \mathbf{y}} \left( \frac{\partial \mathbf{g}}{\partial \mathbf{y}} \right)^{-1} \frac{\partial \mathbf{g}}{\partial \mathbf{x}} \right] \quad (1.31)$$

is the so called reduced Jacobian whose eigenvalues are used for small signal stability analysis of the system.

### 1.5.2 Transient stability

Among the large disturbances which could affect the transient stability of the system, short circuits and possibly subsequent tripping of the faulted transmission line are the most common. Instability which may arise from these severe disturbances is often characterised by a constantly increasing angular separation without any periodicity. This kind of behaviour is often referred to as first swing instability.

As it is the case in small signal stability non oscillatory unstable behaviour was largely eliminated by the widespread use of fast acting regulators. Most common instability behaviour is therefore in the form of large oscillations with increasing amplitude among generators of different areas.

In actual power system the classification based on the nature of the disturbance could result quite artificial. Some real occurrences of system instability, although caused by large disturbances, i.e. generator tripping, manifested as small signal stability problem, i.e. oscillations of growing amplitude. Detailed analytical and numerical analysis reported in [26] showed that the blackout of August 10, 1996 in Western American power system was caused by a Hopf bifurcation due to the eigenvalue associated to the  $0.25Hz$  mode passing from left half plane to right half plane as tie line loading increased after generators tripping. A global bifurcation due to the collapse of a stable limit cycle with an unstable one resulted in the eventual collapse.



While the study of small signal stability is usually tackled by means of the analysis of the linearization around an equilibrium point of interest, the study of transient stability mainly relies on nonlinear numerical simulations of some fault scenarios. In order to avoid the use of numerical simulations an enormous amount of research has been devoted to methods based on energetic principles, like the Lyapunov direct method [27, 28] which allow to determine an estimate of the attraction region  $X_s$  in the form:  $\mathbf{x} \in X_s \Leftrightarrow \mathcal{V}(\mathbf{x}) < \mathcal{V}_{critical}$ , where  $\mathcal{V}$  is a Lyapunov function.

## 1.6 Voltage stability

While small signal and transient instability phenomena are mostly related to synchronous generators and their control, voltage stability is mostly related to network and loads. Voltage stability can be defined as the ability of a power system to maintain voltage magnitude at all buses within acceptable limits after the system has experienced a disturbance. The loss of equilibrium between load demand and load supply is the main cause of voltage instability, which results in unacceptable low voltages across the network [29, 30]. Voltage instability phenomena often appear as a sudden decrease of voltage therefore called *voltage collapse*.

Many loads supplied by a power system are controlled in such a way as to have some sort of restorative behaviour. Large industrial motors drives, thermostatically controlled heating loads, tap-changing transformers are examples of loads that respond to disturbances trying to restore their power consumption. This restorative action has the effect to further increase the stress on an already stressed system. In particular reactive power demand could increase beyond the available capability, leading to the intervention of limiting protections such as overexcitation limiters in synchronous generators [29].

Most power system blackouts were caused by voltage instability resulting in voltage collapse. It has been demonstrated that the blackout experienced by Western American power system on July 2, 1996 was caused by loss of steady state equilibrium subsequent to a saddle-node bifurcation eventually leading to voltage collapse [26].

## 1.7 Subsynchronous oscillations

As described in previous sections, oscillations of synchronous generator rotor with respect to network reference is usually in the range of  $0.2 \div 2\text{Hz}$ . This is, however, a result of the simplifying assumptions used in generator's rotor representation, which is considered to be constituted by a single rigid mass. The rotor of an actual generating unit is a very complex mechanical system obtained by the interconnection of several shaft sections. This structure has therefore several torsional modes of vibration, with each section oscillating against the others [15]. Such oscillations can appear at both subsynchronous and supersynchronous frequencies, ranging from few tens to few hundreds of Hz.

Potentially dangerous undamped subsynchronous oscillations appear as a result of the interaction of torsional modes with synchronous generators' controllers or series capacitor compensated transmission lines. In the latter case, adverse interactions result in the so-called subsynchronous resonance (SSR) phenomena [31].

## Chapter 2

---

# Power system modelling

---

### Summary

*Stability of electric power system depends upon an equilibrium between power produced by generators and power drawn by loads. Stability analysis therefore requires suitable models of each component of the system. In the chapter models commonly used for the description of synchronous generators are introduced. The most common controllers associated with synchronous generators with the aim of increasing system's stability are also described. Models of loads and power balance equations at transmission network level are introduced.*

### 2.1 Synchronous generator

Almost all synchronous generators in operation are of three phase construction. A simplified schematic diagram of a three phase synchronous machine is reported in Fig. 2.1. Voltages are induced in the three stator windings, displaced by 120 degrees each others, by the rotating magnetic field produced by the field winding which is on the rotor [32]. Direct current, produced by an excitation system, flows through the field winding. Rotor revolves at synchronous speed given, in revolutions per minute, by:

$$n_{rpm} = \frac{120f}{p_f} \quad (2.1)$$

where  $f$  is the synchronous AC frequency, and  $p_f$  is the number of field poles. Figure 2.1 shows a two pole machine. An higher number of poles could be required

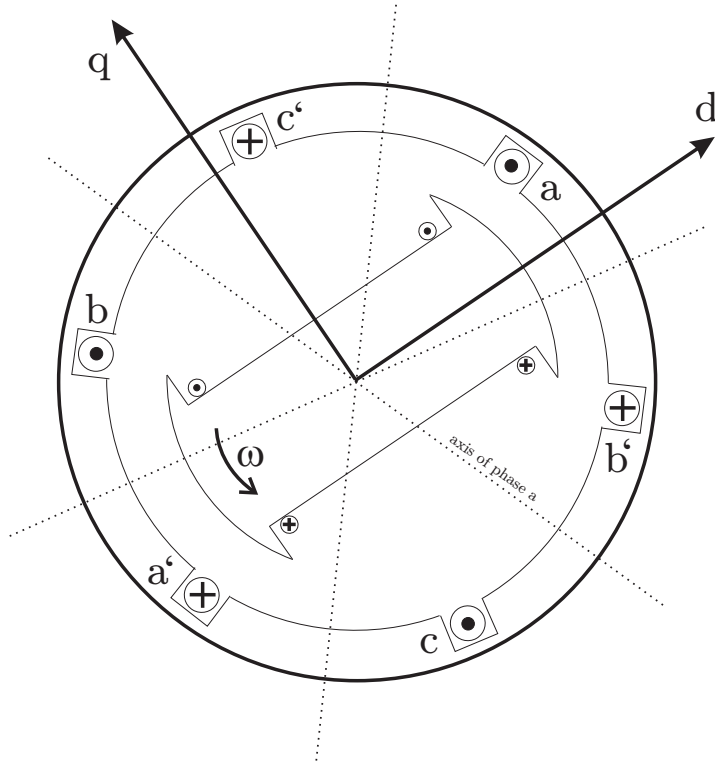


Figure 2.1: Schematic diagram of a three-phase synchronous machine

in machines operated at low speed, such as those connected to hydraulic turbines.

### 2.1.1 Mechanical equations

Steady state operation is characterised by a balance between the applied mechanical torque and the produced electromagnetic torque. In this condition the rotor is stationary with respect to a reference frame rotating at the synchronous angular speed  $\omega_0$ . Any unbalance which results in a deviation from the equilibrium, causes also a variation of the angle  $\delta$  that the rotor axis forms with the synchronously moving reference. The dynamics of rotor angle  $\delta$  and velocity  $\omega$  is described by the so called *swing equations*:

$$\frac{d\Delta\omega}{dt} = \frac{1}{2H} [T_m - T_e - D\Delta\omega] \quad (2.2)$$

$$\frac{d\delta}{dt} = \omega_0 \Delta\omega \quad (2.3)$$

where  $\Delta\omega = \omega - \omega_0$  is the deviation, in *rad/s* of rotor angular velocity from synchronous velocity  $\omega_0 = 2\pi f_0$ ,  $H$  is the *p.u.* inertia constant,  $T_m$  and  $T_e$  are

the *p.u.* mechanical and electromagnetic torque, respectively,  $D$  is the damping coefficient.

### 2.1.2 Electrical equations

Although machine's equations can be derived in a three phase reference frame, a great simplification is attained if electrical quantities are referred to a rotating reference moving at synchronous speed. The  $dq0$  transformation, also known as Blondel-Park transformation, is used to decompose stator quantities into two rotating components: the direct axis component which is aligned with the rotor and the field winding axis, and the quadrature axis component which is orthogonal to the field axis. Several models with different levels of detail are available for the description of electrical equations [33]. These models differs in the number of differential equations and hence of the state variables necessary to describe the electrical subsystem. In all subsequent equations quantities are expressed in per unit, except for the time which is given in seconds.

#### Eight order model

This model uses eight differential equations, six of them to describe the electrical variables and the two swing equations (2.2)-(2.3) to describe the mechanical motion [34].

**Stator equations** Two of the six differential equations are used to describe the  $d$  and  $q$  axis components of the stator fluxes as follows:

$$\dot{\psi}_d = e_d + \psi_q \omega + r i_d \quad (2.4)$$

$$\dot{\psi}_q = e_q - \psi_d \omega + r i_q \quad (2.5)$$

where:

$\psi_d$ : direct axis component of stator flux

$\psi_q$ : quadrature axis component of stator flux

$e_d$ : direct axis component of stator voltage

$e_q$ : quadrature axis component of stator voltage

$i_d$ : direct axis component of stator current

$i_q$ : quadrature axis component of stator current

$e_d$ : direct axis component of stator voltage

$r$ : stator resistance

**Rotor equations** Four differential equations are required to describe rotor electrical dynamics in the four windings assumed to be lying on the rotor. One of them is the field winding necessary to produce the magnetic field that induces voltages in the stator. The other three are used to represent damping due to eddy current flowing in short-circuited damper windings and in the rotor body. This damping is modelled assuming one damper winding in the  $d$  axis, and two in the  $q$  axis. The resulting equations are as follows:

$$\begin{aligned} \dot{E}'_q = & \frac{1}{T'_{d0}} \left[ E_{fd} - E'_q - E'_q \frac{(x'_d - x''_d)(x_d - x'_d)}{(x'_d - x_l)^2} \right. \\ & \left. + \psi_{kd} \frac{(x'_d - x''_d)(x_d - x'_d)}{(x'_d - x_l)^2} - i_d \frac{(x''_d - x_l)(x_d - x'_d)}{(x'_d - x_l)^2} \right] \end{aligned} \quad (2.6)$$

$$\begin{aligned} \dot{E}'_d = & \frac{1}{T'_{q0}} \left[ -E'_d + E'_d \frac{(x'_q - x''_q)(x_q - x'_q)}{(x'_q - x_l)^2} \right. \\ & \left. - \psi_{kq} \frac{(x'_q - x''_q)(x_q - x'_q)}{(x'_q - x_l)^2} + i_q \frac{(x''_q - x_l)(x_q - x'_q)}{(x'_q - x_l)^2} \right] \end{aligned} \quad (2.7)$$

$$\dot{\psi}_{kd} = \frac{1}{T''_{d0}} \left[ -\psi_{kd} + E'_q - (x'_d - x_l)i_d \right] \quad (2.8)$$

$$\dot{\psi}_{kq} = \frac{1}{T''_{q0}} \left[ -\psi_{kq} - E'_d - (x'_q - x_l)i_q \right] \quad (2.9)$$

where:

$E'_d$ : direct axis transient voltage

$E'_q$ : quadrature axis transient voltage

$\psi_{kd}$ : direct axis damper flux linkage

$\psi_{kq}$ : quadrature axis damper flux linkage

$E_{fd}$ : Exciter voltage

$x_d, x'_d, x''_d$ : synchronous, transient and subtransient direct axis reactances

$x_q, x'_q, x''_q$ : synchronous, transient and subtransient quadrature axis reactances

$x_l$ : leakage reactance

$T'_{d0}, T''_{d0}$ : transient and subtransient direct axis time constants (in seconds)

$T'_{q0}, T''_{q0}$ : transient and subtransient quadrature axis time constants (in seconds)

The following algebraic equations:

$$\psi_d = E'_q \frac{x''_d - x_l}{x'_d - x_l} + \psi_{kd} \frac{x'_d - x''_d}{x'_d - x_l} - x''_d i_d \quad (2.10)$$

$$\psi_q = -E'_d \frac{x''_q - x_l}{x'_q - x_l} + \psi_{kq} \frac{x'_q - x''_q}{x'_q - x_l} - x''_q i_q \quad (2.11)$$

which relate internal voltages and fluxes with output stator currents, along with the following relationship for the electromagnetic torque:

$$T_e = \psi_d i_q - \psi_q i_d \quad (2.12)$$

complete the model.

### Sixth order model

Sixth order model is basically the same as eight order model except that stator transients are considered so fast as to be negligible as far as transient stability and its associated slow rotor oscillations, are concerned. Furthermore rotor velocity is assumed to be constant in stator equations. A discussion of these approximations is reported in [15].

Stator differential equations (2.4) collapse into the following algebraic equations:

$$0 = e_d + \psi_q + r i_d \quad (2.13)$$

$$0 = e_q - \psi_d + r i_d \quad (2.14)$$

Rotor equations (2.6)-(2.9) remain the same, as well as the algebraic constraints (2.10)-(2.11) and (2.12).

### Third order model

The third order model is frequently employed in stability and control analysis thanks to its simplicity. Damping effects due to damper winding and rotor body eddy currents are neglected. In order to account for damping the coefficient  $D$  in the mechanical equation (2.2), which is usually zero in higher order models, has to be appropriately tuned. Only one equation is used to model the rotor:

$$\dot{E}'_q = \frac{1}{T'_{d0}} \left[ E_{fd} - E'_q + (x_d - x'_d)i_d \right] \quad (2.15)$$

Algebraic equations for output voltages are:

$$v_d = -x_q i_q - r i_d \quad (2.16)$$

$$v_q = E'_q + x'_d i_d - r i_q \quad (2.17)$$

while electromagnetic torque is given by:

$$T_e = v_d i_d + v_q i_q = E'_q i_q + (x'_d - x_q) i_d i_q - r(i_d^2 + i_q^2) \quad (2.18)$$

### Second order model

Most simplified analysis are carried out by means of the so called classical model. It only takes the two mechanical states  $\delta, \omega$  and their equations (2.2)-(2.3) into account. A constant voltage  $E'$  behind the transient reactance  $x'_d$  is considered as the output of the generator.

#### 2.1.3 Generator-network interface equations

Each generator of an interconnected power system has an its own  $dq$  reference frame, synchronously rotating with its own rotor. In order to study the behaviour of a multimachine system, it is necessary to interface all machines with a common reference, i.e. the network one, denoted as  $\mathcal{DQ}$ , which rotates at the synchronous frequency. This is done by means of the orthogonal transformation illustrated in Fig. 2.2 and given by:

$$\begin{bmatrix} \mathcal{D} \\ \mathcal{Q} \end{bmatrix} = \begin{bmatrix} \cos \delta_i & -\sin \delta_i \\ \sin \delta_i & \cos \delta_i \end{bmatrix} \cdot \begin{bmatrix} d \\ q \end{bmatrix} \quad (2.19)$$

$$\begin{bmatrix} d \\ q \end{bmatrix} = \begin{bmatrix} \cos \delta_i & \sin \delta_i \\ -\sin \delta_i & \cos \delta_i \end{bmatrix} \cdot \begin{bmatrix} \mathcal{D} \\ \mathcal{Q} \end{bmatrix} \quad (2.20)$$



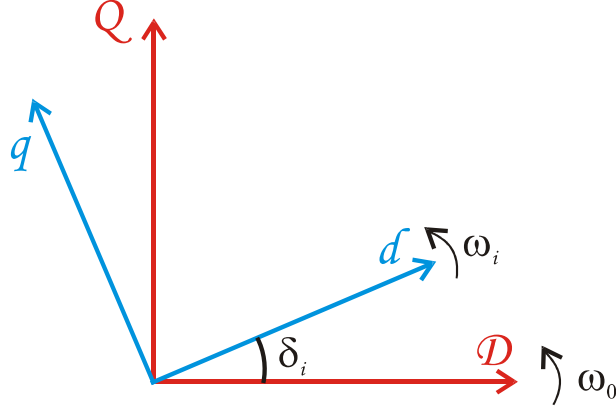


Figure 2.2: Transformation for interfacing machine reference with network reference

#### 2.1.4 Torsional dynamics

Mechanical equations (2.2)-(2.3) describe the motion of a single rotating mass subject to an accelerating or decelerating torque. In case more masses are to be considered in order to take unsynchronous oscillations into account, two equations for each additional mass have to be added. In the case of a four masses shaft the following system of equations describe the mechanical dynamics:

$$\text{Gen} : \begin{cases} \Delta\dot{\omega}_G = \frac{1}{2H_G} [K_{LP-G}(\delta_{LP} - \delta_G) - K_{G-Ex}(\delta_G - \delta_{Ex}) \\ \quad - D_G\Delta\omega_G - T_e] \\ \dot{\delta}_G = \omega_0\Delta\omega_G \end{cases} \quad (2.21)$$

$$\text{Exc} : \begin{cases} \Delta\dot{\omega}_{Ex} = \frac{1}{2H_{Exc}} [K_{G-Ex}(\delta_G - \delta_{Ex}) - D_{Ex}\Delta\omega_{Ex}] \\ \dot{\delta}_{Ex} = \omega_0\Delta\omega_{Ex} \end{cases} \quad (2.22)$$

$$\text{LP} : \begin{cases} \Delta\dot{\omega}_{LP} = \frac{1}{2H_{LP}} [K_{HP-LP}(\delta_{HP} - \delta_{LP}) - K_{LP-G}(\delta_{LP} - \delta_G) \\ \quad - D_{LP}\Delta\omega_{LP} + T_{LP}] \\ \dot{\delta}_{LP} = \omega_0\Delta\omega_{LP} \end{cases} \quad (2.23)$$

$$\text{HP} : \begin{cases} \Delta\dot{\omega}_{HP} = \frac{1}{2H_{HP}} [-K_{HP-LP}(\delta_{HP} - \delta_{LP}) - D_{HP}\Delta\omega_{HP} + T_{HP}] \\ \dot{\delta}_{HP} = \omega_0\Delta\omega_{HP} \end{cases} \quad (2.24)$$

where:

$\Delta\omega_G, \Delta\omega_{Ex}, \Delta\omega_{LP}, \Delta\omega_{HP}$  are the deviation from synchronous velocity of the generator, exciter, low pressure and high pressure turbine sections, respectively;

$\delta_G, \delta_{Ex}, \delta_{LP}, \delta_{HP}$  are the angular positions, with respect to a synchronously rotating reference of the generator, exciter, low pressure and high pressure turbine sections, respectively;

$H_G, H_{Ex}, H_{LP}, H_{HP}$  are the inertia constants of turbine shaft sections;

$D_G, D_{Ex}, D_{LP}, D_{HP}$  are the damping coefficients of turbine shaft sections;

$K_{LP-G}, K_{G-Ex}, K_{HP-LP}$  are the stiffness of the shaft between the respective masses;

$T_{LP}, T_{HP}$  are the mechanical torques developed by the Low pressure and High pressure turbine sections, respectively.

## 2.2 Generator's controllers

Steady state operation of the synchronous generator is guaranteed by the action provided by several control devices. The main feedback controllers are the turbine governor which determines the mechanical torque input to the machine, the Automatic Voltage Regulator (AVR) whose aim is to control the output voltage and the Power System Stabilizer (PSS) which provides a damping action to rotor oscillations.

### 2.2.1 Turbine governor

In most simplified analyses of power system dynamics, especially for short term studies, the mechanical torque input to the synchronous generator is assumed to be constant. In case of detailed analysis the dynamical model of the turbine and the role of the governor in adjusting the mechanical input to the generator are to be considered. IEEE working groups prepared detailed models of both steam and hydroelectric turbines [35, 36].

A common used simplified model from [37] is reported in Fig. 2.3, which, according to [35], could accommodate most of the types of turbine models. Coefficients  $K_2, K_3, K_4$  determine the contributes of the various turbine sections to the developed mechanical torque. Each turbine section is modelled as first order

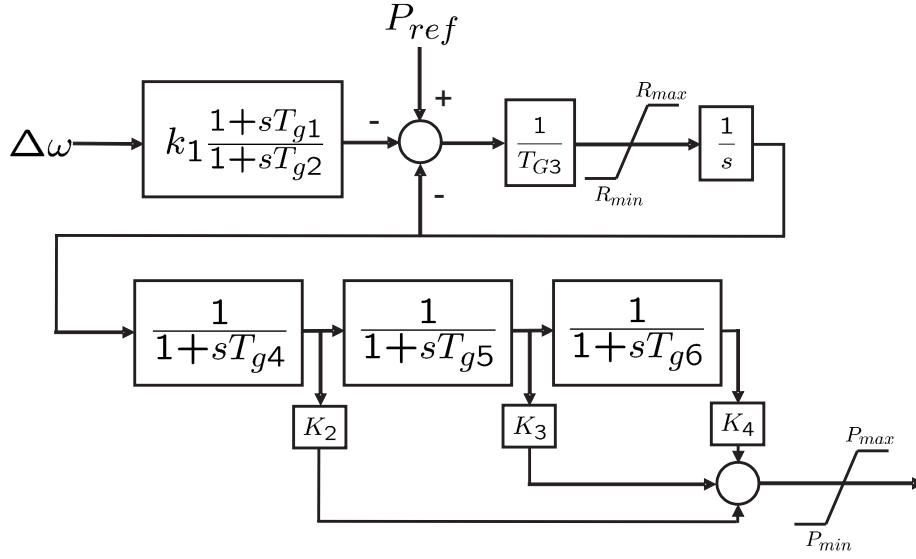


Figure 2.3: Turbine and governor

system. The governor comprises an integral control in order to guarantee zero speed deviation in steady state.

### 2.2.2 Automatic Voltage Regulator

Automatic voltage regulators control generator's output voltage magnitude by acting on the field excitation voltage  $E_{fd}$ . Although several excitation systems have been proposed in the past, the most widely used nowadays are based on static thyristor converters with high gain amplifiers. A schematic of this kind of commonly used exciter is reported in Fig. 2.4 [38, 39].

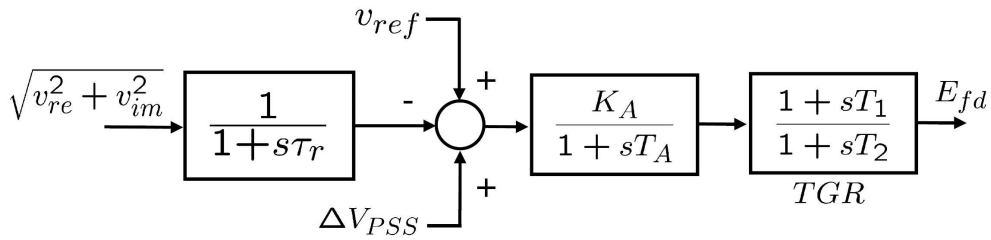


Figure 2.4: Thyristor exciter

A low pass filter is usually added to the voltage measurement. The gain  $K_A$  is usually high for obtaining a rapid response, while the time constant of the exciter is very small and often neglected. In some cases a too rapid response could

negatively affect generator's stability. In these cases a Transient Gain Reduction (TGR), with a lead/lag compensator, is introduced.

### 2.2.3 Power System Stabilizer

Power System Stabilizers (PSS) were introduced to provide additional damping to generator's rotor oscillations and therefore to reduce problems connected to local and interarea oscillations [40, 41]. A common structure for PSS is reported in Fig. 2.5. The input is the speed deviation, however other signals, such as the frequency or the output power deviation, are also used. The first stage is usually an high-pass filter often called wash-out filter, which provides zero output in steady state conditions. One or more, most commonly two, lead/lag filters are employed to provide sufficient phase compensation between  $\Delta\omega$  and the output torque [22]. The PSS output provides an additional input signal to the AVR. Alternative PSS structures have been proposed recently, such as the multiband PSS [42].

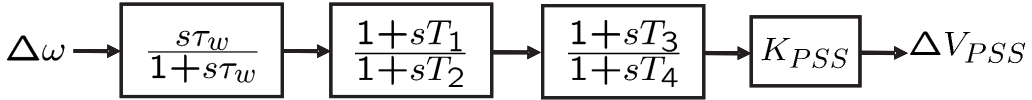


Figure 2.5: PSS

## 2.3 Transmission network and loads

The role of transmission network is to deliver power produced in generators' stations to loads.

The transmission network is made up by the interconnection of a number of transmission lines which can be as long as several hundreds of kilometers. The most detailed mathematical description of a line is in the form of partial differential equation, which takes propagation wave phenomena into account. Since power system stability usually involves slow oscillations and study time intervals of several second, this level of detail is often unnecessary. A detailed discussion of the subject is deferred to the following chapter. In commonly used models all transients associated with transmission lines are neglected and the network is assumed constantly in steady-state, therefore the following algebraic

equations are used to relate injected node currents and node voltages [43]:

$$\bar{\mathbf{I}} = \dot{\mathbf{Y}}_{bus} \bar{\mathbf{V}} \quad (2.25)$$

where:

$\bar{\mathbf{I}}$  is the vector of injected node currents

$\bar{\mathbf{V}} = [V_1 e^{j\theta_1}, \dots, V_n e^{j\theta_n}]^\top$  is the vector of node voltages

$\dot{\mathbf{Y}}_{bus}$  is the bus admittance matrix whose generic entry is  $\dot{\mathbf{Y}}_{bus}^{i,k} = G_{i,k} + jB_{i,k}$

### 2.3.1 Load flow equations

From eq. (2.25) active and reactive power injection at the  $i$ -th busbar are easily derived as:

$$P_i = \sum_{k=1}^n V_i V_k [G_{i,k} \cos(\theta_i - \theta_k) + B_{i,k} \sin(\theta_i - \theta_k)] \quad (2.26)$$

$$Q_i = \sum_{k=1}^n V_i V_k [G_{i,k} \sin(\theta_i - \theta_k) - B_{i,k} \cos(\theta_i - \theta_k)] \quad (2.27)$$

Load flow equations constitute the power balance relationships at each transmission network bus. Active and reactive power injections given by (2.26)-(2.27) must be equal to the opposite of the active and reactive power absorbed by loads:

$$P_i + P_{L,i} = 0 \quad (2.28)$$

$$Q_i + Q_{L,i} = 0 \quad (2.29)$$

### 2.3.2 Load modelling

Active and reactive powers absorbed by loads can either be considered as fixed constants or function of local bus quantities such as voltage magnitude and frequency. Load modelling in power system stability study is a widely debated topic and no definitive model exists [44, 45]. In some studies it could be sufficient to use constant power load models, while in other cases, in particular when loads are the driving force of instability as it is the case for voltage collapse, detailed load modelling is required. A commonly used model is the so called ZIP model which

is a weighted sum of constant impedance (Z), constant current (I) and constant power (P) loads:

$$P_{L,i} = P_{i,0} \left[ p_{i,0} + p_{i,1} \left( \frac{V_i}{V_{i,0}} \right) + p_{i,2} \left( \frac{V_i}{V_{i,0}} \right)^2 \right] \quad (2.30)$$

$$Q_{L,i} = Q_{i,0} \left[ q_{i,0} + q_{i,1} \left( \frac{V_i}{V_{i,0}} \right) + q_{i,2} \left( \frac{V_i}{V_{i,0}} \right)^2 \right] \quad (2.31)$$

where  $P_{i,0}, Q_{i,0}$  are the  $i$ -th load nominal active and reactive power, respectively,  $V_{i,0}$  is the nominal voltage at busbar  $i$  and  $p_{i,0}, p_{i,1}, p_{i,2}, q_{i,0}, q_{i,1}, q_{i,2}$  are appropriate coefficients.

Induction motors account for a large percentage of industrial loads. In many cases their models are necessary to properly describe system's dynamics [15]. Other types of dynamic load models have also been proposed to capture load dynamics useful to describe voltage instability related phenomena[46]. One simple load model that will be also used in numerical simulations reported in later chapter is given by [47, 48]:

$$\dot{G}_i = \frac{1}{\tau_{P_i}} \left[ P_{i,0} - G_i (V_i/V_{i,0})^2 \right] \quad (2.32)$$

$$\dot{B}_i = \frac{1}{\tau_{Q_i}} \left[ -Q_{i,0} - B_i (V_i/V_{i,0})^2 \right] \quad (2.33)$$

### Example 2.1

Consider the Single Machine Infinite Bus (SMIB) system of fig. 2.6 constituted by a machine connected through a transmission line to a constant voltage bus.

The generator is modelled using the classical model, i.e. a constant voltage behind the transient reactance, with mechanical dynamics given by eqs. (2.2)-(2.3). A fault is applied at node 1, cleared after  $t_{cl}$  seconds by opening line 2.

The electrical torque  $T_e$  is given by:

$$T_e = \Re(E' e^{j\delta} \cdot \bar{I}^*) \quad (2.34)$$

where:

$$\bar{I} = \frac{1}{j(x'_d + x_t)} (E' e^{j\delta} - \bar{V}_1) \quad (2.35)$$

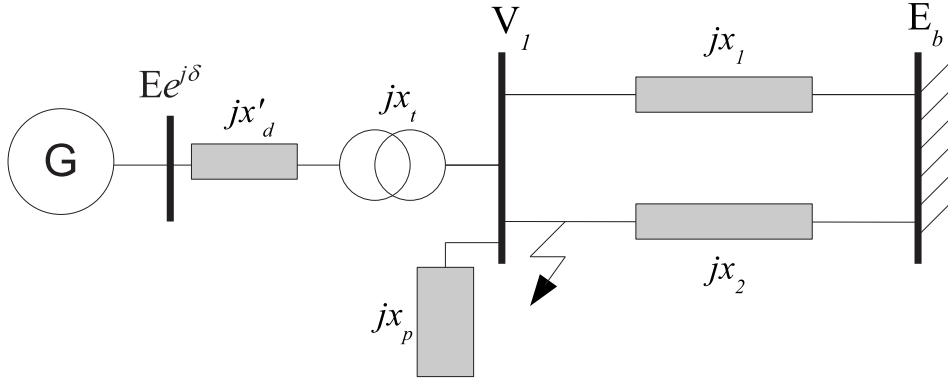


Figure 2.6: SMIB

$$\begin{aligned}
 \bar{V}_1 &= \frac{1}{Y_{prefault}} \left( \frac{1}{j(x'_d + x_t)} E' e^{j\delta} + \frac{1}{jx_1} E_b + \frac{1}{jx_2} E_b \right) & t < t_{fault} \\
 \bar{V}_1 &= 0 & t_{fault} \leq t < t_{fault} + t_{cl} \\
 \bar{V}_1 &= \frac{1}{Y_{postfault}} \left( \frac{1}{j(x'_d + x_t)} E' e^{j\delta} + \frac{1}{jx_1} E_b \right) & t \geq t_{fault} + t_{cl}
 \end{aligned} \tag{2.36}$$

and:

$$\begin{aligned}
 \dot{Y}_{prefault} &= \frac{1}{j(x'_d + x_t)} + \frac{1}{jx_1} + \frac{1}{jx_2} + \frac{1}{jx_p} \\
 \dot{Y}_{postfault} &= \frac{1}{j(x'_d + x_t)} + \frac{1}{jx_1} + \frac{1}{jx_p}
 \end{aligned}$$

With the following parameters, adapted from [15]:

$$x_1 = 0.5, x_2 = 0.93, x_t = 0.15, x'_d = 0.3, E' = 1.1626, E_b = 0.90081, H = 3.5, T_m = 0.9, D = 5$$

equations (2.2)-(2.3) result in the equations 1.19 of Ex.1.1.  $\square$





## Chapter 3

---

# Flexible AC Transmission Systems

---

### Summary

*Flexible Alternating Current Transmission Systems are attracting a great amount of research interest thanks to their ability to exploit power electronic based converters for rapid and effective regulation of power flows in transmission networks. In the chapter, after a brief review of basic concepts related to power flow control, parallel and series compensation are introduced. Two devices belonging to the FACTS family, namely the STATCOM and the SSSC, are described, as well as their ability to provide real-time control of nodal voltage magnitude and line impedance. The enhancement of power system stability achieved through reactive power control is demonstrated by means of power-angle curves and stability region enlargement.*

### 3.1 FACTS role in modern power systems

Electric power systems are undergoing continuous changes and restructuring due to a constant increase in power demand, thus operating in scenarios which can significantly differ from those envisaged years ago, when their main infrastructures were initially planned and designed. Higher power demands lead to increased power flows which in turn result in decreased stability margins. Furthermore, stressed power systems are more prone to lightly damped interarea oscillations which could more easily grow unstable.

The advent of deregulated markets has further increased the importance of some critical problems related to the vulnerability of the interconnected power systems [49]. These problems require more and more effective measures directed to enhance transient and oscillatory stability as far as possible. In deregulated environment the threat of losing stability could be one of the consequences of the heavily loaded transmission lines, due to the power transactions between producers and buyers, aiming at their economic satisfaction. Dispatcher has to realise the balance between load and generation in every elementary time interval, getting respectively their bids and requests compatibly with power system reliability and security.

Although the increased power demand could be satisfied by building new generation and transmission facilities, this solution is seldom viable due to economic and environmental concerns which usually constitute obstacles that cannot be overcome. Electric power utilities are therefore rarely willing to build new generation facilities and transmission lines, instead they would prefer solutions towards a full utilisation of the capabilities of existing equipment.

Flexible Alternating Current Transmission System (FACTS) is the most promising technology that provide a viable solution to these requirements. Based on the use of power electronics, FACTS devices, complemented with modern telecommunication and control technologies, allow power system operators to optimally control the network, both in steady state operation and following disturbances.

FACTS devices can be defined as alternating current transmission systems based on active static converters capable of generating and absorbing a controllable amount of reactive power in order to modify and regulate network quantities such as the voltage at the point of common coupling or current and power flow over a transmission line. Coupling a static converter with a power source or a storage device allows also exchange of active power.

Benefits provided by FACTS devices are twofold: they are capable of increasing power transfer over transmission lines and can make these power transfers fully controllable [50, 51, 52]. Coupled with their extremely fast action, granted by the use of power semiconductor devices and rapidly responding controllers, real time control for the stability enhancement of the system as well as damping of local and interarea oscillations, become viable possibilities [15, 22].

The last decade has witnessed a wide interest in design and application of FACTS devices, both from academic and industrial research. Several enhance-

ment in semiconductor technologies and manufacturing have made power electronic devices capable of handling high power levels (GTO, IGBT, IGCT) commercially available [53].

Many devices have been proposed in the past within the FACTS family, some of them based on thyristor switched reactors like the Thyristor Controlled Series Compensator (TCSC) and the StaticVar [54], while others, like the Static Compensator (STATCOM) [55], the Static Synchronous Series Compensator (SSSC) [56], the Unified Power Flow Controller (UPFC) [57] and the Superconducting Magnetic Energy Storage systems (SMES) [58], employ power electronic converters. This latter choice guarantees the best flexibility in control and rapidity of response.

### 3.2 Active and reactive power flow control through shunt and series compensators

Active and reactive power flow on a transmission line depend on the magnitude and phase of sending and receiving ends voltages, and on the line impedance. For the simple model in Fig. 3.1 which represents a simplified equivalent model of a generator at the sending end connected through a transmission line to an infinite bus at the receiving end, active and reactive power at the sending end can be derived as follows:

$$\dot{S}_s = P_s + jQ_s = \bar{V}_s \bar{I}^* \quad (3.1)$$

where:

$$P_s = \frac{V_s V_r}{X} \sin \delta = P_{\max} \sin \delta \quad (3.2)$$

$$Q_s = \frac{V_s^2 - V_s V_r \cos \delta}{X} \quad (3.3)$$

while at the receiving end:

$$P_r = \frac{V_s V_r}{X} \sin \delta = P_{\max} \sin \delta \quad (3.4)$$

$$Q_r = \frac{V_s V_r \cos \delta - V_r^2}{X} \quad (3.5)$$

Active power, due to lossless transmission line, is equal at both ends and its power-angle relationship is plotted in Fig. 3.2.

Steady state operating point is obtained in Fig 3.2 by the intersection of the power-angle curve with the red line representing mechanical power input at the

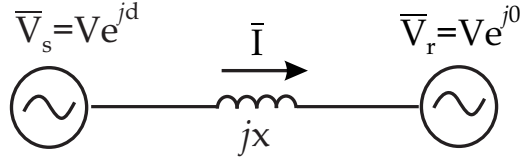


Figure 3.1: A simple two buses power system representing a generator connected to a stiff bus through a lossless transmission line

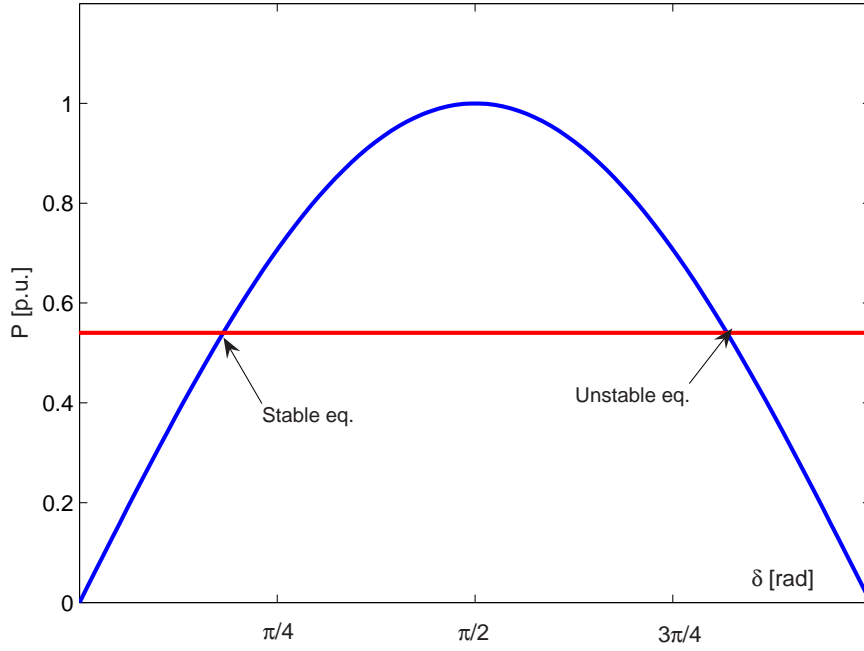


Figure 3.2: Power-angle relationship for the SMIB system in Fig. 3.1

sending end. Depending on the sign of  $dP_e/d\delta$  the equilibrium point is classified as stable or unstable. Indeed, it is easily verified that if  $dP_e/d\delta < 0$  the Jacobian of the second order system without damping has one positive eigenvalue\*, whereas  $dP_e/d\delta > 0$  results in a stable oscillatory mode, with Jacobian matrix having

---

\* For the classical second order SMIB system:

$$\begin{aligned}\dot{\delta} &= \omega \\ \dot{\omega} &= \frac{1}{M}[P_m - P_e]\end{aligned}$$

the Jacobian matrix is:

$$\mathbf{J} = \begin{bmatrix} 0 & 1 \\ -\frac{1}{M} \frac{\partial P_e}{\partial \delta} & 0 \end{bmatrix}$$

purely imaginary eigenvalues. For angles below  $\pi/2$  rad. the equilibrium point is stable, while it is unstable for angles above  $\pi/2$ . In order to provide a sufficient margin for stable operation the power angle over transmission lines is usually kept below 45 deg. From eq. (3.2) it can be recognized that active power flow depends mainly on the power angle, and its sign influences the direction of power flow. On the other hand, reactive power flow mainly depends on the values of voltage magnitudes, and its direction is from the higher voltage bus to the lower voltage bus. Higher values of the angle  $\delta$  and of the transmitted power result in an higher reactive power demand at the sending end, that could further threaten system's security.

From the above discussion, it can be concluded that steady-state active and reactive power flows over a transmission line, depend on line's reactance and on the relative magnitudes and phases of voltages at both line's ends. FACTS controllers are aimed at controlling power transmission over the network performing a regulation of one or more of these parameters. The role of FACTS in power systems is not limited to steady-state regulation. Indeed, their intrinsic capabilities in rapidly adjusting their output in response to system's transients, make them the technology of choice for real-time power systems control.

Several devices belonging to the FACTS family have been proposed in the technical literature. Among them STATCOM and SSSC will be analysed in the following, as examples of shunt connected and series connected devices, respectively. The STATCOM can be employed to regulate the voltage magnitude at the point of common coupling, therefore providing reactive power support and regulating power flows in the network, whereas the SSSC achieves power flow control by modifying the equivalent series reactance of the line to which it is connected.

### 3.3 Static compensator (STATCOM)

The STATic COMpensator can be defined as a synchronous static generator which operates as a shuntly-connected reactive power static compensator. Its output current can be fully controlled in both the capacitive and inductive range, independently of AC network voltage. It is basically constituted by a Voltage

---

whose characteristic equation is:

$$\lambda^2 + \frac{1}{M} \frac{\partial P_e}{\partial \delta} = 0 \quad (3.6)$$

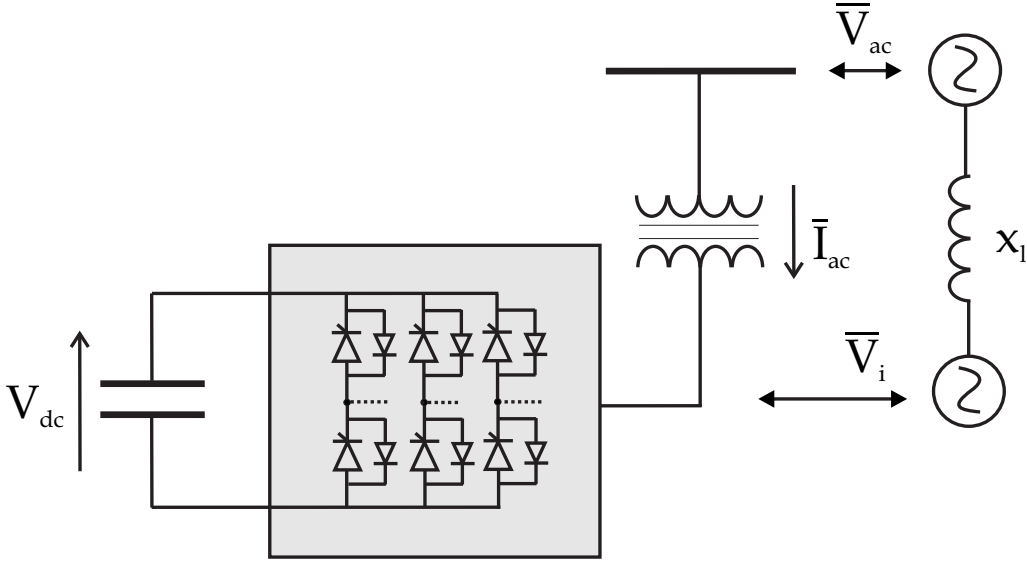


Figure 3.3: Basic structure and equivalent circuit of a STATCOM

Source Inverter (VSI), a coupling transformer with leakage reactance  $x_l$  shuntly connected with the network, and a DC capacitor. A schematic diagram of a STATCOM, its network interface and equivalent circuit is reported in Fig. 3.3. A STATCOM draws, at the point of common coupling, a practically sinusoidal current, whose amplitude is fully controllable, and kept almost in quadrature with respect to network voltage. It therefore acts as a controllable shunt capacitive or inductive reactance, thus allowing regulation of network voltage which is its main function. A supplementary feedback controller can be added in order to enhance damping of system's oscillations. Reactive power is exchanged through the leakage reactance of the coupling transformer. STATCOM operation, as summarised in Fig. 3.4, depends on the relative values of inverter output voltage  $\bar{V}_i$  and network voltage  $\bar{V}_{ac}$ . When inverter voltage magnitude is lower than network voltage, the STATCOM acts as an inductor drawing reactive power from the network. On the other hand, when inverter voltage is higher than network voltage the STATCOM operates as a capacitor injecting capacitive reactive power into the network. Although not apparent from the above discussion, proper operation of the STATCOM requires also the inverter to draw an amount of active power necessary to compensate for VSI and transformer's losses, as to maintain the required voltage across DC capacitor. It is therefore required that inverter voltage  $\bar{V}_i$  lag network voltage  $\bar{V}_{ac}$  of a small angle. It should be highlighted that

several inverter controller proposed for FACTS applications are able to control only the phase of output voltage and not its magnitude which is proportional to DC voltage. In these cases, output voltage regulation is achieved by angle control which determines active power exchange with the network to charge or discharge the DC capacitor [59, 60].

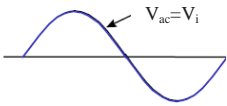
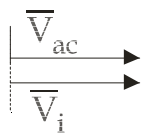
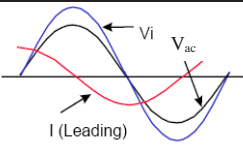
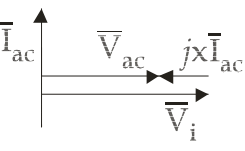
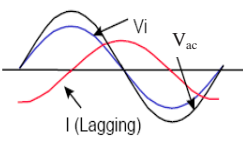
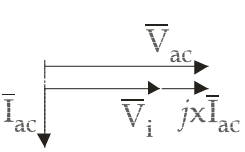
Mode	Waveforms	Phasor diagram	Description
No load			$\bar{V}_{ac} = \bar{V}_i \Rightarrow \bar{I}_{ac} = 0$
Capacitive operating mode			<p>If <math> \bar{V}_{ac}  &lt;  \bar{V}_i </math>, <math>\bar{I}</math> leads <math>\bar{V}</math> of <math>90^\circ</math>. Current amplitude is fully controllable by adjusting <math>\bar{V}_i</math>.</p> <p>The STATCOM will draw capacitive (leading) current, acting as a capacitor with fully controllable reactance</p>
Inductive operating mode			<p>If <math> \bar{V}_{ac}  &gt;  \bar{V}_i </math>, <math>\bar{I}</math> lags <math>\bar{V}</math> of <math>90^\circ</math>.</p> <p>Current amplitude is fully controllable by adjusting <math>\bar{V}_i</math>.</p> <p>The STATCOM will draw inductive (lagging) current, acting as an inductor with fully controllable reactance</p>

Figure 3.4: Operating modes, waveforms and phasor diagram illustrating STATCOM operation

Reactive power exchange achieved by the STATCOM is independent of network voltage, differently from compensation achieved with fixed capacitor's banks or switched capacitor based compensator such as the SaticVAR [54], thus reactive power support can also be provided at low voltages, when it is most required.

As detailed in a later chapter, if DC voltage is supported by an external energy source or storage device, STATCOM can also exchange active power. This possibility can further enhance FACTS capabilities to improve power system stability [61, 62].

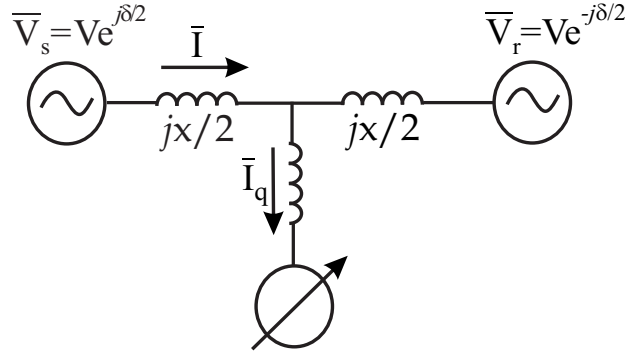


Figure 3.5: Midpoint compensation of a transmission line

It has been demonstrated in eqs. (3.2)-(3.4) that the active power flow over an uncompensated transmission line, as represented in Fig. 3.5 with  $\bar{I}_q = 0$ , is given by:

$$P = \frac{V^2}{X} \sin \delta \quad (3.7)$$

assuming equal magnitude voltages at both line ends. The power-angle relationship in eq. (3.7) is represented by the blue line in Fig. 3.6. If compensation is such that the voltage magnitude at midpoint location\* is  $V$ , then the power flow is increased to:

$$P = 2 \frac{V^2}{X} \sin \frac{\delta}{2} \quad (3.8)$$

which is plotted in red line in Fig. 3.6. Transmissible power can be doubled with perfect compensation. Practical constraints on the maximum magnitude of STATCOM current limit the transmissible power, whose dependence on the angle is given by:

$$P = \frac{V^2}{X} \sin \delta + \frac{V I_{q,max}}{2} \sin \frac{\delta}{2} \quad (3.9)$$

Several power-angle curves for  $I_q$  ranging from  $0.2p.u.$  to  $2p.u.$  are reported in Fig. 3.6 in light blue.

### 3.4 Static synchronous series compensator (SSSC)

Series reactive power compensation is obtained by controlling the equivalent impedance of a transmission line, as to regulate the power flow through the

---

\*Midpoint siting is often considered as the best option for FACTS devices [63].



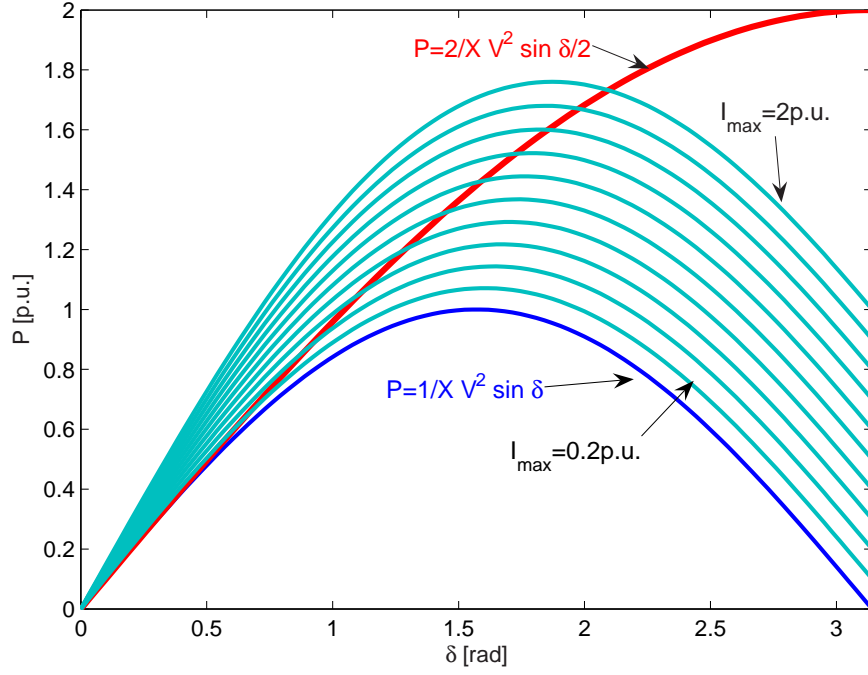


Figure 3.6: Power-angle relationship for midpoint compensated line

line. Series connection of capacitors banks was the first method of series compensation. However, the impossibility to control in real time the level of compensation and the risk of initiating potentially dangerous resonances constitute serious drawbacks to this solution. As for shunt compensation, the utilisation of fully controllable devices based on power electronics converters, provides the most flexible solution for series compensation.

The SSSC can be defined as a static synchronous generator which acts as a series compensator whose output voltage is fully controllable, independent of line current and kept in quadrature with it, with the aim of increasing or decreasing the voltage drop across the line, therefore controlling the power flow.

The basic structure of an SSSC and its connection with the network is reported in Fig. 3.7.

SSSC operation is illustrated by the equivalent circuit of a lossless transmission line of Fig. 3.8 where the compensator injects a voltage  $\bar{V}_q$ . The corresponding phasor diagram is reported in Fig. 3.9. Series injected voltage  $\bar{V}_q$  is in quadrature with respect to line current, and can either provide capacitive com-

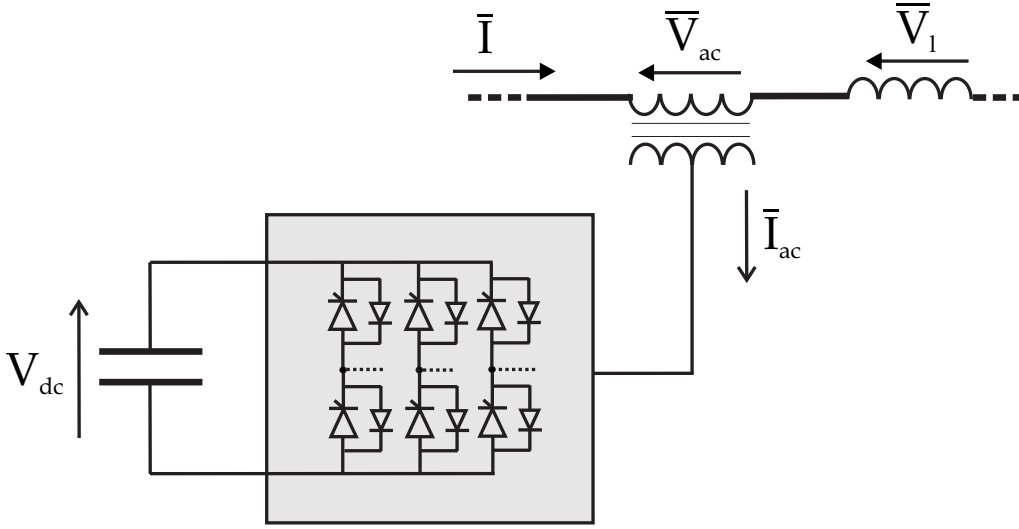


Figure 3.7: Basic structure of an SSSC

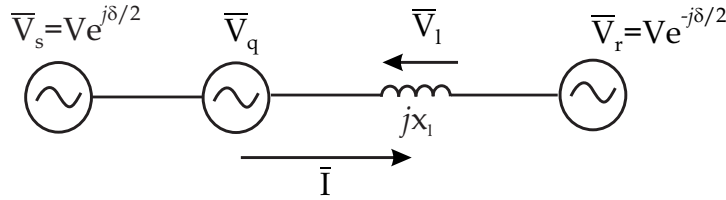


Figure 3.8: A series compensated transmission line

pensation if  $\bar{V}_q$  leads  $\bar{I}$  by  $\pi/2rad.$  or inductive compensation if  $\bar{V}_q$  lags  $\bar{I}$  by  $\pi/2rad.$  A relatively small active power exchange is required to compensate for coupling transformer and switching losses, and maintain the required DC voltage.

From the phasor diagram of Fig. 3.9, it can be concluded that the SSSC increases the voltage drop across line inductance and hence power flow, if it emulates capacitive compensation. Differently from series compensation achieved by means of either fixed or switched reactors, the SSSC can inject a voltage that is independent of line current, whose amplitude can be fully controlled. Indeed, the SSSC can be controlled in two different operation modes: constant reactance mode and constant quadrature voltage mode. If SSSC is in constant reactance mode of operation, active power transfer over the transmission line of Fig. 3.7 is

$$P = \frac{V_s V_r}{x_l(1-s)} \sin \delta \quad (3.10)$$

where  $s = x_c/x_l$  is the degree of series compensation. If SSSC is operated in constant quadrature voltage mode, assuming  $V_s = V_r = V$  active power transfer

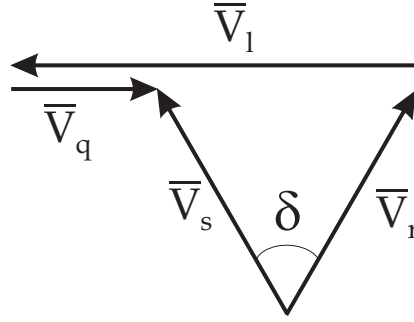


Figure 3.9: Phasor diagram of the series compensated transmission line in Fig. 3.8

is:

$$P = \frac{V^2}{x_l} \sin \delta + \frac{V}{x_l} V_q \cos \frac{\delta}{2} \quad (3.11)$$

Power-angle relationships (3.10)-(3.11) are reported for different values of compensation in Fig. 3.10 for both constant reactance and constant quadrature voltage mode of operation.

A comprehensive analysis of the different modes of operation of the SSSC and their influence on power system stability is reported in [64].

### 3.5 Shunt and series reactive compensation and stability region

The potentiality of FACTS devices in enlarging the stability region can be easily argued from the already reported power angle relationships, by keeping in mind the well known equal area criterion [15].

An alternative way for investigating the increasing of the critical clearing time obtained by use of FACTS devices is their incidence on the stable manifold of the controlling unstable equilibrium point, which is contained in the boundary of the asymptotic stability region of post-fault stable equilibrium. Recently an interesting characterisation of this manifold has been proposed based upon a quadratic approximation\* [66, 65, 67].

\*The quadratic approximation of the boundary of the stability region of the stable equilibrium point  $\mathbf{x}_e$  for the system  $\dot{\mathbf{x}} = \mathbf{f}(\mathbf{x})$  is obtained in [65] as:

$$\mathbf{W}_s(\mathbf{x}_e) = [\mathbf{x} - \mathbf{x}_e]^\top \cdot \boldsymbol{\eta} + \frac{1}{2} [\mathbf{x} - \mathbf{x}_e]^\top \cdot \mathbf{Q} [\mathbf{x} - \mathbf{x}_e] \quad (3.12)$$

Where  $\mu$  is the unique unstable eigenvalue,  $\boldsymbol{\eta}$  is the corresponding left eigenvector of the Jacobian

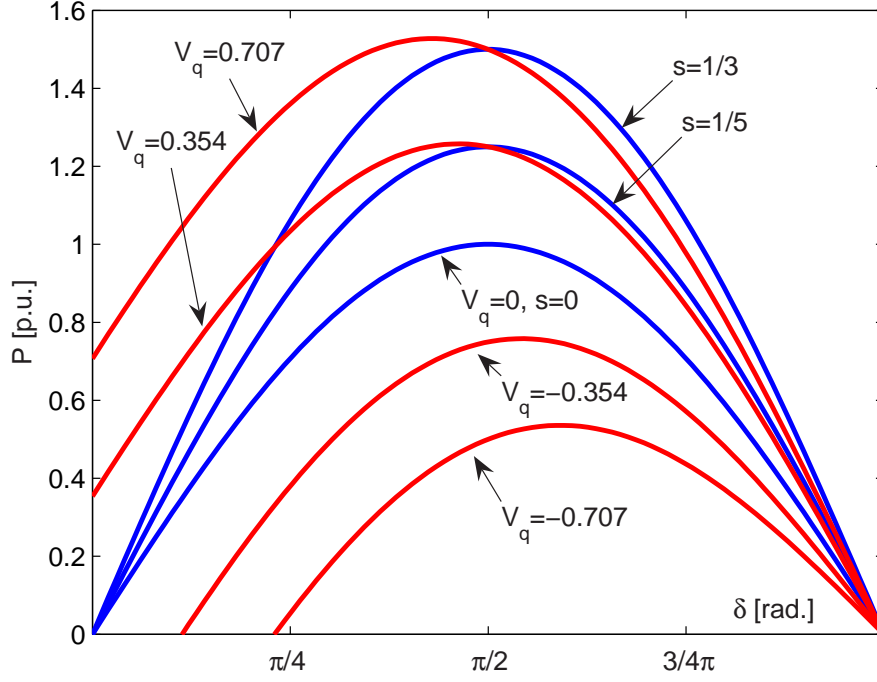


Figure 3.10: Power-angle relationship for series compensated transmission line, with constant reactance and constant quadrature voltage mode of operation

The simple SMIB power system in Fig. 3.11 is adapted from [15], adding a series compensator in one of the two parallel transmission lines and a shunt connected compensator at the intermediate bus.

Figures 3.12-3.12 show the phase portrait of the SMIB power system where the synchronous generator is represented by the classical second order model,

matrix  $\mathbf{J}$  and  $\mathbf{Q}$  is the solution of the following Lyapunov matrix equation:

$$\mathbf{C} \cdot \mathbf{Q} + \mathbf{Q} \cdot \mathbf{C}^\top = \mathbf{H} \quad (3.13)$$

where:

$$\begin{aligned} \mathbf{H} &= \sum_j \eta_j \mathbf{H}_j \\ \mathbf{H}_j &= \frac{\partial^2 f_j}{\partial x_i \partial x_k} \\ \mathbf{C} &= \mu \mathbf{I} / 2 - \mathbf{J}^\top \\ \mathbf{J}^\top \cdot \boldsymbol{\eta} &= \mu \boldsymbol{\eta} \end{aligned}$$

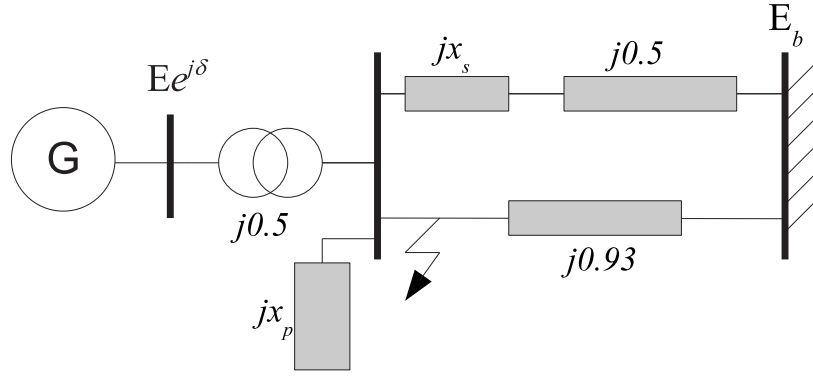


Figure 3.11: Single Machine power system coupled to an infinite bus, with series and parallel connected compensators.

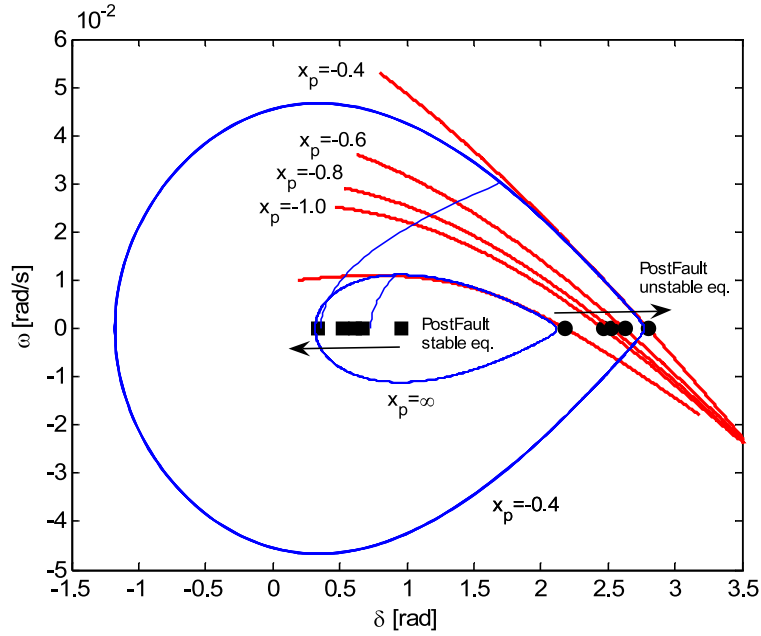


Figure 3.12: Stability region and quadratic approximation of its boundary as effected by shunt compensation

for the shunt and series compensation, respectively. Trajectories on the verge of instability, as well as the quadratic approximation of the stability boundary for several values of the compensation clearly show the enlargement of the stability region as a result of the action of reactive compensation achieved by FACTS devices.

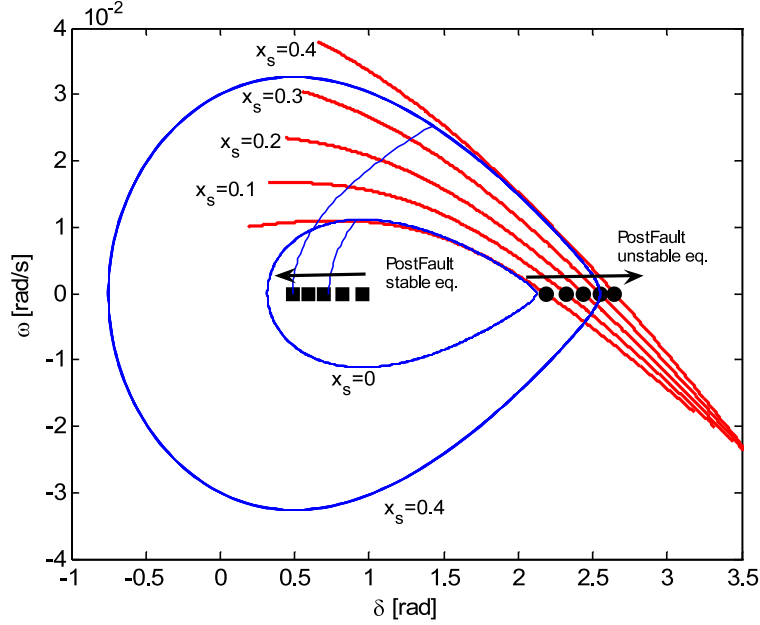


Figure 3.13: Stability region and quadratic approximation of its boundary as effected by capacitive series compensation

### 3.6 FACTS devices with active power compensation capabilities

Although many benefits in terms of increased power flow possibility and consequently of higher stability margins are achieved through reactive power compensation, it has been recognised that much better performances can be obtained if FACTS devices are complemented with active power compensation capabilities. Active power compensation capabilities in FACTS devices can be exploited to achieve a better damping of power system oscillations. Indeed, interarea oscillations appear as poorly damped, low frequency oscillations of active power exchange between different areas, therefore active power modulation is potentially much more effective in increasing damping than reactive power modulation only [61].

One of the most viable opportunity for high power storage is the use of superconducting coils, in which energy is stored in a large lossless inductor. This solution results in the so called Superconducting Magnetic Energy Storage system (SMES).

Beside stability improvement applications of SMES devices, other applications were proposed in the past, such as load levelling and spinning reserve however, costs associated with huge energy storage requirements, discouraged utilities from practical realisation.

The use of a proportional-integral controller for oscillation damping applied to a SMES with a power-flow error control signal is demonstrated in [61, 62], while robust control is used in [68, 69].

### 3.7 Conclusion

In the present chapter, operating principles and main benefits achievable with the use of power electronic converters-based compensating devices have been introduced. Series and shunt connected FACTS devices have been reviewed. Their capability to provide reactive power support has been shown to increase power flow and stability margins. It has been highlighted that FACTS devices can be augmented with supplementary controllers which can provide additional benefits such as increased damping of power system oscillations. One such controller, based on the use of Lyapunov theory will be proposed in chapter 5, after appropriate modelling and mathematical properties are reviewed.

It has also been underlined that, beside reactive power support, both STATCOM and SSSC can be capable of active power exchange when a storage device is connected to them.

A novel topology for power conditioning system for series and parallel compensators will be proposed in chapter 6. The same configuration will also be used for SMES-based FACTS devices.





## Chapter 4

---

# Phasor dynamics influence on electric power system performances

---

### Summary

*Dynamic behavior analysis of electric power system has always played a vital role in operation and planning of power systems. This analysis relies on computer simulation which are usually based on simplifying assumptions which aim at rendering system modelling more amenable to numerical solution. However, it is well known that uncertainties and unmodelled dynamics could in some cases lead to unexpected results. A simplified dynamic model of transmission network is employed to evaluate the influence of network transients on dynamic behavior of power systems. Although simplified, this model can easily capture usually neglected dynamics. Applications of this modelling is proposed with respect to two test systems, highlighting the effects of usually unmodelled dynamics.*

### 4.1 Introduction

Actual power system result from the interconnections of a large number of devices, comprising synchronous machines, transformers, lines, loads etc. each of them with its own dynamics, which can evolve over very different time scales.

Traditionally, power systems are modelled as a coupled set of differential and algebraic equations (DAE). This modelling is motivated by the assumption that the electrical system is operating in sinusoidal steady-state, network transients being much faster than electromechanical ones, due to generator dynamics. Angular rotor oscillations are indeed usually in the range  $0.1 \div 3\text{Hz}$  while network transients are expected to be orders of magnitude faster, thus decaying very rapidly [15]. As far as transient stability is concerned, fast network dynamics are traditionally neglected, thus simplifying modelling and alleviating the computational burden of simulating large electrical power systems which consist of hundreds of generators and thousands of lines and loads.

Fast network transient are then considered as instantaneous and their associated differential equations collapse into algebraic ones. The result is a set of DAE in the form [70]:

$$\begin{aligned}\dot{\mathbf{x}} &= \mathbf{f}(\mathbf{x}, \mathbf{y}) \\ \mathbf{0} &= \mathbf{g}(\mathbf{x}, \mathbf{y})\end{aligned}\tag{4.1}$$

where algebraic variables  $\mathbf{y}$  (voltage magnitude and phase) are functions of dynamic states  $\mathbf{x}$  (mechanical and electrical generators state variables). The extremely fast and ideally instantaneous network dynamics make all electric variables perfectly sinusoidal signals at synchronous frequency (60 or 50 Hz), thus being easily described by quasi-stationary phasors, whose magnitude and phase variations are much slower than the synchronous frequency. This quasi-stationary assumption is questioned when fast phenomena happen in power systems, such as subsynchronous resonance [71], voltage instability or the control action of FACTS regulating devices [72]. Fast time-varying phasors and their dynamics have been proposed to overcome such modelling limitations [73]-[74]. Even though the most accurate model of the transmission network is in the form of algebraic equations with time-delays [75]-[76], time-varying phasors provide a simple but effective environment for the study of fast network transients. Time-varying phasors have also been used as a tool to examine the interactions of load and transmission network transients in [47], in deriving a simple simulation environment with didactic purposes in [77] and to provide a simple method for testing robustness of controllers against network's unmodelled dynamics [71]. An alternative, yet similar derivation is reported in [78] employing the definition of complex envelope and the Hilbert transform.

As power systems become more and more loaded and operated near their stability margins, accuracy in modelling increases its importance, for planning and control decisions. Although unmodelled dynamics are unlikely to contribute in great modifications in system's response, their inclusion into simulations will result in a more accurate assessment of the overall dynamic behaviour. It is known, for example, that an accurate prediction of damping is a prerequisite for optimal tuning of generators' controllers and FACTS devices [79].

In the chapter, after some useful definitions and properties are presented, numerical simulations of a simple SMIB test system and a multimachine one, are presented in order to highlight the incidence of network modelling on the dynamic behaviour of electric power systems.

## 4.2 Time-varying phasors and their dynamics

Dynamic phasors are a tool to analytically describe time varying almost periodic signals, such as those arising from the use of power electronic converters. They were firstly introduced to model dc-dc converters in [80], and then applied to the description of AC machines [81] [82], asymmetrical faults in power systems [83], subsynchronous phenomena [84], and FACTS devices such as the Unified Power Flow Controller (UPFC) [85], and the Thyristor Controlled Series Compensator [86]. Model based estimation of dynamic phasor is the subject of [87]. A power systems computer simulator based on dynamic phasor modelling is proposed in [88] [89], along with a discussion of computational efficiency of various approaches.

The definition of dynamic phasors is derived by recognizing that, according to Fourier theory, any square integrable function  $x(\tau)$  could be expanded as:

$$x(\tau) = \sum_{k=-\infty}^{\infty} X_k(t) e^{jk\omega_0\tau}, \quad \forall \tau \in (t-T, t] \quad (4.2)$$

where  $\omega_0 = \frac{2\pi}{T}$ . The complex Fourier coefficients  $X_k(t)$ , which will be referred to as *dynamic phasors*, are given by:

$$X_k(t) = \frac{1}{T} \int_{t-T}^t x(\tau) e^{-jk\omega_0\tau} d\tau =: \langle x \rangle_k(t) \quad (4.3)$$

The definition could be straightforwardly extended to three phase systems [83] [87]. By taking the derivative of (4.3) with respect to time and using integration

by parts, it results:

$$\frac{dX_k}{dt} = \frac{1}{T} \left[ x(\tau)e^{-jk\omega_0\tau} \right]_{t-T}^t = \int_{t-T}^t \frac{dx(\tau)}{d\tau} e^{-jk\omega_0\tau} d\tau - jk\omega_0 \int_{t-T}^t x(\tau)e^{-jk\omega_0\tau} d\tau \quad (4.4)$$

which yields the key property of the derivative of dynamic phasors:

$$\frac{dX_k}{dt}(t) = \left\langle \frac{dx}{d\tau} \right\rangle_k(t) - jk\omega_0 X_k(t) \quad (4.5)$$

Differently from power converters, in most cases of practical interests in power system analysis, only very few dynamic phasors are needed for a precise description of transient phenomena, since almost all state variables are (possibly time-varying) sinusoids. In the following, it will be considered the case in which only the first coefficient of (4.2) is sufficient for a precise description. In this context the definition of time-varying phasor is introduced as follows, as a straightforward extension of the well known classical phasor definition. Let  $e(t)$  be a generic sinusoidal signal with time varying amplitude and phase:

$$e(t) = E(t) \cos(\omega t + \delta(t)) \quad (4.6)$$

Its associated phasor is the complex quantity:

$$\bar{E}(t) = \mathcal{P}[e(t)] = E(t)e^{j\delta(t)} \quad (4.7)$$

obtained by applying the phasor operator  $\mathcal{P}$  to the signal  $e(t)$ . The operator  $\mathcal{P}$  is linear, thus linear relationships valid in time domain, such as Kirchhoff laws, also apply to phasor domain. Active and reactive powers are defined as usual:

$$P + jQ = \Re\{\mathcal{P}[e(t)]\mathcal{P}^*[i(t)]\} + j\Im\{\mathcal{P}[e(t)]\mathcal{P}^*[i(t)]\} \quad (4.8)$$

where  $e(t)$ ,  $i(t)$  are the voltage across a branch and the current flowing through it, respectively. Under the assumption that  $e_k(t)$  and  $i_k(t)$  are bandpass signals, it is proven in [73] that instantaneous power balance equations is valid also for time-varying phasors, that is:

$$\sum_{k=1}^n e_k(t)i_k(t) = 0 \iff \sum_{k=1}^n \bar{E}_k(t)\bar{I}_k(t)^* = 0 \quad (4.9)$$

This property is fundamental for using time-varying phasor in power system simulations since some network relationships are given in the form of power balance.

Consider now a current  $i(t) = I(t) \cos(\omega t + \delta(t))$  flowing through an inductance  $L$ . The voltage across the inductor is then:

$$\begin{aligned}
v_L(t) &= L \frac{di_L(t)}{dt} = L\dot{I}(t) \cos(\omega t + \delta(t)) - L(\omega + \dot{\delta}(t))I(t) \sin(\omega t + \delta(t)) \\
&= L\dot{I}(t) \cos(\omega t + \delta(t)) + L\dot{\delta}(t)I(t) \cos(\omega t + \delta(t) + \pi/2) \\
&+ L\omega I(t) \cos(\omega t + \delta(t) + \pi/2)
\end{aligned} \tag{4.10}$$

Its associated phasor is then:

$$\begin{aligned}
\overline{V}_L(t) = \mathcal{P}(v_L(t)) &= L\dot{I}(t)e^{j\delta(t)} + Lj\dot{\delta}(t)I(t)e^{j\delta(t)} + j\omega LI(t)e^{j\delta(t)} \\
&= L \frac{d}{dt} [I(t)e^{j\delta(t)}] + j\omega LI(t)e^{j\delta(t)}
\end{aligned} \tag{4.11}$$

thus, its evolution in time is described by the following differential equation:

$$\overline{V}_L(t) = L \frac{d}{dt} \overline{I}_L(t) + j\omega L \overline{I}_L(t) \tag{4.12}$$

Analogously, the current flowing through a capacitance  $C$  with an applied sinusoidal voltage, is:

$$\begin{aligned}
i_C(t) &= C \frac{dv_C(t)}{dt} \\
&= C\dot{V}_C(t) \cos(\omega t + \delta(t)) + CV_C(t)\dot{\delta}(t) \cos(\omega t + \delta(t) + \pi/2) \\
&+ \omega CV_C(t) \cos(\omega t + \delta(t) + \pi/2)
\end{aligned} \tag{4.13}$$

Its associated phasor is then described by:

$$\overline{I}_C(t) = C \frac{d}{dt} \overline{V}_C(t) + j\omega C \overline{V}_C(t) \tag{4.14}$$

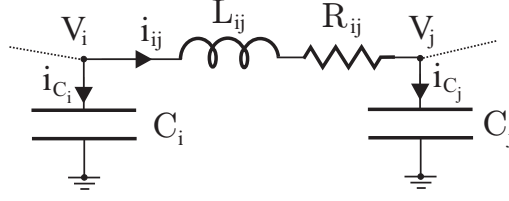
Both (4.12) and (4.14) can also be derived by direct application of property (4.5) to inductance and capacitance constitutive relationships with  $k = 1$ :

$$v_L(t) = L \frac{di(t)}{dt} \rightarrow \frac{dI_1}{dt}(t) = \left\langle \frac{1}{L} v_L \right\rangle_1(t) - j\omega I_1(t) \tag{4.15}$$

$$i_C(t) = C \frac{dv(t)}{dt} \rightarrow \frac{dV_1}{dt}(t) = \left\langle \frac{1}{C} i_C \right\rangle_1(t) - j\omega V_1(t) \tag{4.16}$$

Time-varying phasor are complex-valued function, thus being the sum of two orthogonal components, denoted in the following as real and imaginary part:  $\overline{E}(t) = E_{RE}(t) + jE_{IM}(t)$ .

Let consider now the 2-port  $\Pi$  circuit with lumped RLC in Fig. (4.1), which can be considered as an approximate equivalent of a transmission line. The validity of this approximation is discussed in [76].

Figure 4.1:  $\Pi$  circuit

Time evolution of voltage and current phasors described by eqs. (4.12) and (4.14), are rewritten here in p.u. and in state-space form, separating their real and imaginary parts:

$$\frac{1}{\omega} \begin{bmatrix} \dot{I}_{ijRE} \\ \dot{I}_{ijIM} \end{bmatrix} = \begin{bmatrix} -r_{ij}/l_{ij} & 1 \\ -1 & -r_{ij}/l_{ij} \end{bmatrix} \cdot \begin{bmatrix} I_{ijRE} \\ I_{ijIM} \end{bmatrix} + \begin{bmatrix} 1/l_{ij} & 0 \\ 0 & 1/l_{ij} \end{bmatrix} \cdot \begin{bmatrix} V_{iRE} - V_{jRE} \\ V_{iIM} - V_{jIM} \end{bmatrix} \quad (4.17)$$

$$\frac{1}{\omega} \begin{bmatrix} \dot{V}_{iRE} \\ \dot{V}_{iIM} \end{bmatrix} = \begin{bmatrix} 0 & 1 \\ -1 & 0 \end{bmatrix} \cdot \begin{bmatrix} V_{iRE} \\ V_{iIM} \end{bmatrix} + \begin{bmatrix} 1/c_i & 0 \\ 0 & 1/c_i \end{bmatrix} \cdot \begin{bmatrix} I_{CiRE} \\ I_{CiIM} \end{bmatrix} \quad (4.18)$$

where all values are expressed in per unit. Neglecting transients results in the traditional stationary model, which is readily derived from (4.17) and (4.18) by substituting their left-hand side with zeros, resulting in the following algebraic relationships:

$$\begin{bmatrix} i_{ijRE} \\ i_{ijIM} \end{bmatrix} = \frac{1}{r^2 + l^2} \begin{bmatrix} r & l \\ -l & r \end{bmatrix} \cdot \begin{bmatrix} v_{iRE} - v_{jRE} \\ v_{iIM} - v_{jIM} \end{bmatrix} \quad (4.19)$$

$$\begin{bmatrix} v_{iRE} \\ v_{iIM} \end{bmatrix} = \frac{1}{c} \begin{bmatrix} 0 & 1 \\ -1 & 0 \end{bmatrix} \cdot \begin{bmatrix} i_{CiRE} \\ i_{CiIM} \end{bmatrix} \quad (4.20)$$

Systems with different time-scale dynamics are known as singularly perturbed systems [11]-[29]. They are usually written in the form:

$$\begin{aligned} \dot{\mathbf{x}} &= \mathbf{f}(\mathbf{x}, \mathbf{y}, \varepsilon) \\ \varepsilon \dot{\mathbf{y}} &= \mathbf{g}(\mathbf{x}, \mathbf{y}, \varepsilon) \end{aligned} \quad (4.21)$$

where  $\varepsilon$  is a small parameter. The coefficient  $1/\omega$  in (4.17)-(4.18) plays the role of  $\varepsilon$  in (4.21). Setting  $\varepsilon = 0$  results in the DAE formulation:

$$\begin{aligned}\dot{\mathbf{x}}_s &= \mathbf{f}(\mathbf{x}_s, \mathbf{y}_s) \\ \mathbf{0} &= \mathbf{g}(\mathbf{x}_s, \mathbf{y}_s)\end{aligned}\tag{4.22}$$

where  $\mathbf{x}_s$  and  $\mathbf{y}_s$  are the approximation of  $\mathbf{x}$  and  $\mathbf{y}$ , respectively.  $\mathbf{y}_s$  is often referred to as the slow manifold. Under some regularity and stability assumptions, Tikhonov theorem establishes that the error  $\mathbf{x} - \mathbf{x}_s$  is in the order of  $\varepsilon$ , i.e. it vanishes as a linear function of  $\varepsilon$  as  $\varepsilon \rightarrow 0$ .

DAE modeling of power system implies that network variables (voltages and currents) evolve along the slow manifold as a function of the slow variables (machines rotor angles). The separation of states into slow and fast subsystems could in principle be effected employing the knowledge of the physical meaning of system's dynamics. However, when several variables evolve on different time-scales, the interaction could not be negligible and time-scale separation could be questionable. Following [90] a linear system:

$$\begin{bmatrix} \dot{\mathbf{x}} \\ \varepsilon \dot{\mathbf{y}} \end{bmatrix} = \begin{bmatrix} \mathbf{A} & \mathbf{B} \\ \mathbf{C} & \mathbf{D} \end{bmatrix} \begin{bmatrix} \mathbf{x} \\ \mathbf{y} \end{bmatrix}\tag{4.23}$$

has a two-time-scale dynamics if it can be put in the form \*

$$\begin{bmatrix} \dot{\mathbf{x}} \\ \eta \end{bmatrix} = \begin{bmatrix} \mathbf{F}_1 & \mathbf{B} \\ \mathbf{0} & \mathbf{F}_2 \end{bmatrix} \begin{bmatrix} \mathbf{x} \\ \eta \end{bmatrix}\tag{4.24}$$

where the greatest eigenvalue of  $\mathbf{F}_1$  is less then the minimum eigenvalue of  $\mathbf{F}_2$ , i.e.:

$$\rho_{slow} = \max_i |\lambda_i(\mathbf{F}_1)| < \min_j |\lambda_j(\mathbf{F}_2)| = \rho_{fast}\tag{4.25}$$

A measure of time-scale separation should therefore be related to the ratio  $\rho_{fast}/\rho_{slow}$ . Analogous considerations hold for nonlinear systems, employing Jacobian matrix in (4.23).

---

\*The transformation from (4.23) to (4.24) can be obtained by the linear mapping

$$\eta = \mathbf{y} + \mathbf{L}\mathbf{x}$$

with  $\mathbf{F}_1, \mathbf{F}_2$  such that:

$$\begin{aligned}\mathbf{F}_1 &= \mathbf{A} - \mathbf{B}\mathbf{L} \\ \mathbf{F}_2 &= \mathbf{D} + \mathbf{B}\mathbf{L}\end{aligned}$$

and  $\mathbf{L}$  solution of the non-symmetric Riccati equation  $\mathbf{0} = \mathbf{D}\mathbf{L} - \mathbf{L}\mathbf{A} + \mathbf{L}\mathbf{B}\mathbf{L} - \mathbf{C}$ [91]

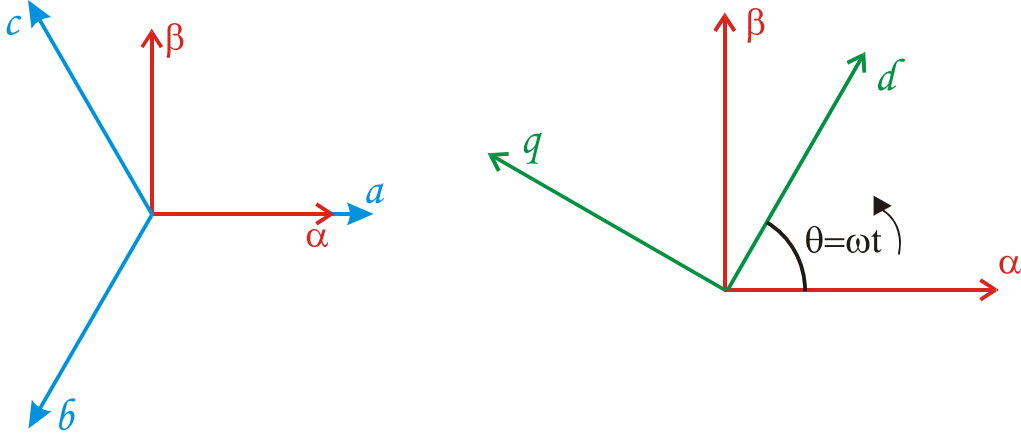


Figure 4.2: Three-phase abc to rectangular transformation

### 4.3 Three-phase to rectangular reference transformation

The two rectangular components of the time-varying phasors of network quantities identified as  $Re$  and  $Im$  can in principle be derived and practically extracted from a set of balanced three-phase signals by means of the classical  $abc/dq$  transformation which is easily derived from Fig. 4.2. The transformation comprises two steps, the first of which entails projecting the balanced three-phase signals onto the so-called  $\alpha - \beta$  fixed rectangular reference system:

$$\begin{bmatrix} \alpha \\ \beta \\ 0 \end{bmatrix} = \begin{bmatrix} 1 & \cos \frac{-2\pi}{3} & \cos \frac{2\pi}{3} \\ 0 & \sin \frac{-2\pi}{3} & \sin \frac{2\pi}{3} \\ 1/3 & 1/3 & 1/3 \end{bmatrix} \cdot \begin{bmatrix} a \\ b \\ c \end{bmatrix} \quad (4.26)$$

Due to the balanced nature of the original three-phase system, the 0 component is always zero, therefore the three signals  $a(t), b(t), c(t)$  can be retrieved from the two signals  $\alpha(t), \beta(t)$ . The fixed rectangular reference frame can then be projected onto a synchronously rotating reference frame usually called  $dq$  reference as follows:

$$\begin{bmatrix} d \\ q \end{bmatrix} = \begin{bmatrix} \cos \omega t & \sin \omega t \\ -\sin \omega t & \cos \omega t \end{bmatrix} \cdot \begin{bmatrix} \alpha \\ \beta \end{bmatrix} \quad (4.27)$$

$Re$  and  $Im$  components of voltages and currents can then be identified with  $dq$  components of the corresponding three-phase quantities.

Transformation from three-phase to rotating rectangular reference also allows to simulate detailed three-phase models of components such as loads or converters



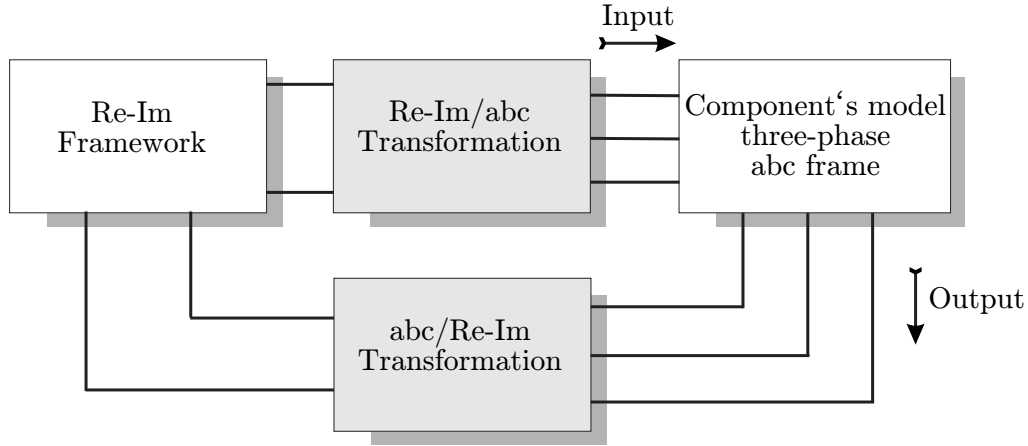


Figure 4.3: Framework for Re-Im/abc coupled simulations: the component is modelled in three-phase abc frame

in transient stability simulations which employ a phasor modelling of the remaining part of the power system, as reported in previous sections. Figure 4.3 shows a framework for coupled three-phase reference/rectangular reference simulations which will be used in a later chapter to simulate the detailed internal behaviour of an inverter for FACTS applications, embedded in a transient stability simulation.

The opposite situation, i.e. embedding models of components in rectangular reference into three-phase simulations, is equally possible, as depicted in Fig. 4.4.

The nature of the input and the output quantities into and from the component, as depicted in Figs. 4.3,4.4 depends on the connection of the component. For a series connected component the input is the current that enters one of its terminal and the output is the injected voltage. The opposite applies to shunt connected components, where the input is the voltage at the point of common coupling and the output is the current it injects into the network.

## 4.4 Comparison of transmission line modellings

By means of the framework introduced in the previous section and reported in Fig. 4.4, both the dynamic modelling in Eqs. (4.17)-(4.18) and the algebraic model in Eqs. (4.19)-(4.20) for transmission lines in rectangular reference frame are compared with a detailed three-phase model in order to check their accuracy. A simple system with a three-phase generator, a 300 km transmission line

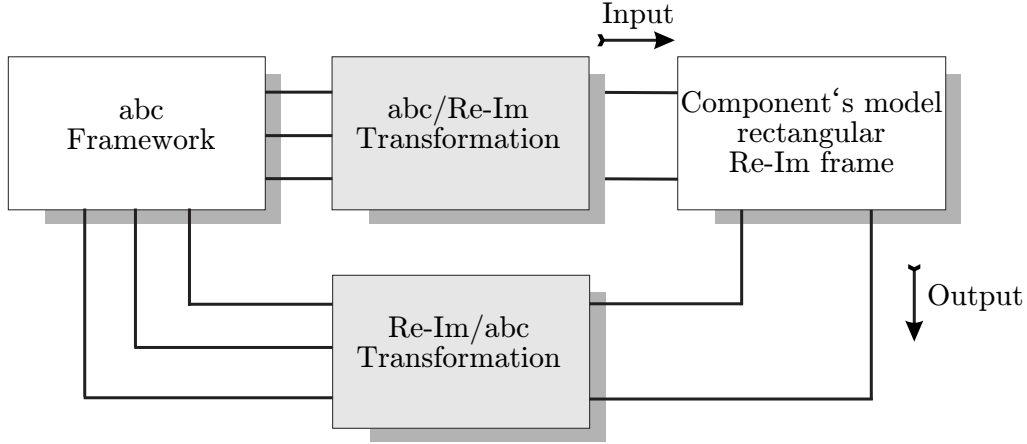


Figure 4.4: Framework for Re-Im/abc coupled simulations: the component is modelled in rectangular Re-Im framework

and a linear  $RL$  load is considered \*. In the detailed three-phase simulation the transmission line is modelled according to the Bergeron's travelling wave model which simulate a distributed parameter line (DPL) [92, 93, 94]. In sinusoidal steady-state no noticeable difference is obtained among the three different models of the transmission line. In order to check the accuracy of each model in transient situations a modulation has been applied first to the magnitude and then to the phase of the generator. Figure 4.5 shows the results of the simulation of the system when a 10 Hz modulation of 0.5  $p.u.$  is applied to generator's voltage magnitude. Phase a load current is depicted for the three different models. Dynamic model (4.17)-(4.18) gives very accurate results shown in Fig. 4.5(a),(c), while algebraic model (4.19)-(4.20) gives a difference with the most accurate DPL model nearly four times bigger as demonstrated by Fig. 4.5(b),(d). Analogous conclusions can be obtained when a 10 Hz modulation of 45 degrees is applied to generator's voltage angle, as reported in Fig. 4.6. While dynamic model always provides very accurate results compared with the most detailed DPL model, algebraic model gives a difference that grows even bigger when longer transmission lines are considered and/or higher frequency variations of voltages or currents are applied.

---

\* $r_{line}=0.0127 \Omega/Km$ ,  $l_{line}=0.934 \cdot 10^{-3} H/Km$ ,  $c_{line}=12.7 \cdot 10^{-9} F/Km$

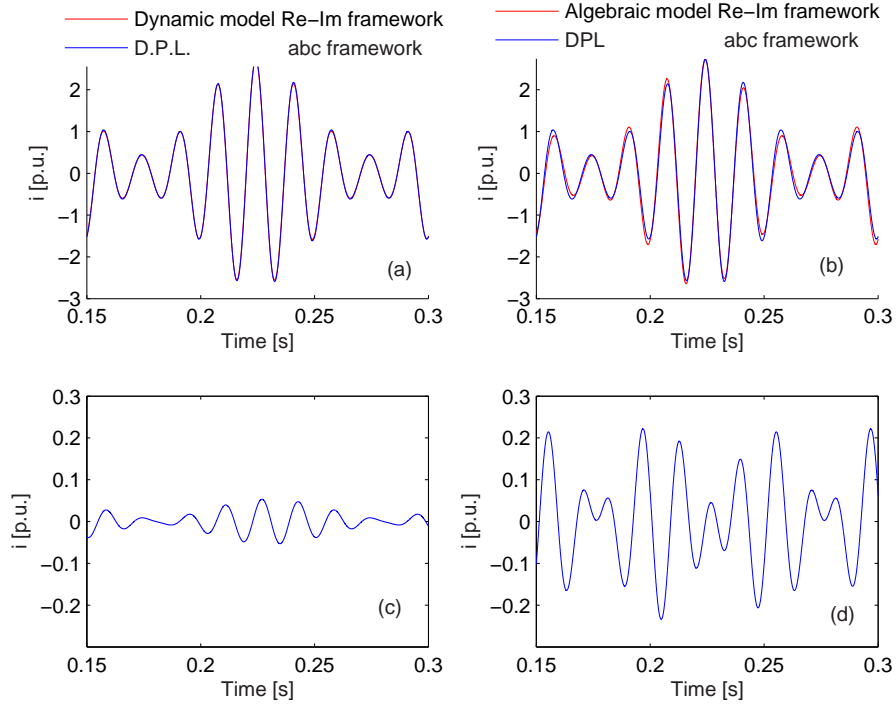


Figure 4.5: Transmission line models comparison:  $0.5p.u.$ , 10 Hz modulation of generator's voltage magnitude. (a): phase  $a$  load current  $i_{DPL}$  with Bergeron's model (blue) and Dynamic model  $i_{Dynamic}$  (red) 4.17-4.18 of the transmission line; (b): phase  $a$  load current with Bergeron's model  $i_{DPL}$  (blue) and Algebraic model  $i_{Algebraic}$  (red) 4.19-4.20 of the transmission line; (c):  $i_{DPL} - i_{Dynamic}$ ; (d):  $i_{DPL} - i_{Algebraic}$

## 4.5 Numerical results

In the present section the slow and fast transients for a simplified SMIB power system are identified, then a comprehensive analysis is carried out with respect to a 4-machine 11-bus test system, with detailed models of machines internal dynamics.

### 4.5.1 SMIB test system

Let consider the SMIB system in Fig. (4.7). The classical second order swing equations are:

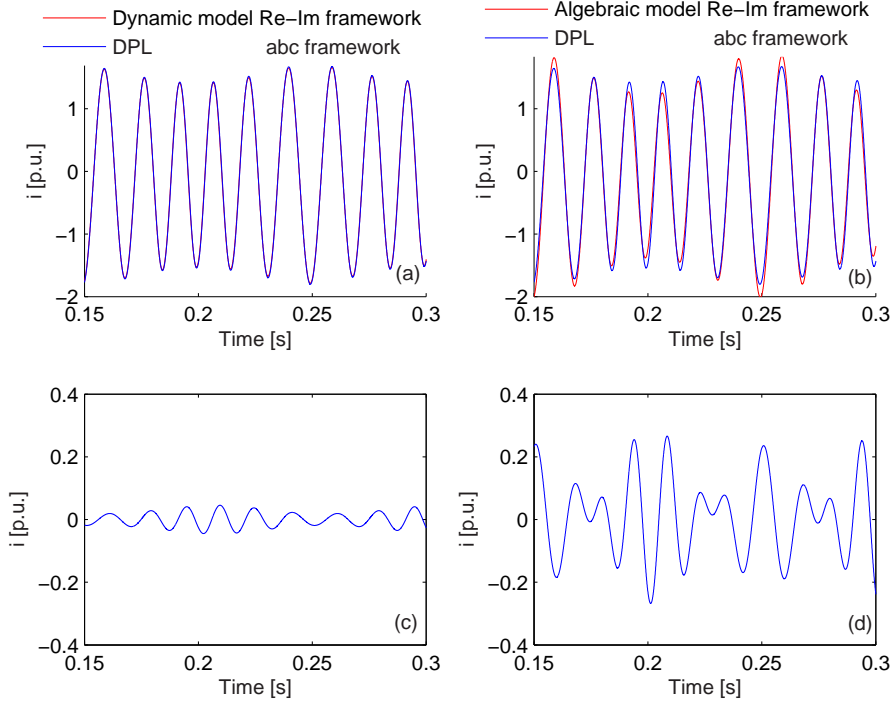


Figure 4.6: Transmission line models comparison: 45 degrees, 10 Hz modulation of generator's voltage phase. (a): phase *a* load current  $i_{DPL}$  with Bergeron's model (blue) and Dynamic model  $i_{Dynamic}$  (red) 4.17-4.18 of the transmission line; (b): phase *a* load current with Bergeron's model  $i_{DPL}$  (blue) and Algebraic model  $i_{Algebraic}$  (red) 4.19-4.20 of the transmission line; (c):  $i_{DPL} - i_{Dynamic}$ ; (d):  $i_{DPL} - i_{Algebraic}$

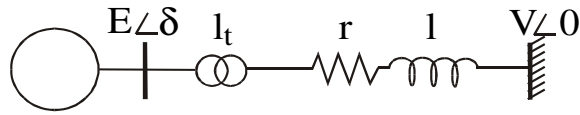


Figure 4.7: SMIB power system

$$\begin{aligned} \dot{\delta} &= \Delta\omega \\ \Delta\dot{\omega} &= \frac{1}{M} [P_m - P_e - D\Delta\omega] \end{aligned} \quad (4.28)$$

where all parameters and variables are defined as usual. The electrical power is given by:

$$P_e = \Re\{\bar{E} \cdot \bar{I}^*\} = EI_{RE} \cos \delta + EI_{IM} \sin \delta \quad (4.29)$$

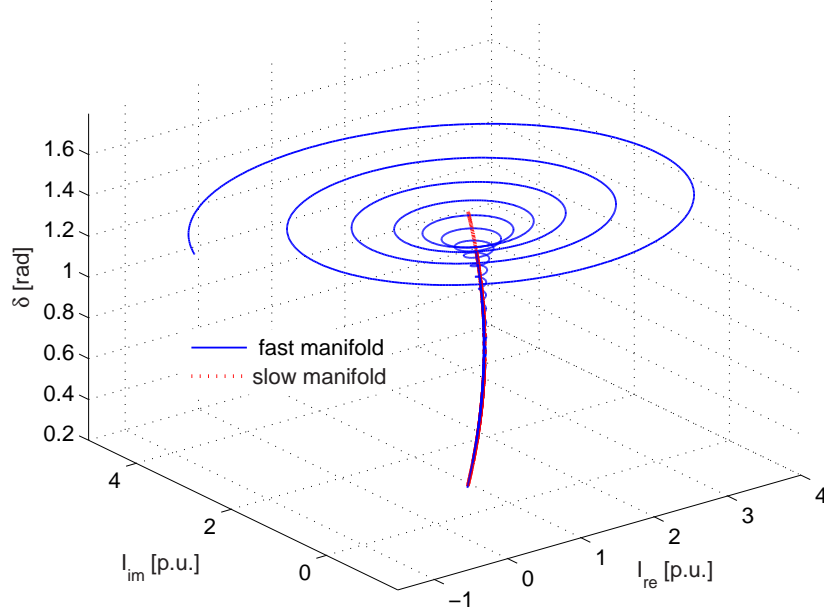


Figure 4.8: Projection on  $\delta - I_{RE} - I_{IM}$  axes of the phase portrait of SMIB system

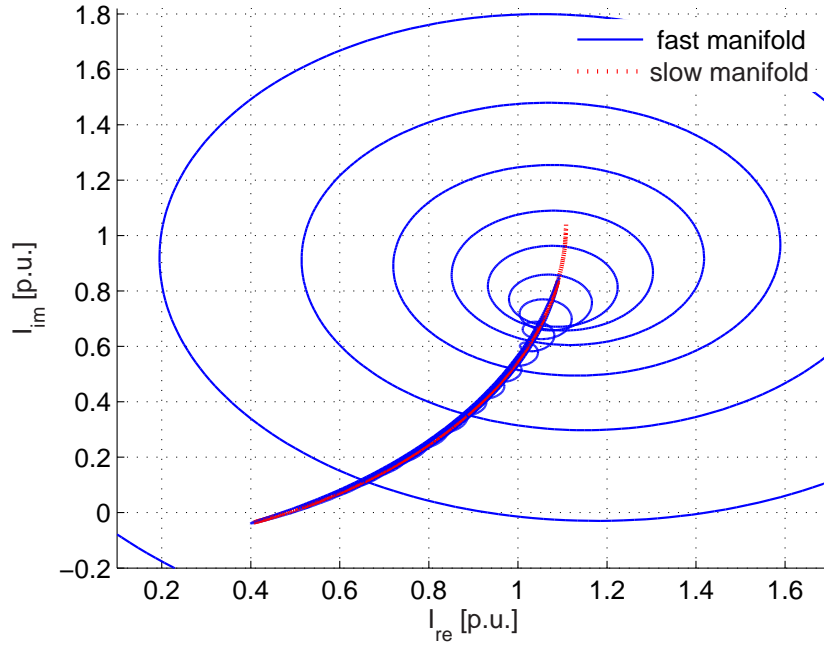
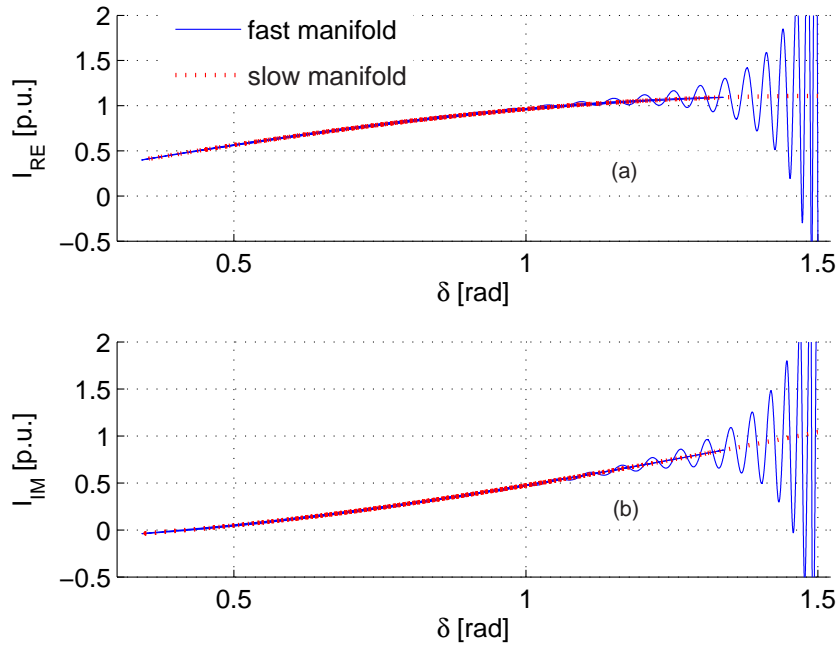
The two current component are given by:

$$\frac{1}{\omega} \begin{bmatrix} \dot{I}_{RE} \\ \dot{I}_{IM} \end{bmatrix} = \begin{bmatrix} -r/l & 1 \\ -1 & -r/l \end{bmatrix} \cdot \begin{bmatrix} I_{RE} \\ I_{IM} \end{bmatrix} + \begin{bmatrix} 1/l & 0 \\ 0 & 1/l \end{bmatrix} \cdot \begin{bmatrix} E \cos \delta - V \\ E \sin \delta \end{bmatrix} \quad (4.30)$$

The slow manifold can be obtained by setting the LHS of (4.30) to zero, and solving for the currents as functions of the slow variable  $\delta$ :

$$\begin{bmatrix} I_{RE} \\ I_{IM} \end{bmatrix} = \frac{1}{r^2 + l^2} \begin{bmatrix} r & l \\ -l & r \end{bmatrix} \cdot \begin{bmatrix} E \cos \delta - V \\ E \sin \delta \end{bmatrix} \quad (4.31)$$

Figs. (4.8-4.11) report results of simulation of a sample SMIB test system whose parameters are reported in Appendix. It is clearly visible from figs. (4.8-4.11) how fast variables evolve in a neighborhood of the slow manifold once the fast transients decay. Applying the procedure (4.23-4.25) to the linearised version of (4.28-4.30) about the equilibrium point results in  $\rho_{fast} = 377.7$ ,  $\rho_{slow} = 6.77$ . Dynamics of currents are therefore about 55 times faster than angle dynamics. Their transients can thus be neglected without significant loss of accuracy in the evaluation of angle behaviour.

Figure 4.9: Projection on  $I_{RE} - I_{IM}$  axes of the phase portrait of SMIB systemFigure 4.10: Projection on (a):  $\delta - I_{RE}$ , (b):  $\delta - I_{IM}$  axes of the phase portrait of SMIB system

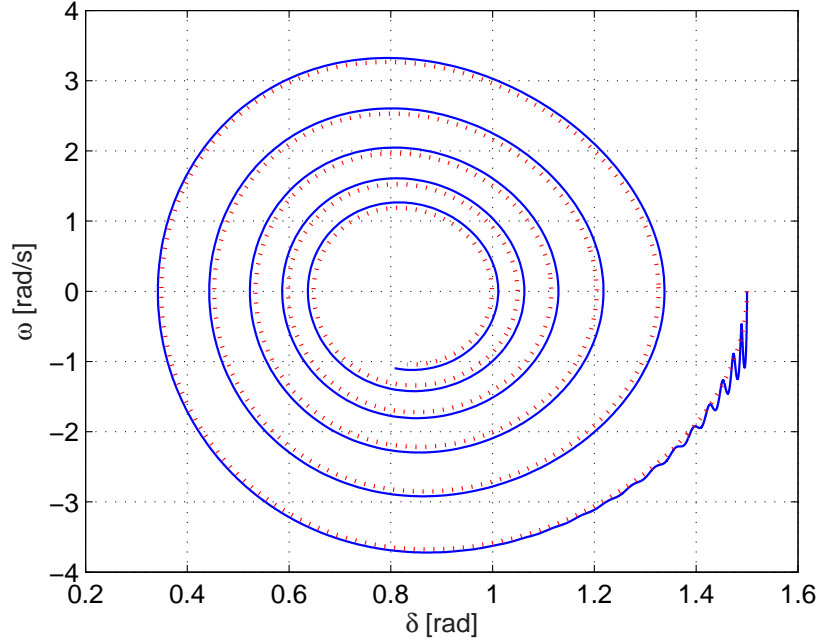


Figure 4.11: Projection on  $\delta - \omega$  axes of the phase portrait of SMIB system

#### 4.5.2 4-machine test system

Simulations for the four-machine two-area test system in Fig. (A.1) are reported. For each generator the two-axis subtransient model is used, according to the equations (2.6)-(2.9)

Each generator is equipped with a high gain thyristor exciter, a power system stabilizer and a governor-turbine system, whose block diagrams are reported in 2. Parameters used in simulations are given in Appendix A. Each transformer and transmission line is modelled with the  $\Pi$ -equivalent circuit as detailed in the previous sections. Loads are modelled with constant impedance for the reactive component of power and constant current for the active component. Load models are known to have a significant impact on power system stability evaluation [95]. Several load models have been proposed in the past, ranging from static (e.g. the so called ZIP model) to dynamic [79][46]. Other load modelling have also been considered and although different results have been obtained with respect to transient responses, similar conclusions are drawn regarding the differences in system's behaviour when fast network dynamics are modelled or not. Loads are slightly different from those given in [15] in order to simulate a more stressed

system, characterised by a lower damping in the interarea mode: in particular load 7 is lowered by 3% while load 9 is increased by 3%. In Figs. (4.12)-(4.15) results of simulations are reported. Oscillations are triggered by a three-phase fault at bus 8 cleared after 0.12s. Rotor angle and velocities of machines, as well as power flow on tie lines 7 – 8 and voltage at node 8 are shown, both for the case where line dynamics are modelled according (4.17)-(4.18), referred to as dynamic model, and for the case where line dynamics are neglected according to (4.19)-(4.20), this latter case being referred to as algebraic model. Differently damped oscillations are clearly identifiable in transient response. Linearization of state equations about the stable equilibrium point has been performed. Eigenvalues are shown in Fig. (4.16), again comparing the dynamic model with the algebraic one. The inclusion of faster network dynamics, not only adds faster oscillatory modes, but also contributes to a slight variation of slower electromechanical ones. Local and interarea modes, identified with selective modal analysis and participation factors [96], are reported in Tab. (4.1). In stressed systems with lightly damped oscillations this differences could result in non negligible variations in nonlinear simulations results. In well damped systems smaller differences have been found. When all machines and their controls are modelled, time-scale separation could not be strong. In the present case it results  $\rho_{slow} = 97.67$ ,  $\rho_{fast} = 377.67$ , meaning that internal generators' control dynamics are not much slower than network's ones. Differences are also found in critical clearing time  $t_{cr}$  evaluation, resulting in  $t_{cr} = 0.124s$  for the dynamic model, and  $t_{cr} = 0.135s$  for the algebraic model.

The final model results in a system of 110 differential equations. This system is clearly stiff. Efficient algorithms are available for solving this kind of problem such as those which combine implicit forward and backward differentiation that are also available in MATLAB [97].

## 4.6 Subsynchronous oscillations phenomena

This section aims at showing the necessity to include a more detailed description of network's dynamics in order to evaluate how they could negatively interact with torsional modes of generation units. Figure 4.17 depicts the second IEEE benchmark model for subsynchronous resonance [31]. The dynamics of the mechanical subsystem is described by the interaction of four rotating masses as described in a previous chapter and illustrated in Fig. (4.18).



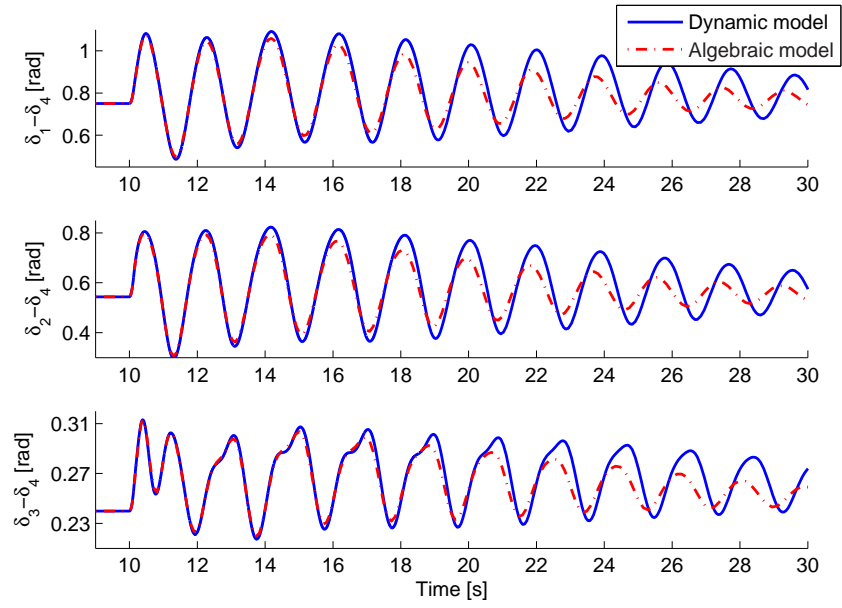


Figure 4.12: Angle oscillations of machines 1 ÷ 3 versus machine 4

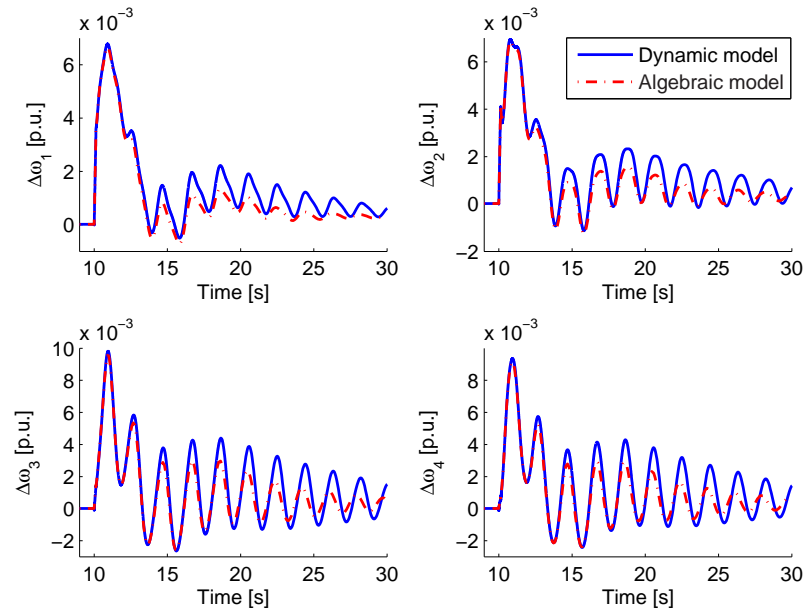


Figure 4.13: Speed deviation of generators

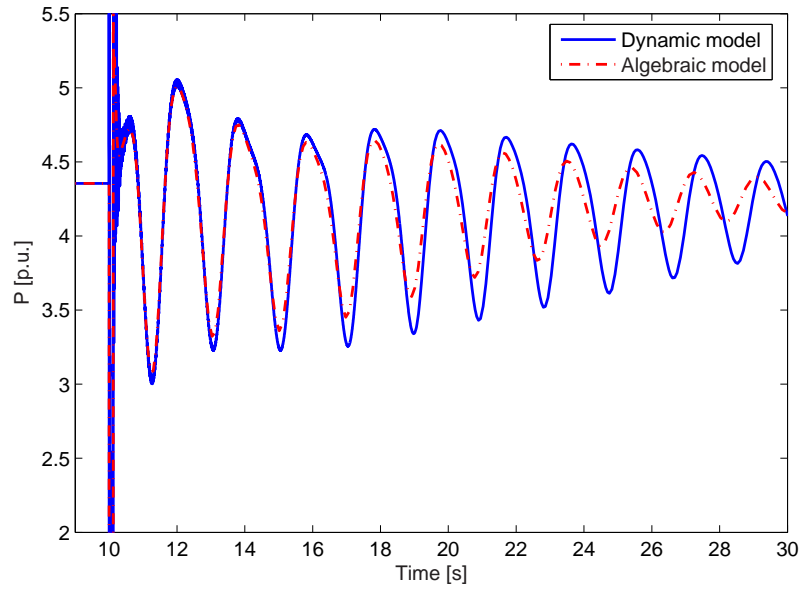


Figure 4.14: Active power flow on tie lines 7 – 8

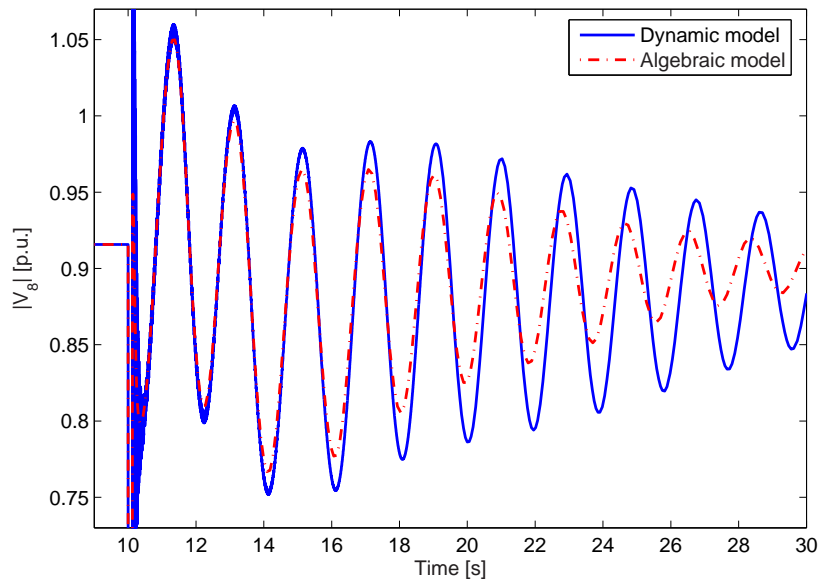


Figure 4.15: Voltage at bus 8

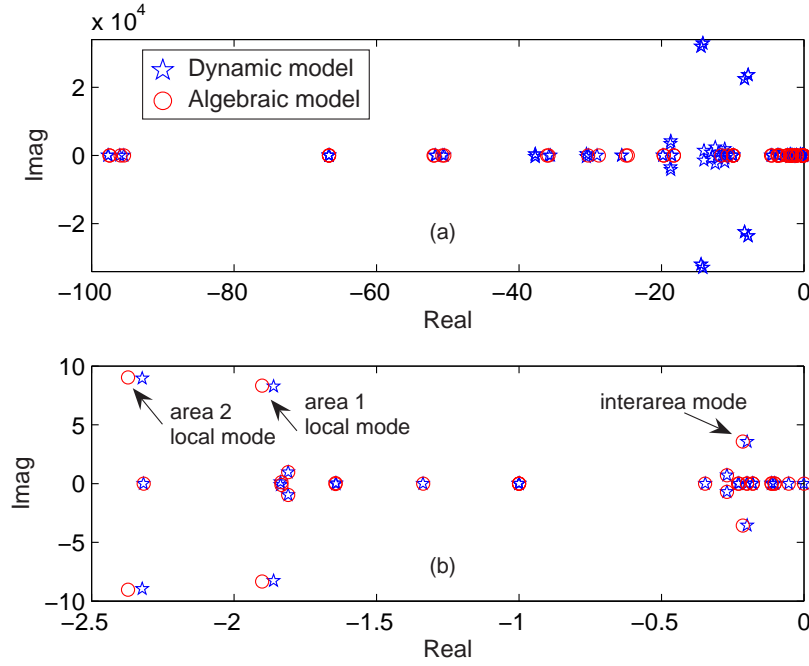


Figure 4.16: (a): Eigenvalues of the linearised system about the stable equilibrium point. (b): A zoomed area of the eigenvalues with modulus less than 10

Mode	Algebraic model	Dynamic model
area 1 (G1-G2)	$-1.901 \pm 8.335j$	$-1.861 \pm 8.268j$
area 2 (G3-G4)	$-2.372 \pm 9.030j$	$-2.321 \pm 8.946j$
interarea	$-0.215 \pm 3.569j$	$-0.199 \pm 3.560j$

Table 4.1: Local and interarea modes

The capacitive compensation of line 1 in the original *2nd* benchmark model is substituted by a FACTS series compensator, namely an SSSC, which is usually thought as being immune to resonance phenomena [56]. A simple PI controller shown in Fig. 4.19 is used to regulate power flow over line 1, by modulating SSSC equivalent capacitive reactance  $x_{eq-SSSC}$ .

It has been recently demonstrated that, subsynchronous oscillations can take place in systems with FACTS devices, despite the physical absence of series capacitors, as parameters of controllers are varied [98]. It has also been shown that constant power control of thyristor-controlled series capacitor can result in undamped subsynchronous oscillations [99]. Several occurrences of unstable sub-

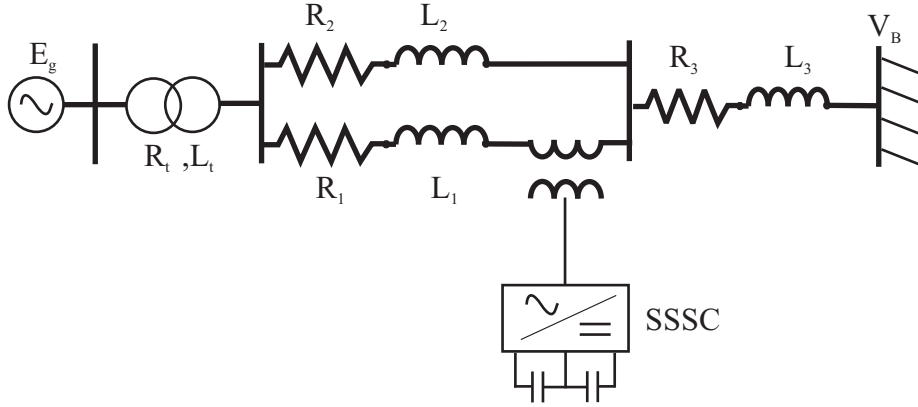


Figure 4.17: IEEE second benchmark model for subsynchronous resonance with a SSSC

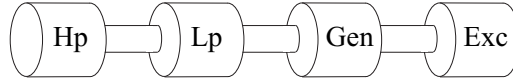


Figure 4.18: Four masses mechanical subsystem

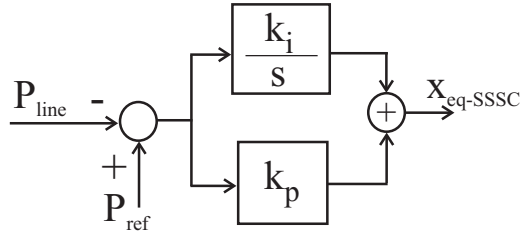


Figure 4.19: Equivalent SSSC reactance PI power flow controller

synchronous oscillations determined by poorly designed HVDC controllers were also reported in literature [15]. One widely cited case was the destabilisation of the first torsional mode of a generating station near the Square Butte HVDC link in North Dakota, due to the interaction between the torsional mode and the HVDC supplementary damping controller.

For the system in Fig. 4.17 a modal analysis has been carried out, using both the algebraic modeling of the transmission lines (4.19)-(4.20), and the differential one (4.17)-(4.18). Figure 4.20 and 4.21 show the eigenvalues and some of their associated modes for the algebraic and the differential model, respectively, with  $K_i = 0.05$  and  $K_p = K_i/30$ . Network's dynamics produce eigenvalues absent in the algebraic model of Fig. 4.20 which could adversely interact with

torsional dynamics. The eigenvalue locus for the algebraic model as controller gain is increased from  $K_i = 0.05$  to  $K_i = 20$ , with  $K_p = K_i/30$ , is reported in Fig. 4.22. A better damping of electromechanical oscillation is to be expected as a result of controller's gain increase and therefore of its velocity in regulation. However, due to unmodelled network's dynamics, eigenvalues associated with torsional modes do not vary as controller's parameters change. Using differential models of transmission lines allows to catch torsional mode instability as controller's gain increase. Indeed, fig. 4.23 and the zoomed region in fig. 4.24 show how the first torsional mode crosses the imaginary axis going into the positive-real half-plane, as  $K_i > 5$ . Results of time domain simulations are reported in fig. 4.25, which shows active power flow on line 1 for different values of  $K_i$ , and fig. 4.26 which shows the mechanical torque between  $HP - LP$  and  $LP - GEN$  masses at the onset of subsynchronous instability. Oscillations are initiated by a three-phase fault at busbar 2, self-cleared after  $0.07s$ . As it is to be expected from linearized analysis, the higher the gain of the controller and hence of its velocity, the higher the damping of electromechanical oscillations. However, controller's gain greater than approximately 5 determines a destabilizing interaction between line dynamics and the first torsional mode, which does not occur with algebraic modelling.

## 4.7 Conclusion

In the chapter, after relevant definitions and properties of time-varying phasors are summarised, the application of these concepts to power system's dynamic simulations is presented, firstly with respect to a simple SMIB system, then to a multimachine one, and finally to a benchmark model for subsynchronous oscillations study. Results of nonlinear simulations as well as linearised analysis are presented, showing the influence of network's dynamics in transient stability assessment. Efficient algorithms are available for solving the resulting stiff differential equations, thus providing tools for simulation without excessive computational burden.

The proposed network modelling will be used in the next chapter to introduce a novel extended Lyapunov function and derive, by means of the concept of control Lyapunov function, stabilising control laws for FACTS devices.

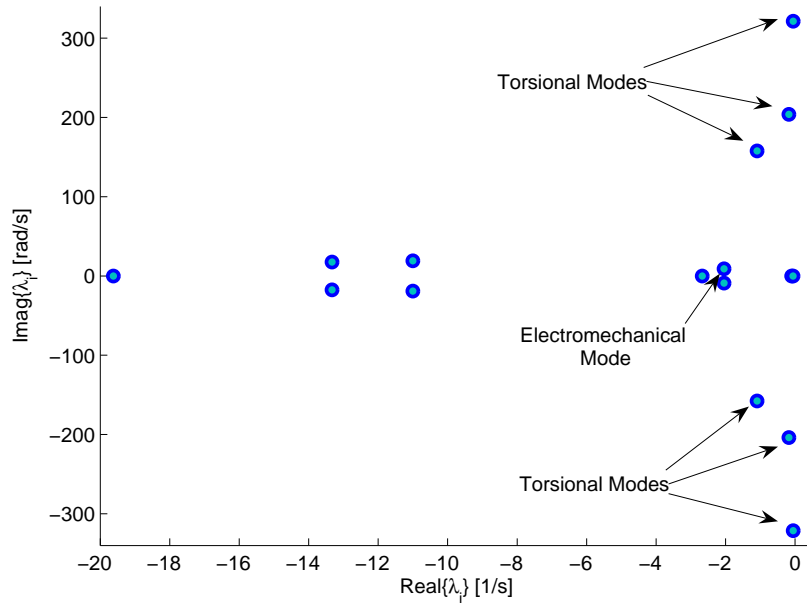


Figure 4.20: Eigenvalues of system with algebraic model.  $K = 0.05$

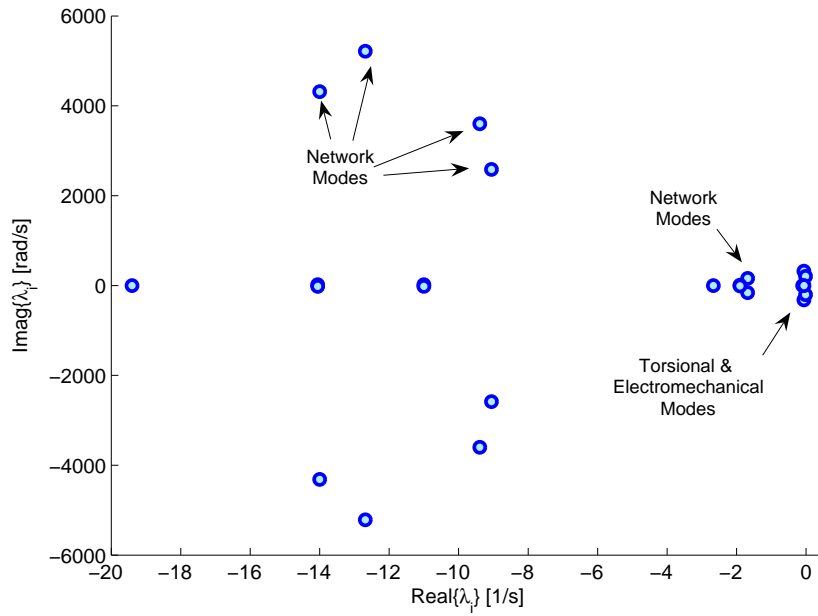
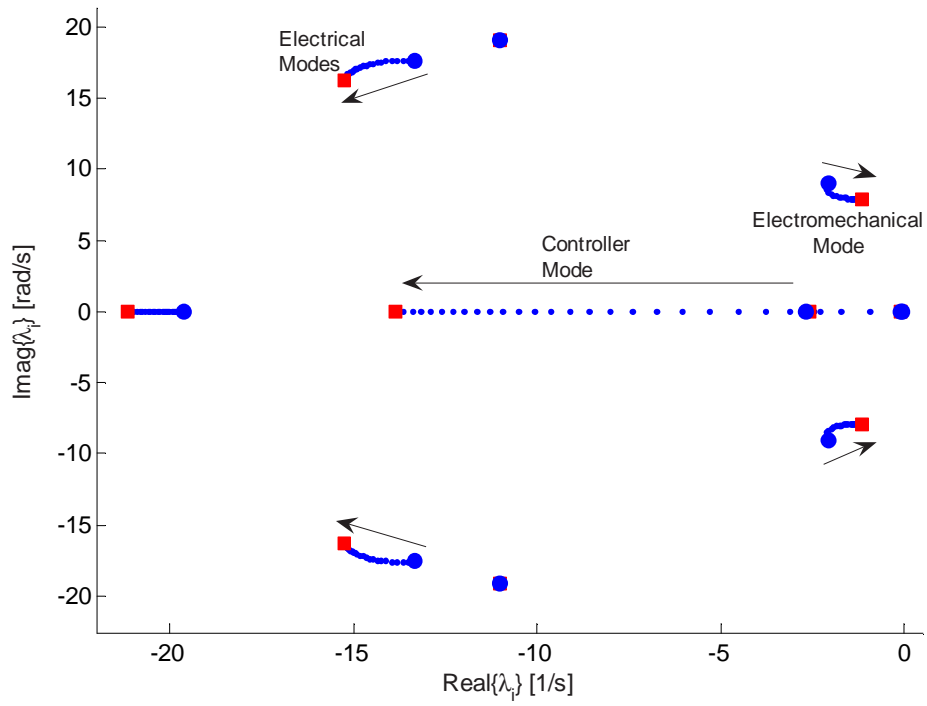
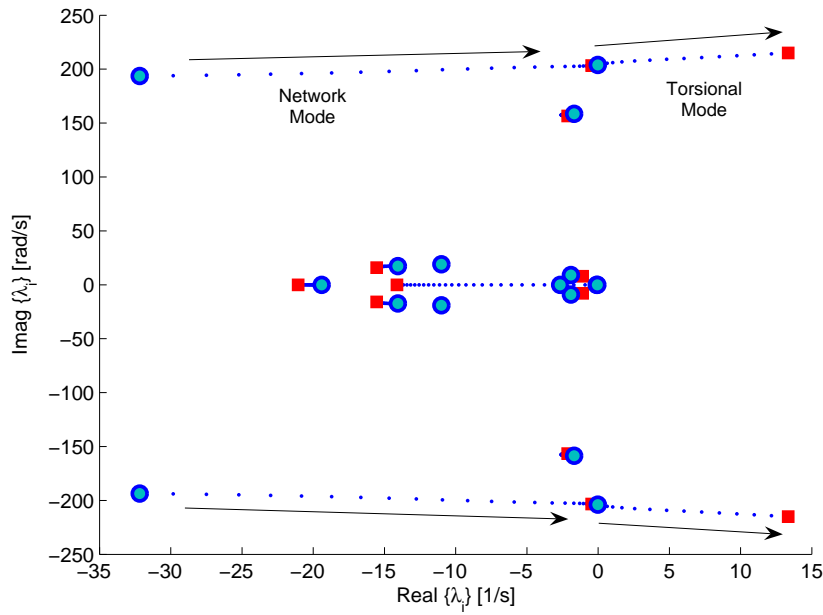


Figure 4.21: Eigenvalues of system with algebraic model.  $K = 0.05$

Figure 4.22: Eigenvalues of system with algebraic model.  $K = 0.05 \div 20$ Figure 4.23: Eigenvalues of system with dynamic model.  $K = 0.05 \div 20$

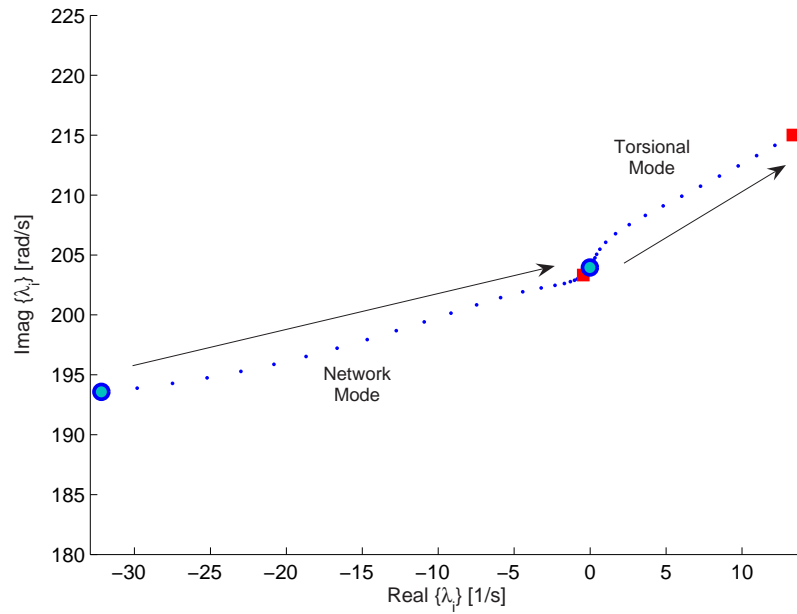
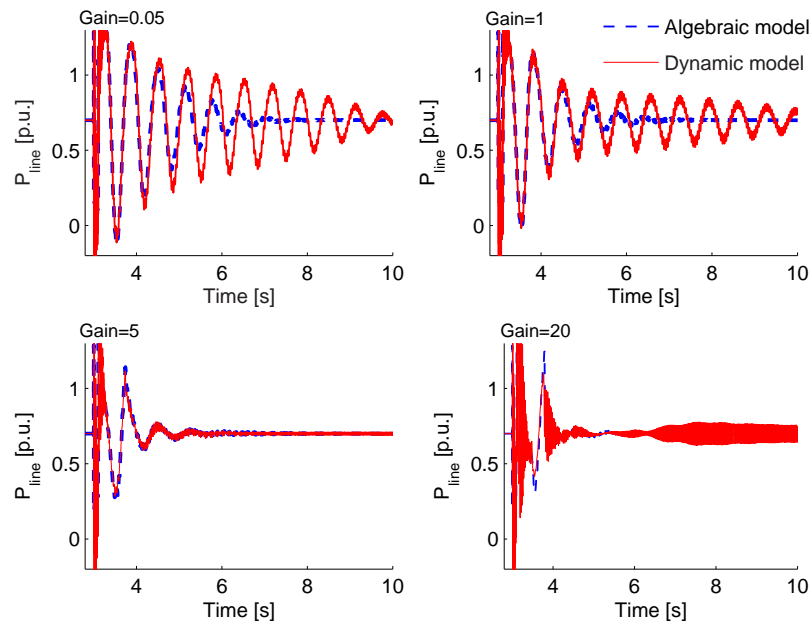
Figure 4.24: Eigenvalues of system with dynamic model.  $K = 0.05 \div 20$ 

Figure 4.25: Active power flow



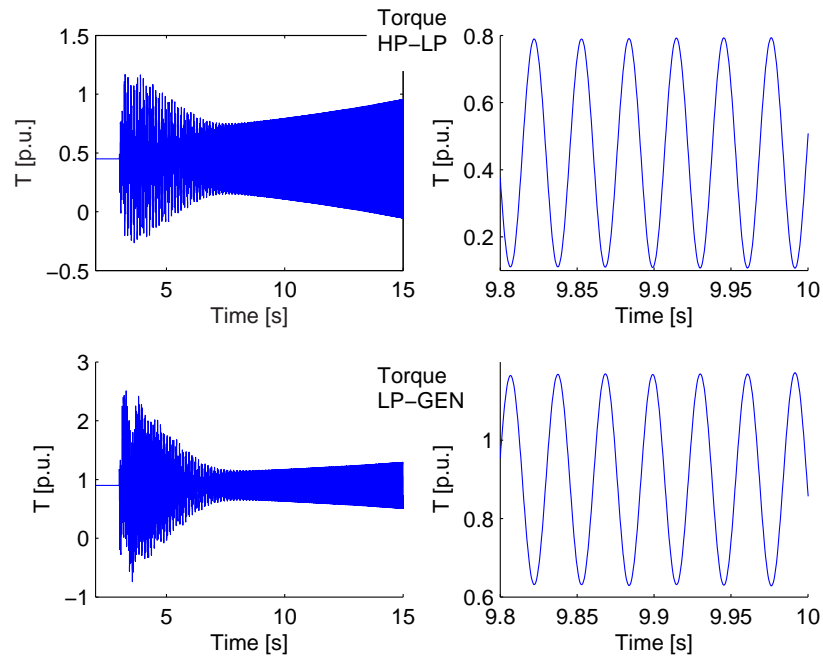


Figure 4.26: Torque between HP-LP (top panel) and LP-GEN (bottom panel) shaft sections. On the right an expanded region is reported to better show oscillations in the subsynchronous range



## Chapter 5

---

# Lyapunov's theory for stability and control

---

### Summary

*In the chapter the direct method of Lyapunov is introduced. It relates stability of a dynamical system with the value of a scalar function, which, roughly speaking, measures some energetic content of the system. A Lyapunov function commonly employed for power system analysis is reviewed. The presence of transfer conductances in load flow equations poses a limit on the possibility to derive true Lyapunov functions for power systems. Extended invariance principle have been proposed to circumvent this problem. A new Extended Lyapunov function which takes the network modelling presented in previous chapter into account, is proposed. Lyapunov function are also used to derive control actions to provide wider stability margins. A control law for series and shunt compensators based upon the proposed Extended Lyapunov function is given. An adaptive equilibrium point estimation technique, needed for practical application of the proposed control strategy, is also presented.*

### 5.1 Lyapunov's direct method

The idea of relating stability of a dynamical system to the associated energy is an old one, dating back to the early work of Torricelli, Laplace and Lagrange.

A. M. Lyapunov proposed the first mathematical formalisation of this approach [14].

The Lyapunov's theorem is stated in the following, with respect to the equilibrium point  $\mathbf{x} = \mathbf{0}$  for the nonlinear system  $\dot{\mathbf{x}} = \mathbf{f}(\mathbf{x})$ . A straightforward change of coordinates is necessary if the actual equilibrium point of the system under investigation is different from the origin. The following definitions are given beforehand.

**Locally positive semi-definite function:** A scalar function  $\mathcal{V}(\mathbf{x})$  is said to be *locally positive semi-definite* in a domain  $\mathcal{D} \subseteq \mathbb{R}^n$  containing the origin  $\mathbf{x} = \mathbf{0}$ , if:

$$\mathcal{V}(\mathbf{0}) = 0 \quad (5.1)$$

$$\mathcal{V}(\mathbf{x}) \geq 0 \quad \forall \mathbf{x} \in \mathcal{D} \quad (5.2)$$

If  $\mathcal{D} = \mathbb{R}^n$  than  $\mathcal{V}(\mathbf{x})$  is said to be *globally positive semi-definite*.

**Locally positive definite function:** A scalar function  $\mathcal{V}(\mathbf{x})$  is said to be *locally positive definite* in a domain  $\mathcal{D} \subseteq \mathbb{R}^n$  containing the origin  $\mathbf{x} = \mathbf{0}$ , if:

$$\mathcal{V}(\mathbf{0}) = 0 \quad (5.3)$$

$$\mathcal{V}(\mathbf{x}) > 0 \quad \forall \mathbf{x} \in \mathcal{D} \quad (5.4)$$

If  $\mathcal{D} = \mathbb{R}^n$  than  $\mathcal{V}(\mathbf{x})$  is said to be *globally positive definite*.

**Locally negative (semi-)definite function:** A scalar function  $\mathcal{V}(\mathbf{x})$  is said to be *locally negative (semi-)definite* in a domain  $\mathcal{D} \subseteq \mathbb{R}^n$  containing the origin  $\mathbf{x} = \mathbf{0}$ , if  $-\mathcal{V}(\mathbf{x})$  is locally positive (semi-)definite.

For a given dynamical system  $\dot{\mathbf{x}} = \mathbf{f}(\mathbf{x})$  the following theorem is the basis for stability analysis via energy functions [13, 12].

**Lyapunov theorem for local stability** If there exists a scalar function  $\mathcal{V}(\mathbf{x})$  with continuous first partial derivatives such that:

- $\mathcal{V}(\mathbf{x})$  is locally positive definite in  $\mathcal{D}$
- $\dot{\mathcal{V}}(\mathbf{x}) = \frac{\partial \mathcal{V}}{\partial \mathbf{x}} \cdot \mathbf{f}(\mathbf{x})^*$  is locally negative semi-definite in  $\mathcal{D}$

the equilibrium point  $\mathbf{x} = \mathbf{0}$  is stable. If:

---

\*  $\mathcal{L}_f := \frac{\partial \mathcal{V}}{\partial \mathbf{x}} \cdot \mathbf{f}(\mathbf{x})$  is known as the *Lie derivative* of  $\mathcal{V}(\mathbf{x})$  along  $\mathbf{f}(\mathbf{x})$ .

- $\dot{\mathcal{V}}(\mathbf{x})$  is locally negative definite in  $\mathcal{D}$

then the equilibrium point is asymptotically stable.

A global version of the stability theorem can equally be given.

**Lyapunov function** A scalar function  $\mathcal{V}(\mathbf{x})$  is said to be a *Lyapunov function* if it verifies the hypotheses of the Lyapunov theorem, i.e. it is locally positive definite and has a locally negative semi-definite time derivative.

Although there does not exist a general and simple procedure for determining a Lyapunov function for a given system, *converse theorems of Lyapunov* guarantee the existence of a local Lyapunov function for a system with a stable equilibrium point [11].

### LaSalle's invariance principle

In Lyapunov stability theorem the hypothesis of  $\mathcal{V}(\mathbf{x})$  being locally positive definite is not always necessary to conclude stability of the equilibrium point. Further, even if  $\dot{\mathcal{V}}(\mathbf{x})$  is only locally negative semi-definite, in some cases, one can still conclude that the equilibrium point is indeed asymptotically stable. These extensions to stability theorems are guaranteed by LaSalle's invariance principle which is stated next, after the following definition:

**Invariant set** A set  $\mathcal{M} \subset \mathbb{R}^n$  is said to be an *invariant set* for the dynamical system  $\dot{\mathbf{x}} = \mathbf{f}(\mathbf{x})$ , if, given the initial condition  $\mathbf{x}(t_0) = \mathbf{x}_0$ :

$$\mathbf{x}(t) \in \mathcal{M} \quad \forall \mathbf{x}_0 \in \mathcal{M}, \quad \forall t > t_0 \quad (5.5)$$

**LaSalle's invariance principle** Let  $\mathcal{V}(\mathbf{x}) : \mathbb{R}^n \rightarrow \mathbb{R}$  be a continuously differentiable function. Let  $l$  be a constant such that

$$\Omega_l = \{\mathbf{x} \in \mathbb{R}^n : \mathcal{V}(\mathbf{x}) < l\} \quad (5.6)$$

is bounded, and

$$\dot{\mathcal{V}}(\mathbf{x}) \leq 0 \quad \forall \mathbf{x} \in \Omega_l \quad (5.7)$$

Then  $\forall \mathbf{x}_0 \in \Omega_l$ ,  $\mathbf{x}$  approaches the largest invariant set  $^* \mathcal{M} \subseteq \mathcal{S}$  as  $t \rightarrow \infty$ , where  $\mathcal{S} \subset \Omega_l$  is defined by:

$$\mathcal{S} = \{\mathbf{x} \in \Omega_l : \dot{\mathcal{V}}(\mathbf{x}) = 0\} \quad (5.8)$$

---

\*A set  $\mathcal{M}$  is said to be *invariant* if  $\mathbf{x}_0 \in \mathcal{M} \Rightarrow \Phi(\mathbf{x}_0, t) \in \mathcal{M}, \forall t > t_0$ , where  $\Phi(\mathbf{x}_0, t)$  is the solution to the differential equations  $\dot{\mathbf{x}} = \mathbf{f}(\mathbf{x})$  with initial conditions  $\mathbf{x}_0(t_0)$

In practical cases  $\mathcal{S}$  is often constituted only by equilibrium points. In such situations LaSalle's invariance principle allows to demonstrate asymptotic stability of an equilibrium point while  $\dot{\mathcal{V}}(\mathbf{x})$  being only negative semi-definite [13].

## 5.2 Direct methods for power system stability analysis

Power system stability analysis via Lyapunov methods has been the subject of extensive research for several decades. Excellent reviews [100, 70] as well as some books [27, 28] have been published on the subject. The use of direct methods for stability analysis has several advantages over stability assessment based on numerical simulations. Although integration of differential equations provides time domain response of each state variable with any desired level of detail in system modelling, only one contingency can be analysed at a time. Therefore, time domain simulations of a huge number of contingencies could be avoided with the use of direct methods which also provide a measure of the degree of system stability and its proximity to instability, that could be used to derive preventive control actions. On the other hand, direct methods relies on simplified modelling and do not provide time domain response of all state variables.

Direct stability analysis of electric power systems is based on the comparison of the value of an energy function at the post-fault initial point, with a critical value. An energy function has a decreasing value along any system trajectory and cannot be bounded along system trajectories unless the trajectories are bounded too, as formalised in the following definition [70, 101]:

**Energy function** The function  $\mathcal{V}(\mathbf{x}) : \mathbb{R}^n \rightarrow \mathbb{R}$  is said to be an *energy function* if the following conditions hold:

- $\dot{\mathcal{V}}(\mathbf{x}(t)) \leq 0$  along any system trajectories  $\mathbf{x}(t)$
- along any trajectory  $\mathbf{x}(t)$ , except for equilibrium points, the set  $\{t \in \mathbb{R} : \dot{\mathcal{V}}(\mathbf{x}(t)) = 0\}$  has measure zero in  $\mathbb{R}$
- $\mathcal{V}(\mathbf{x}(t))$  bounded  $\Rightarrow \mathbf{x}(t)$  bounded

Energy functions provide a tool for describing the boundary of stability region of dynamical systems. It can be proven that, if the system admits an energy

function, this boundary consist of the union of stable manifolds <sup>\*</sup> of the unstable equilibrium points on the stability boundary [102].

Once an energy function for post-fault system is available, a critical value  $\mathcal{V}_{cr}$  has to be defined. If this critical value is exceeded with post-fault initial conditions, i.e.  $\mathcal{V}(\mathbf{x}_{postfault}) > \mathcal{V}_{cr}$ , the trajectory is considered to be unstable <sup>†</sup>.

One of the challenge in the practical usage of direct methods lies in the choice of  $\mathcal{V}_{cr}$ . An earlier method known as the *closest unstable equilibrium point* method defines  $\mathcal{V}_{cr}$  as the minimum value that the energy function  $\mathcal{V}$  assumes among all equilibrium points on the stability boundary<sup>‡</sup> [103]. More recently the *boundary of stability region based controlling unstable equilibrium point (BCU method)* has been proposed first for network reduced models [104] and then extended to structure preserving models [105]. This method uses as  $\mathcal{V}_{cr}$  the value of  $\mathcal{V}$  at the unstable equilibrium whose stable manifold is hit first by the fault-on unstable trajectory.

### 5.2.1 SMIB system

For the classical SMIB system, whose equations, with the origin translated at the stable equilibrium point  $(\tilde{\delta}, \Delta\tilde{\omega}) = (\delta_s, 0)$ , are:

$$\dot{\delta} = \Delta\omega \quad (5.11)$$

$$\Delta\dot{\omega} = \frac{1}{M} [P_m - P_{max} \sin(\delta + \delta_s)] \quad (5.12)$$

the following local Lyapunov function exists:

$$\mathcal{V}(\delta, \Delta\omega) = \frac{1}{2} M \Delta\omega^2 - P_m(\delta + \delta_s) - P_{max} \cos(\delta + \delta_s) + c \quad (5.13)$$

where  $c$  is a suitable constant such that  $\mathcal{V}(0, 0) = 0$ . The function is plotted in Fig. 5.1, which shows that it is locally positive definite and locally convex, thus the first hypothesis (5.6) of LaSalle's invariance principle is verified.

---

<sup>\*</sup> The stable and unstable manifolds,  $\mathcal{W}^s(\tilde{\mathbf{x}}_0)$  and  $\mathcal{W}^u(\tilde{\mathbf{x}}_0)$ , respectively, of the equilibrium point  $\tilde{\mathbf{x}}_0$  are defined as follows:

$$\mathcal{W}^s(\tilde{\mathbf{x}}_0) := \{\mathbf{x}_0 \in \mathbb{R}^n : \Phi(\mathbf{x}_0, t) \rightarrow \tilde{\mathbf{x}}_0 \text{ as } t \rightarrow \infty\} \quad (5.9)$$

$$\mathcal{W}^u(\tilde{\mathbf{x}}_0) := \{\mathbf{x}_0 \in \mathbb{R}^n : \Phi(\mathbf{x}_0, t) \rightarrow \tilde{\mathbf{x}}_0 \text{ as } t \rightarrow -\infty\} \quad (5.10)$$

where  $\Phi(\mathbf{x}_0, t)$  is the solution of the differential equation  $\dot{\mathbf{x}} = \mathbf{f}(\mathbf{x})$  with initial condition  $\mathbf{x}_0$

<sup>†</sup>Due to the conservative nature of direct methods, a trajectory can be classified as unstable while the actual trajectory is indeed stable.

<sup>‡</sup>All equilibrium points on the boundary of the stability region are unstable.

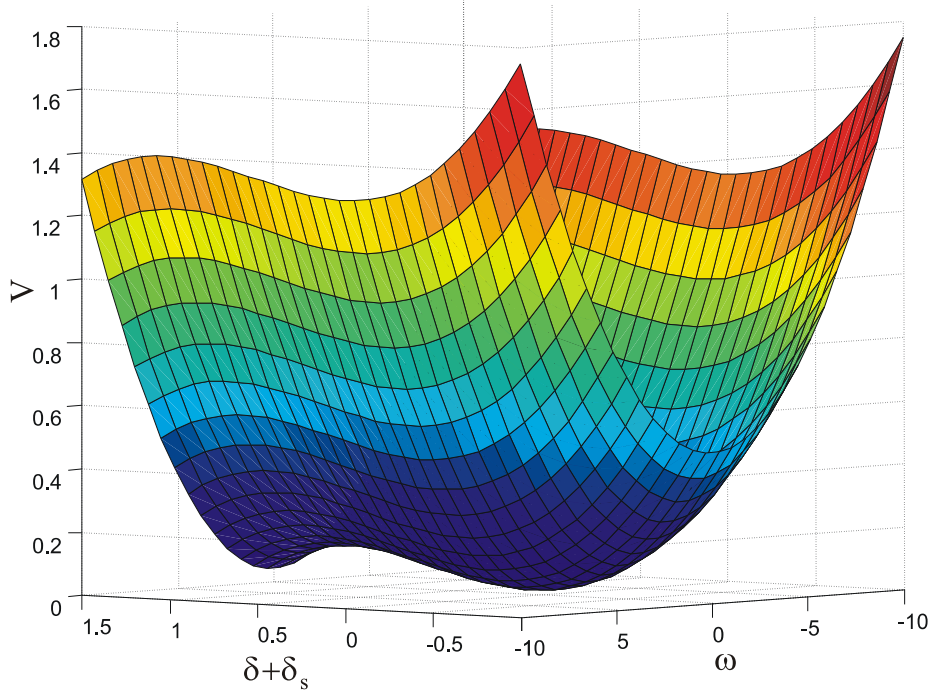


Figure 5.1: Lyapunov function for SMIB power system

The time derivative of the Lyapunov function (5.13) is given by:

$$\dot{\mathcal{V}} = \frac{\partial \mathcal{V}}{\partial \delta} \frac{\partial \delta}{\partial t} + \frac{\partial \mathcal{V}}{\partial \Delta \omega} \frac{\partial \Delta \omega}{\partial t} = -D \Delta \omega^2 \leq 0 \quad (5.14)$$

thus being negative semi-definite.

### 5.2.2 Lyapunov function for structure preserving models

Earlier efforts to derive a Lyapunov function for multimachine power system models made use of the reduced network modelling in which the network structure is lost by elimination of algebraic equations [27]. Lyapunov function for structure preserving power system models were first introduced by Tsolas, Arapostathis and Varaiya in a widely cited paper [106], and then proposed to include higher order generators models [28], dynamic load models [107], HVDC links [108] and FACTS devices [109]. For multimachine power systems, using the third order model for synchronous generator, as detailed in chapter 1, the following energy function has been proposed [110]:

$$\mathcal{V}(\omega, \delta, E'_q, V, \theta) = \mathcal{V}_1 + \sum_{k=1}^8 \mathcal{V}_{2k} + c_0 \quad (5.15)$$



which is the sum of the following terms, the first of which represents the kinetic energy of the generators, while the others account for the potential energy associated with the generators and the network:

$$\begin{aligned}
\mathcal{V}_1 &= \frac{1}{2} \sum_{k=1}^M M_k \omega_k^2 \\
\mathcal{V}_{21} &= - \sum_{k=1}^M P_{mk} \delta_k \\
\mathcal{V}_{22} &= - \sum_{k=M+1}^{M+N} P_{Lk} \theta_k \\
\mathcal{V}_{23} &= - \sum_{k=M+1}^{M+N} \int \frac{Q_{Lk}}{V_k} dV_k : \\
\mathcal{V}_{24} &= \sum_{k=M+1}^{M+N} \frac{1}{2x'_{dk-M}} [E'^2_{qk-M} + V_k^2 - 2E'_{qk-M} V_k \cos(\delta_{k-M} - \theta_k)] \quad (5.16) \\
\mathcal{V}_{25} &= - \frac{1}{2} \sum_{k=M+1}^{M+N} \sum_{j=M+1}^{M+N} B_{kj} V_k V_j \cos(\theta_k - \theta_j) \\
\mathcal{V}_{26} &= \sum_{k=M+1}^{2M} \frac{x'_{dk-M} - x_{qk-M}}{4x'_{dk-M} x_{qk-M}} [V_k^2 - V_k^2 \cos(2(\delta_{k-M} - \theta_k))] \\
\mathcal{V}_{27} &= - \sum_{k=1}^M \frac{E_{fdk} E'_{qk}}{x_{dk} - x'_{dk}} \\
\mathcal{V}_{28} &= \sum_{k=1}^M \frac{E'^2_{qk}}{2(x_{dk} - x'_{dk})}
\end{aligned}$$

As it can be easily demonstrated, the time derivative of the Lyapunov function (5.15), neglecting the transmission system transfer conductances, evaluated along the trajectories of the system is given by:

$$\begin{aligned}
\dot{\mathcal{V}}(\mathbf{x}) &= - \sum_{k=1}^M D_k \omega_k^2 - \sum_{k=1}^M \frac{T'_{d0k}}{x_{dk} - x'_{dk}} (\dot{E}'_{qk})^2 + \\
&\quad \sum_{k=1}^N \underbrace{(P_{Lk} + P_k)}_{=0} \dot{\theta}_k + \sum_{k=1}^N \underbrace{(Q_{Lk} + Q_k)}_{=0} \frac{\dot{V}_k}{V_k} \leq 0 \quad (5.17)
\end{aligned}$$

Since  $x_d > x'_d$  the time derivative is negative semi-definite.

### 5.3 Transfer conductances and the extended invariance principle

Almost all classical energy functions for power systems stability analysis make use of a power network model consisting of nodes and buses connected by lossless transmission lines. The node admittance matrix representing the network is therefore given by  $\dot{\mathbf{Y}} = [Y_{h,k}] = j[B_{h,k}]$ , with all transfer conductances  $G_{h,k}$  being neglected. All attempts to utilise a more detailed modelling including transfer conductances to derive an analytical energy function have been in vain [111]. The presence of transfer conductances in the model gives rise to path-dependant integrals into the energy function itself, therefore preventing its analytical calculation. Due to these path-dependent integrals these functions fail to satisfy the requirements of an energy function [112]. Furthermore, Narasimhamurthi demonstrated that there does not exist any smooth transformation that transform an energy function for the lossless case into an energy function for the system with losses [111].

Many power system controllers for stability improvement are also designed neglecting losses. The design of a stabilising excitation controller for multimachine power systems explicitly accounting for transfer conductances is the subject of [113].

#### 5.3.1 Extended invariance principle

An extension to the classical LaSalle's invariance principle has been proposed to circumvent the difficulty in finding a Lyapunov function for a generic system. Indeed, its application does not require  $\dot{\mathcal{V}}$  be negative semi-definite. Instead,  $\dot{\mathcal{V}}$  is allowed to be positive along system's trajectories in some regions of the state space. The extended invariance principle was first applied to derive an estimate of the attractor of single and coupled Lorenz systems [114], and then utilised in power system analysis for dealing with systems whose transfer conductances are not negligible [115].

**The extended invariance principle** Let the scalar function  $\mathcal{V}(\mathbf{x}) : \mathbb{R}^n \rightarrow \mathbb{R}$  be continuous with its first derivatives. Let

$$\Omega_{\mathcal{L}} = \{\mathbf{x} \in \mathbb{R}^n : \mathcal{V}(\mathbf{x}) < \mathcal{L}\} \quad (5.18)$$

be a bounded set where  $\mathcal{L}$  is an appropriate constant value. Define the set:

$$\mathcal{C} = \{\mathbf{x} \in \Omega_{\mathcal{L}} : \dot{\mathcal{V}}(\mathbf{x}) > 0\} \quad (5.19)$$

Assuming that:

$$\sup_{\mathbf{x} \in \mathcal{C}} \mathcal{V}(\mathbf{x}) = l < \mathcal{L} \quad (5.20)$$

then every solution of  $\dot{\mathbf{x}} = \mathbf{f}(\mathbf{x})$  starting in  $\Omega_{\mathcal{L}}$  converges as  $t \rightarrow \infty$  to the largest invariant set contained in:

$$\mathcal{E} = \{\mathbf{x} \in \Omega_{\mathcal{L}} : \dot{\mathcal{V}}(\mathbf{x}) = 0\} \cup \overline{\Omega}_l \quad (5.21)$$

where:

$$\overline{\Omega}_l = \{\mathbf{x} \in \mathbb{R}^n : \mathcal{V}(\mathbf{x}) < l\} \quad (5.22)$$

□

A pictorial illustration of the level sets involved in the statement of the extended invariance principle in the case of a one-dimensional system is given in Fig. 5.2.

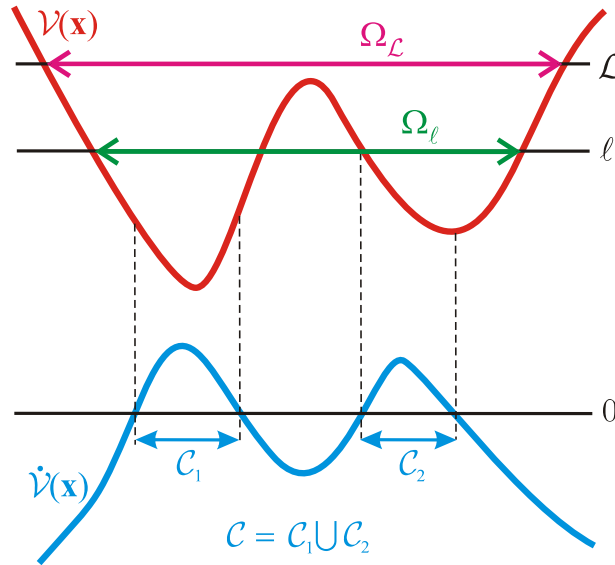


Figure 5.2: A one-dimensional graphical illustration of the level sets involved in the statement of the extended invariance principle.

Differently from the LaSalle's invariance principle the time derivative of  $\mathcal{V}$  is no longer needed to be negative semi-definite since in the bounded region  $\mathcal{C}$  it

can even be positive definite. However, this less stringent requirement results in the impossibility of demonstrating asymptotic stability of the equilibrium point. Instead, since the set  $\bar{\Omega}_l$  is in general nonempty, one can only determine an estimate of the region in which trajectories are bounded.

The possibility of using functions whose time derivative are not negative definite was exploited in [115] to derive an energy function for power systems with non-negligible transfer conductances.

In the following, exploiting the dynamic phasor modelling of the transmission network introduced in an earlier chapter, an extended Lyapunov function will be given [116]. After the relevant definitions, this extended Lyapunov function will be used to derive stabilising controls for series and shunt compensators.

## 5.4 A new extended Lyapunov function

An extended Lyapunov function is proposed. Although higher order models may be employed as well, the third order model for synchronous generators is used in the following derivation, due to its simplicity. The model is repeated here for ease of reference:

$$\dot{\delta}_i = \omega_i \quad (5.23)$$

$$\dot{\omega}_i = \frac{1}{M_i} [P_{m,i} - P_{e,i} - D_i \omega_i] \quad (5.24)$$

$$\dot{E}'_{q,i} = \frac{1}{T'_{d0,i}} [E_{fd,i} - E'_{q,i} + (x_{d,i} - x'_{d,i}) I_{d,i}] \quad (5.25)$$

$$P_{e,i} = V_{d,i} I_{d,i} + V_{q,i} I_{q,i} \quad (5.26)$$

$$V_{d,i} = -x_{q,i} I_{q,i} \quad (5.27)$$

$$V_{q,i} = E'_{q,i} + x'_{d,i} I_{d,i} \quad (5.28)$$

$$\begin{bmatrix} I_{d,i} \\ I_{q,i} \end{bmatrix} = \begin{bmatrix} -\sin \delta_i & \cos \delta_i \\ \cos \delta_i & \sin \delta_i \end{bmatrix} \cdot \begin{bmatrix} I_{gen,i_{RE}} \\ I_{gen,i_{IM}} \end{bmatrix} \quad (5.29)$$

$$\begin{bmatrix} V_{gen,i_{RE}} \\ V_{gen,i_{IM}} \end{bmatrix} = \begin{bmatrix} -\sin \delta_i & \cos \delta_i \\ \cos \delta_i & \sin \delta_i \end{bmatrix} \cdot \begin{bmatrix} V_{d,i} \\ V_{q,i} \end{bmatrix} \quad (5.30)$$

Each transmission line and RL load is described by eqs. (4.17)-(4.18) as detailed in chapter 3.

The proposed extended Lyapunov function is given by the summation of the

following terms:

$$\mathcal{V}_1 = \frac{1}{2} \sum_{i=1}^m M_i \omega_i^2 \quad (5.31)$$

$$\begin{aligned} \mathcal{V}_2 &= - \sum_{i=1}^m \int (P_{m,i} - P_{e,i}) d\delta \\ &= - \sum_{i=1}^m [P_{m,i} \delta_i - E'_{q,i} (I_{gen,i_{RE}} \sin \delta_i - I_{gen,i_{IM}} \cos \delta_i)] \\ &\quad + \sum_{i=1}^m (x'_{d,i} - x_{q,i}) \left[ -\frac{1}{4} (I_{gen,i_{IM}}^2 - I_{gen,i_{RE}}^2) \cos 2\delta_i \right. \\ &\quad \left. + \frac{1}{2} I_{gen,i_{RE}} I_{gen,i_{IM}} \sin 2\delta_i \right] \end{aligned} \quad (5.32)$$

$$\mathcal{V}_3 = - \sum_{i=1}^m \frac{E_{fd,i} E'_{q,i}}{x_{d,i} - x'_{d,i}} + \sum_{i=1}^m \frac{(E'_{q,i})^2}{2(x_{d,i} - x'_{d,i})} \quad (5.33)$$

$$\mathcal{V}_4 = \sum_{i=1}^m [I_{gen,i_{RE}}^2 + I_{gen,i_{IM}}^2] \quad (5.34)$$

$$\mathcal{V}_l = \sum_{i,j \in \mathcal{N}, i \neq j} \frac{1}{2} \frac{l_{ij}}{\omega_0} [(I_{ij_{RE}} - I_{ij_{RE}}^*)^2 + (I_{ij_{IM}} - I_{ij_{IM}}^*)^2] \quad (5.35)$$

$$\mathcal{V}_c = \sum_{i \in \mathcal{N}} \frac{1}{2} \frac{c_i}{\omega_0} [(V_{i_{RE}} - V_{i_{RE}}^*)^2 + (V_{i_{IM}} - V_{i_{IM}}^*)^2] \quad (5.36)$$

Terms (5.31)-(5.33) are derived similarly to the analogous terms in the classical Lyapunov function (5.16). The remaining terms are quadratic functions of voltages and currents in the network, which provide a measure of the stored energy. Starred variables denote the corresponding stable equilibrium point value. Time derivative of the proposed function is obtained by adding the following terms:

$$\dot{\mathcal{V}}_{\delta, \omega, E'_q} = - \sum_{i=1}^m \left[ D_i \omega_i^2 + \frac{T'_{d0,i}}{x_{d,i} - x'_{d,i}} (\dot{E}'_{q,i})^2 \right] \leq 0 \quad (5.37)$$

$$\begin{aligned} \dot{\mathcal{V}}_{I_{gen_{RE}}, I_{gen_{IM}}} &= \sum_{i=1}^m \left[ -V_{gen,i_{RE}} \dot{I}_{gen,i_{IM}} + V_{gen,i_{IM}} \dot{I}_{gen,i_{RE}} \right. \\ &\quad \left. + (1 + x_{q,i}) (I_{gen,i_{RE}} \dot{I}_{gen,i_{RE}} + I_{gen,i_{IM}} \dot{I}_{gen,i_{IM}}) \right] \end{aligned} \quad (5.38)$$

$$\dot{\mathcal{V}}_{I_{RE}, I_{IM}} = \sum_{i \neq j} \frac{l_{ij}}{\omega_0} [(I_{ij_{RE}} - I_{ij_{RE}}^*) \dot{I}_{ij_{RE}} + (I_{ij_{IM}} - I_{ij_{IM}}^*) \dot{I}_{ij_{IM}}] \quad (5.39)$$

$$\dot{\mathcal{V}}_{V_{RE}, V_{IM}} = \sum_{i \in \mathcal{N}} \frac{c_i}{\omega_0} [(V_{i_{RE}} - V_{i_{RE}}^*) \dot{V}_{i_{RE}} + (V_{i_{IM}} - V_{i_{IM}}^*) \dot{V}_{i_{IM}}] \quad (5.40)$$

The term (5.37) is negative semi-definite and is the same as the first term in (5.17). The other terms (5.38)-(5.40) are related to the variation of stored energy

in network's elements. They might be responsible for generating regions in the state-space where  $\dot{\mathcal{V}}$  is positive definite.

In general cases, it is not easy to verify the validity of the hypotheses of the extended invariance principle. In particular, it should be proven that the set  $\Omega_{\mathcal{L}} = \{\mathbf{x} \in \mathbb{R}^n : \mathcal{V}(\mathbf{x}) < \mathcal{L}\}$  is bounded, and that according to (5.20), the supremum of  $\mathcal{V}$  over the region in which  $\dot{\mathcal{V}}$  is allowed to be positive, is less than  $\mathcal{L}$ . It is worth noting that these conditions are verified if the function  $\mathcal{V}$  is convex. In practical cases, the conditions for the extended invariance principle to hold can be numerically checked via constrained optimisation, which was employed in the following one-machine case.

### 5.4.1 SMIB system

A single synchronous generator coupled to an infinite bus provides a simple test case. Figure 5.3 shows two cross sections of the proposed extended Lyapunov function for this SMIB test case.

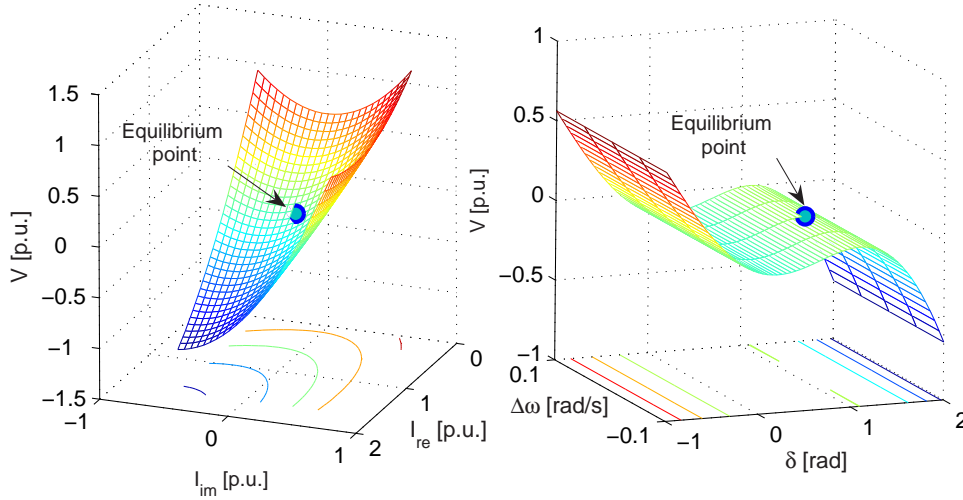


Figure 5.3: Two cross sections of the proposed extended Lyapunov function of the SMIB test case

It can be easily demonstrated, both graphically and using numerical optimisation, that  $\Omega_{\mathcal{L}}$  is bounded in all directions except for increasing  $\delta$ . The presence of quadratic terms in all variables makes all level set closed surfaces in the hypothesis that  $\delta$  is bounded too. This situation is similar to what happens with classical

Lyapunov functions for power system analysis, such as the function reported in eq. (5.13). Indeed, the presence of the term  $-P_m\delta$ , which is also present in the proposed function, makes the level sets unbounded in the direction of increasing  $\delta$ , as it can be also graphically deduced in the plot reported in Fig. 5.1. Since the energy function (5.13) for the second order SMIB system (5.11)-(5.12) is not bounded below, application of the classical LaSalle's invariance principle is possible only if it is known a priori that a trajectory is bounded. In this case the LaSalle's theorem prove that the trajectory asymptotically converge to an equilibrium point, since invariant sets are constituted only by equilibrium points [13]. Differently to this widely known classical result, the application of the extended invariance principle with the proposed modelling, instead of proving asymptotic stability, yields an estimate of the region  $\bar{\Omega}_l$  in which trajectories remain bounded. The extended invariance principle will be applied to demonstrate that a proper selection of control action can reduce the amplitude of this region.

## 5.5 Lyapunov functions and control systems

Although stability analysis of dynamical systems was the first application of Lyapunov's theory, several applications to controlled systems have appeared in literature. Most of them are based on the use of control actions that results in negative definite additional terms to the time derivative of a suitable Lyapunov function [117, 118, 119].

Several applications have also been proposed in the past to power system stability enhancement. In particular stabilising controls appeared in technical literature applied to excitation control [120, 121, 122], controllable series devices [110, 123], UPFC [124], SMES with either network reduced model [125] or structure preserving model [126] and, in general, FACTS devices [127, 128, 129]. The definition of Control Lyapunov function and its use to derive control laws are given next.

### 5.5.1 Control Lyapunov function

Let consider the nonlinear system with control input  $\mathbf{u}$  whose state-space equations are given by:

$$\dot{\mathbf{x}} = \mathbf{f}(\mathbf{x}) + \mathbf{g}(\mathbf{x})\mathbf{u}, \quad \mathbf{x} \in \mathbb{R}^n, \quad \mathbf{u} \in \mathbb{R}^m \quad (5.41)$$

Systems of this kind are commonly referred to as affine in the control, since the state space derivative depends linearly on the control input  $\mathbf{u}$ . Let  $\mathbf{0}$  be the equilibrium point of the uncontrolled part of the system (5.41):

$$\dot{\mathbf{x}}_{\text{un}} = \mathbf{f}(\mathbf{0}) = \mathbf{0} \quad (5.42)$$

If the equilibrium point  $\mathbf{0}$  is stable, the control input  $\mathbf{u}$  can be chosen to achieve asymptotical stability, or to add additional damping to an already stable system.

**Control Lyapunov function** Let  $\mathcal{V}(\mathbf{x})$  be a smooth, positive definite and radially unbounded\* function.  $\mathcal{V}(\mathbf{x})$  is said to be a *Control Lyapunov function* (CLF) for (5.41) if and only if  $\forall \mathbf{x} \neq \mathbf{0}$  the following implication holds:

$$L_g \mathcal{V}(\mathbf{x}) := \frac{\partial \mathcal{V}}{\partial \mathbf{x}} \mathbf{g}(\mathbf{x}) = \mathbf{0} \Rightarrow L_f \mathcal{V}(\mathbf{x}) = \left( \frac{\partial \mathcal{V}}{\partial \mathbf{x}} \right)^\top \cdot \mathbf{f}(\mathbf{x}) < 0 \quad (5.43)$$

This definition means that a CLF is any Lyapunov function whose time derivative can be made negative definite by means of an appropriate control input  $\mathbf{u}$  [117], [119]-[130]. Let  $\mathcal{V}(\mathbf{x})$  be a Lyapunov function for the uncontrolled system:

$$\dot{\mathbf{x}} = \mathbf{f}(\mathbf{x}) \quad (5.44)$$

The time derivative of  $\mathcal{V}$  along the trajectories of the controlled system (5.41) is:

$$\begin{aligned} \dot{\mathcal{V}}(\mathbf{x}) &= \nabla \mathcal{V} \cdot \dot{\mathbf{x}} = \nabla \mathcal{V} \cdot (\mathbf{f}(\mathbf{x}) + \mathbf{g}(\mathbf{x})\mathbf{u}) \\ &= \frac{\partial \mathcal{V}}{\partial \mathbf{x}} \mathbf{f}(\mathbf{x}) + \left( \frac{\partial \mathcal{V}}{\partial \mathbf{x}} \mathbf{g}(\mathbf{x}) \right)^\top \mathbf{u} \\ &= L_f \mathcal{V} + (L_g \mathcal{V})^\top \mathbf{u} \end{aligned} \quad (5.45)$$

Since  $\mathcal{V}$  is a Lyapunov function for the uncontrolled system, the following inequality holds:

$$L_f \mathcal{V} \leq 0 \quad (5.46)$$

The control law:

$$\mathbf{u} = -k(L_g \mathcal{V}) \quad (5.47)$$

known as injection damping, Jurdjevic-Quinn or simply  $L_g \mathcal{V}$  control, adds the negative semidefinite term:

$$-k \|L_g \mathcal{V}\|^2 \quad (5.48)$$

---

\*A scalar function  $\mathcal{V}(\mathbf{x})$  is said to be *radially unbounded* if  $\mathcal{V}(\mathbf{x}) \rightarrow \infty$  as  $\|\mathbf{x}\| \rightarrow \infty$



to the time derivative of  $\mathcal{V}$ , thus increasing the damping to system trajectories and providing asymptotic stability to the system.

A general optimal stabilizing law, obtained from a CLF, was derived by Sontag [119] as:

$$\mathbf{u}_S = \begin{cases} -\mathbf{k} \left( c_0 + \frac{a(\mathbf{x}) + \sqrt{a^2(\mathbf{x}) + (\mathbf{b}^\top(\mathbf{x})\mathbf{b}(\mathbf{x}))^2}}{\mathbf{b}^\top(\mathbf{x})\mathbf{b}(\mathbf{x})} \right) \mathbf{b}(\mathbf{x}) & , \quad \mathbf{b}(\mathbf{x}) \neq \mathbf{0} \\ \mathbf{0} & , \quad \mathbf{b}(\mathbf{x}) = \mathbf{0} \end{cases} \quad (5.49)$$

where:

$$\begin{aligned} a(\mathbf{x}) &= L_f \mathcal{V} \\ \mathbf{b}(\mathbf{x}) &= (L_g \mathcal{V})^\top \end{aligned} \quad (5.50)$$

Both Jurdjević-Quinn and Sontag's, as well as all universal formulas depending upon CLFs can be considered as particular cases of a general parametrization, as described in [131].

### 5.5.2 Extended control Lyapunov function

Control laws derived from a control Lyapunov function, such as injection damping control, can provide asymptotic stability to stable systems, as it can easily be demonstrated via direct application of the LaSalle's invariance principle. In case an extended Lyapunov function is available, the presence of a control which adds a negative definite term to  $\dot{\mathcal{V}}$  has the effect of reducing the region  $\mathcal{C}$  defined in eq. (5.19) in which  $\dot{\mathcal{V}}$  takes positive values to a region  $\mathcal{C}' \subseteq \mathcal{C}$ . This, in turn, results in a shrinking of the state-space region in which trajectories are bounded i.e.:

$$\overline{\Omega}_{l'} \subseteq \overline{\Omega}_l \quad (5.51)$$

where prime denotes the presence of control. The effect of a injection damping control such as  $L_g \mathcal{V}$  control can be graphically deduced from the pictorial representation in Fig. 5.4.

### Extended CLF for series compensator control

The presence of a series connected compensator in a transmission line capable of independent control of active and reactive power, modifies line's equations as

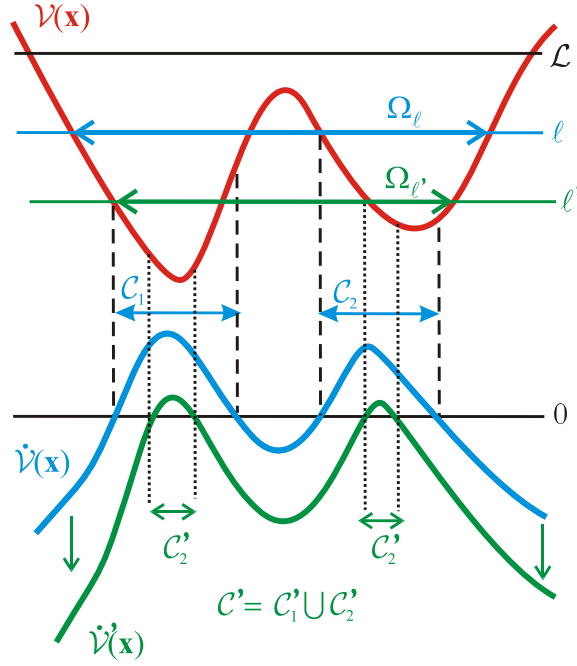


Figure 5.4: A one-dimensional graphical illustration of the effect of a control input which adds a negative definite term to the time derivative of the Lyapunov function, on the level sets involved in the statement of the extended invariance principle.

follows:

$$\begin{aligned} \frac{1}{\omega} \begin{bmatrix} \dot{I}_{ijRE} \\ \dot{I}_{ijIM} \end{bmatrix} &= \begin{bmatrix} -\frac{r_{ij}}{l_{ij}} & 1 \\ 1 & -\frac{r_{ij}}{l_{ij}} \end{bmatrix} \cdot \begin{bmatrix} I_{ijRE} \\ I_{ijIM} \end{bmatrix} + \begin{bmatrix} \frac{1}{l_{ij}} & 0 \\ 0 & \frac{1}{l_{ij}} \end{bmatrix} \cdot \begin{bmatrix} V_{iRE} - V_{jRE} \\ V_{iIM} - V_{jIM} \end{bmatrix} \\ &+ \begin{bmatrix} \frac{1}{l_{ij}} & 0 \\ 0 & \frac{1}{l_{ij}} \end{bmatrix} \cdot \begin{bmatrix} u_{RE} \\ u_{IM} \end{bmatrix} \end{aligned} \quad (5.52)$$

The derivative of  $\mathcal{V}$  modifies as follows:

$$\begin{aligned} \dot{\mathcal{V}}_{I_{ijRE}, I_{ijIM}} &= [(I_{ijRE} - I_{ijRE}^*), (I_{ijIM} - I_{ijIM}^*)] \cdot \left\{ \begin{bmatrix} -r_{ij} & 1 \\ 1 & -r_{ij} \end{bmatrix} \cdot \begin{bmatrix} I_{ijRE} \\ I_{ijIM} \end{bmatrix} \right. \\ &+ \left. \begin{bmatrix} V_{iRE} - V_{jRE} \\ V_{iIM} - V_{jIM} \end{bmatrix} \right\} + [(I_{ijRE} - I_{ijRE}^*), (I_{ijIM} - I_{ijIM}^*)] \cdot \begin{bmatrix} u_{RE} \\ u_{IM} \end{bmatrix} \end{aligned} \quad (5.53)$$

The following choice of control input:

$$\begin{bmatrix} u_{RE} \\ u_{IM} \end{bmatrix} = -\frac{K}{I_{ijRE}^2 + I_{ijIM}^2} \begin{bmatrix} I_{ijRE} - I_{ijRE}^* \\ I_{ijIM} - I_{ijIM}^* \end{bmatrix} \quad (5.54)$$

adds a negative definite term to  $\dot{\mathcal{V}}$  as follows:

$$\dot{\mathcal{V}}' = \dot{\mathcal{V}} - \underbrace{K \left[ \frac{(I_{ijRE} - I_{ijRE}^*)^2 + (I_{ijIM} - I_{ijIM}^*)^2}{I_{ijRE}^2 + I_{ijIM}^2} \right]}_{\leq 0} \quad (5.55)$$

A saturation should be imposed in applications to limit the value of the control law (5.54) to the maximum attainable value given by practical constraints.

### Extended CLF for shunt compensator control

Analogously to the series compensator, the presence of a compensator shunt connected to a bus  $i$ , capable of independent control of active and reactive power, modifies bus voltage equations as follows:

$$\begin{aligned} \frac{1}{\omega} \begin{bmatrix} \dot{V}_{iRE} \\ \dot{V}_{iIM} \end{bmatrix} &= \begin{bmatrix} 0 & 1 \\ -1 & 0 \end{bmatrix} \cdot \begin{bmatrix} V_{iRE} \\ V_{iIM} \end{bmatrix} + \begin{bmatrix} \frac{1}{c_i} & 0 \\ 0 & \frac{1}{c_i} \end{bmatrix} \cdot \begin{bmatrix} I_{ciRE} \\ I_{ciIM} \end{bmatrix} \\ &+ \begin{bmatrix} \frac{1}{c_i} & 0 \\ 0 & \frac{1}{c_i} \end{bmatrix} \cdot \begin{bmatrix} u_{RE} \\ u_{IM} \end{bmatrix} \end{aligned} \quad (5.56)$$

The derivative of  $\mathcal{V}$  modifies as follows:

$$\begin{aligned} \dot{\mathcal{V}}_{V_{iRE}, V_{iIM}} &= \left[ (V_{iRE} - V_{iRE}^*), (V_{iIM} - V_{iIM}^*) \right] \cdot \left\{ \begin{bmatrix} 0 & 1 \\ -1 & 0 \end{bmatrix} \cdot \begin{bmatrix} V_{iRE} \\ V_{iIM} \end{bmatrix} \right. \\ &+ \left. \begin{bmatrix} I_{ciRE} \\ I_{ciIM} \end{bmatrix} \right\} + \left[ (V_{iRE} - V_{iRE}^*), (V_{iIM} - V_{iIM}^*) \right] \cdot \begin{bmatrix} u_{RE} \\ u_{IM} \end{bmatrix} \end{aligned} \quad (5.57)$$

The following choice of control input:

$$\begin{bmatrix} u_{RE} \\ u_{IM} \end{bmatrix} = -\frac{K}{V_{iRE}^2 + V_{iIM}^2} \begin{bmatrix} V_{iRE} - V_{iRE}^* \\ V_{iIM} - V_{iIM}^* \end{bmatrix} \quad (5.58)$$

adds a negative definite term to  $\dot{\mathcal{V}}$  as follows:

$$\dot{\mathcal{V}}' = \dot{\mathcal{V}} - \underbrace{K \left[ \frac{(V_{iRE} - V_{iRE}^*)^2 + (V_{iIM} - V_{iIM}^*)^2}{V_{iRE}^2 + V_{iIM}^2} \right]}_{\leq 0} \quad (5.59)$$

Again a limit should be imposed, according to practical constraints, to the control law in eq. (5.58).

### 5.5.3 Numerical applications: SMIB system with series compensator

The proposed control law for series compensator is applied to the SMIB system already presented in previous chapters. A  $0.15\text{ s}$  fault is applied to produce a deviation from steady-state conditions.

Figs. 5.5-5.6 represent the value of the proposed Lyapunov function  $\mathcal{V}$  and its time derivative  $\dot{\mathcal{V}}$ , respectively, while Figs. 5.7 and 5.8 show  $E'_q, \Delta\omega, \delta$  and  $I_{re}, I_{im}$  sections of the phase-plane, respectively. The improvement in dynamic behaviour is clear from Figs. 5.7-5.8. Critical clearing time is increased of 66%. The value of  $l$  defined by 5.20 has been evaluated by means of numerical constrained optimisation. It has been verified that  $l = 4.15$  for the uncontrolled system, while  $l' = 2.74$  for the controlled system.

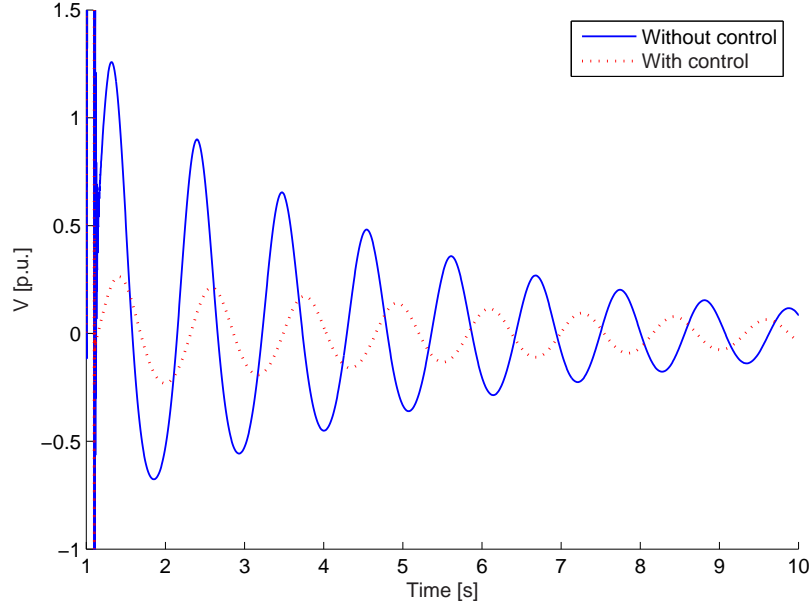
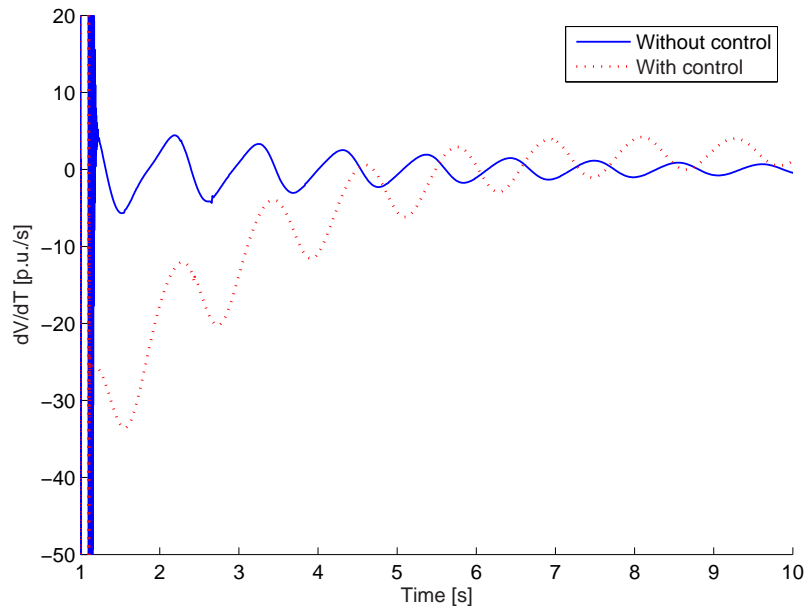
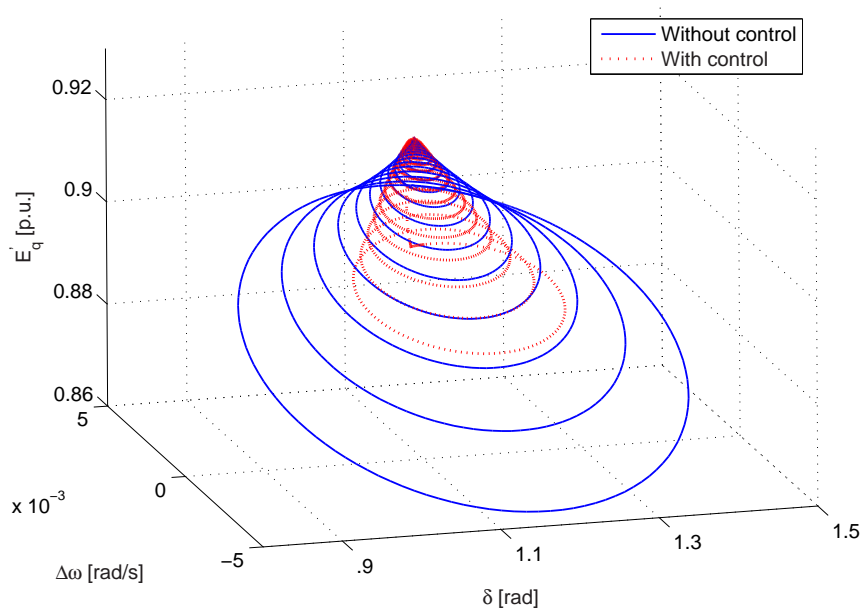


Figure 5.5:  $\mathcal{V}$  with and without control

### 5.5.4 Numerical applications: 2nd benchmark system for subsynchronous resonance

The proposed control law has also been applied to the 2nd benchmark model for subsynchronous resonance already reported in the previous chapter. Active power flow over line 1 obtained with the proposed control law is reported in Fig.

Figure 5.6:  $\dot{V}$  with and without the proposed controlFigure 5.7:  $E'_q, \Delta\omega, \delta$  phase-plane section of the SMIB system with and without the proposed control

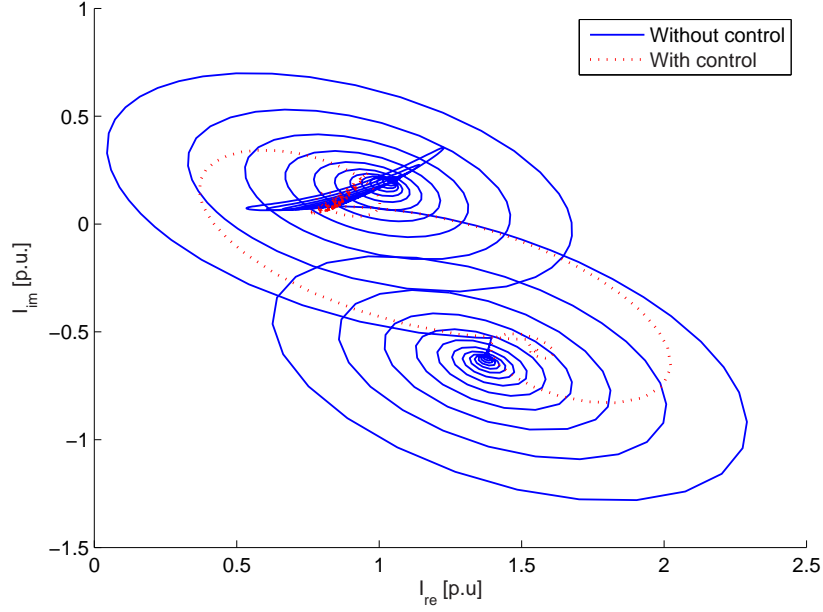


Figure 5.8:  $I_{re}, I_{im}$  phase-plane section of the SMIB system with and without control

5.9, compared with the result of the application of the PI control with  $k = 5$ . The proposed control law, thanks also to active power exchange, is able to damp mechanical oscillations without causing instability in torsional oscillations as PI controller does.

## 5.6 Adaptive equilibrium point estimation

Control laws derived from Lyapunov theory are aimed at stabilising system steering it towards an equilibrium point. The knowledge of this equilibrium point is indeed necessary in the proposed control laws for series and shunt compensators given in eqs. (5.54) and (5.58), respectively. It is worth noting that both control laws do not change the equilibrium point itself, since both control actions vanish as trajectory approaches to the equilibrium point.

In actual control system, steady state equilibrium is seldom available in real time operation. This is also the case in power system control, since post fault equilibrium is not known in advance as it usually depends on protective equipment action following a fault. A common practice is to add wash-out filters,

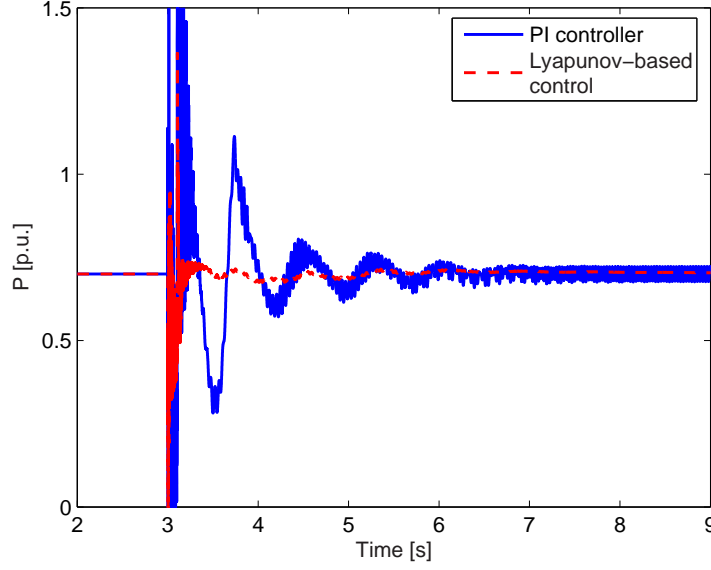


Figure 5.9: Active power flow over line 1. Comparison between PI controller and the Lyapunov based controller

which thanks to a high pass filtering make the controllers respond only to a deviation from steady state, as it is the case with widely used PSS [15]. The problem of designing stabilising controllers with unknown operating point has been recognised and been dealt with in a few papers such as [120, 132, 133] which propose adaptation schemes that provide estimates of the unknown equilibrium point. In particular, it is demonstrated in [120], with a synchronous generator example, that  $L_g\mathcal{V}$  controllers supplemented with an adaptive tracking of the unknown equilibrium point, not only retain their stabilising properties but also increase the amplitude of the attraction region, with respect to the *static*  $L_g\mathcal{V}$  control which assumes the equilibrium point to be known.

The controlled system with the proposed controller can be written as:

$$\dot{\mathbf{x}} = \mathbf{f}(\mathbf{x}) + \mathbf{g}(\mathbf{x}) \cdot \mathbf{u}(\mathbf{x}, \mathbf{x}^*) \quad (5.60)$$

where  $\mathbf{x}^*$  is the stable equilibrium point. As already said  $\mathbf{u}(\mathbf{x}^*, \mathbf{x}^*) = \mathbf{0}$ .

Adopting the adaptive scheme from [120] the controlled system becomes:

$$\dot{\mathbf{x}} = \mathbf{f}(\mathbf{x}) + \mathbf{g}(\mathbf{x}) \cdot \mathbf{u}(\mathbf{x}, \theta) \quad (5.61)$$

$$\dot{\theta} = \mathbf{A} \cdot (\mathbf{x} - \theta) \quad (5.62)$$

where  $\theta$  is the adaptive estimation of the unknown equilibrium point  $\mathbf{x}^*$ . Matrix  $\mathbf{A}$  has to be positive definite. The system augmented with adaptive equilibrium point tracking (5.61)-(5.62) preserves the original equilibria. Indeed, it is easily proven that:

$$\begin{aligned} \mathbf{x}^* \text{ is an eq. point of the open loop system (i.e. } \mathbf{f}(\mathbf{x}^*) = \mathbf{0}) \\ \Updownarrow \\ \begin{bmatrix} x^{*\top}, x^{*\top} \end{bmatrix}^\top \text{ eq. point of (5.61) - (5.62)} \end{aligned} \quad (5.63)$$

The adaptive version of the proposed series compensator control law is obtained modifying eq. (5.54) as follows:

$$\begin{bmatrix} u_{RE} \\ u_{IM} \end{bmatrix} = -\frac{K}{I_{ijRE}^2 + I_{ijIM}^2} \begin{bmatrix} I_{ijRE} - \theta_{RE} \\ I_{ijIM} - \theta_{IM} \end{bmatrix} \quad (5.64)$$

where:

$$\begin{bmatrix} \dot{\theta}_{RE} \\ \dot{\theta}_{IM} \end{bmatrix} = \begin{bmatrix} a_{11} & 0 \\ 0 & a_{22} \end{bmatrix} \cdot \begin{bmatrix} I_{ijRE} - \theta_{RE} \\ I_{ijIM} - \theta_{IM} \end{bmatrix} \quad (5.65)$$

Analogously, for the shunt compensator case, eq. (5.58) augmented with adaptive equilibrium point estimation becomes:

$$\begin{bmatrix} u_{RE} \\ u_{IM} \end{bmatrix} = -\frac{K}{V_{iRE}^2 + V_{iIM}^2} \begin{bmatrix} V_{iRE} - \theta_{RE} \\ V_{iIM} - \theta_{IM} \end{bmatrix} \quad (5.66)$$

where:

$$\begin{bmatrix} \dot{\theta}_{RE} \\ \dot{\theta}_{IM} \end{bmatrix} = \begin{bmatrix} a_{11} & 0 \\ 0 & a_{22} \end{bmatrix} \cdot \begin{bmatrix} V_{iRE} - \theta_{RE} \\ V_{iIM} - \theta_{IM} \end{bmatrix} \quad (5.67)$$

### 5.6.1 Numerical applications: interarea oscillations damping in multimachine power system

The possibility to exploit the proposed control law to damp interarea oscillations has been tested with respect to the two-area test system whose data are reported in Appendix A. A modification in PSS parameter has been made, adding a TGR in order to decrease interarea oscillations damping. The system has been simulated with both series and shunt compensator.

#### Shunt compensator

A compensator shunt connected to bus 8 is first considered. Oscillations are initiated by a three-phase fault at bus 9 self-cleared after 0.1 s, followed by a 1 p.u.



active power load shedding at bus 9, in order to simulate post-fault conditions different from pre-fault and test the equilibrium point tracking technique presented in the previous section. Results of numerical simulations are reported in Figs. 5.10-5.12. Figure 5.10 shows rotor angles of machines 1 to 3 with respect to machine 4, with the supplementary Lyapunov-based control given in eqs. 5.66 compared with the case of fixed reactive compensation alone. Oscillations are clearly damped, as it is also evident from Fig. 5.11 which shows the active power flow from area 1 to area 2, i.e. flowing from bus 8 to 9. Real and imaginary part of bus 8 voltage and adaptive estimate of respective equilibrium points, obtained with eqs. 5.67 with  $a_{11} = a_{22} = 1$  are reported in Fig. 5.12 in blue and red lines, respectively.

### Series compensator

Analogous simulations are reported with respect to a series compensator, which is connected between buses 8A and 8B obtained by splitting bus 8 into two. The same fault sequence as in the previous case has been applied. Again good damping performances are obtained with respect to both rotor angle oscillations as reported in Fig. 5.13 and active power flow in Fig. 5.14. Real and imaginary part of line 8A – 8B current and adaptive estimate of respective equilibrium points, obtained with eqs. 5.65 with  $a_{11} = a_{22} = 1$  are reported in Fig. 5.15 in blue and red lines, respectively.

The series injected voltages will be used as reference values to be tracked by the converter presented in the next chapter.

## 5.7 Conclusion

After a brief introduction to the classical stability analysis via Lyapunov functions, the extended invariance principle is presented. It allows to derive control laws which shrink the region in which trajectories are bounded also for system whose Lyapunov function has time derivative not negative definite. An adaptive procedure is necessary in real-time implementation for estimating the equilibrium point to be stabilised.

The next chapter will describe a novel topology for FACTS devices which will be used to track the reference values obtained using the proposed Lyapunov-based methodology.

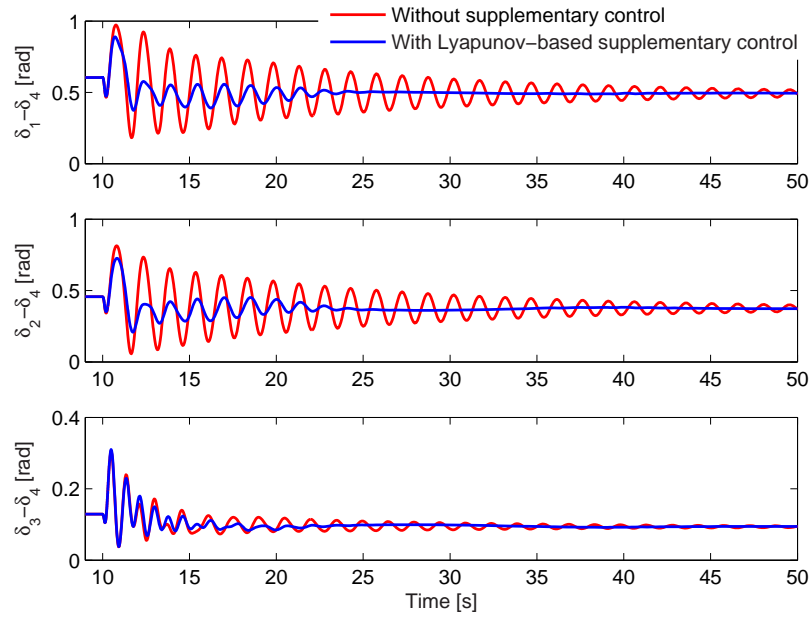


Figure 5.10: Rotor angles of machines 1 ÷ 3 with respect to machine 4, with and without the proposed supplementary control law for the shunt compensator

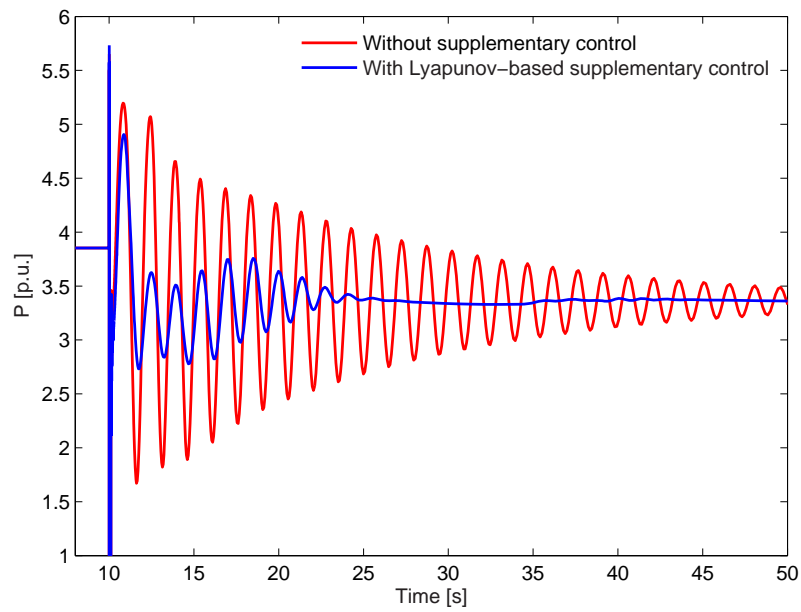


Figure 5.11: Active power flow from area 1 to area 2 with and without the proposed supplementary control law for the shunt compensator

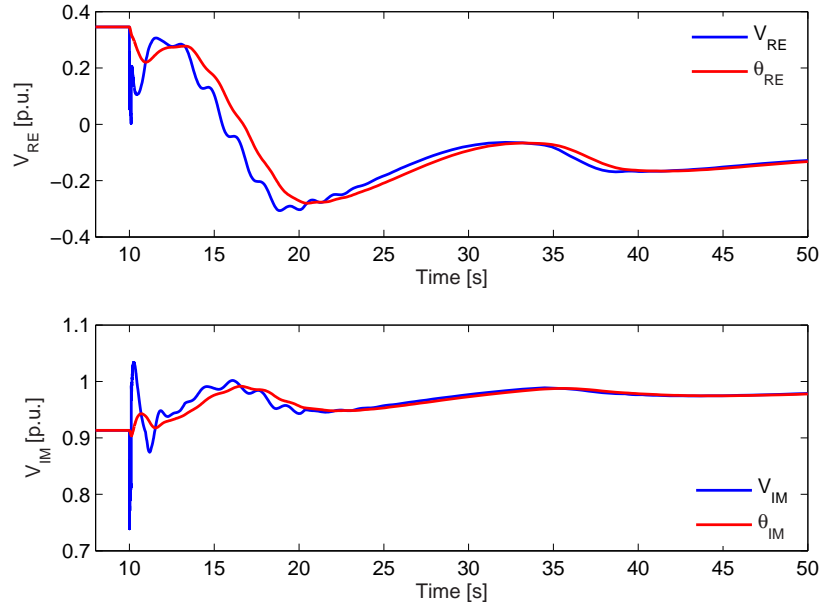


Figure 5.12: Real and Imaginary part of bus 8 voltage (blue line) and adaptive estimate of respective equilibrium point (red line)

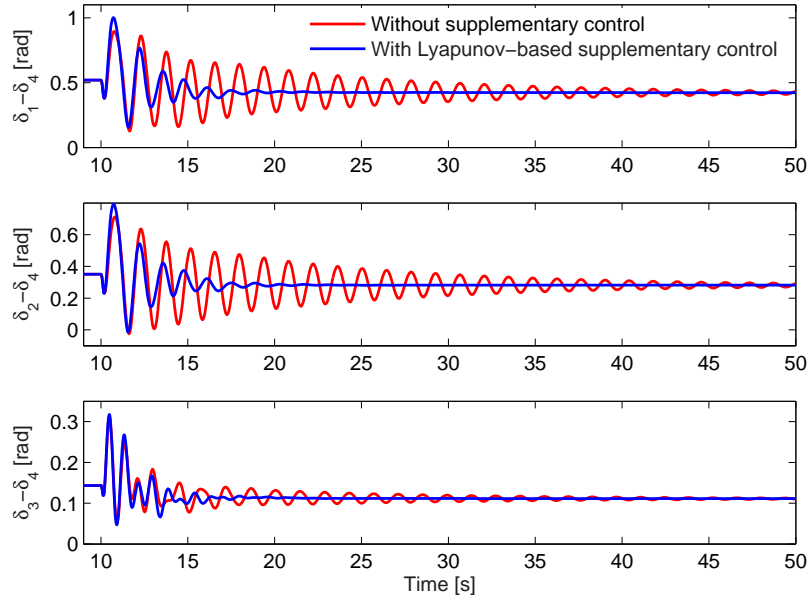


Figure 5.13: Rotor angles of machines 1  $\div$  3 with respect to machine 4, with and without the proposed supplementary control law for the series compensator

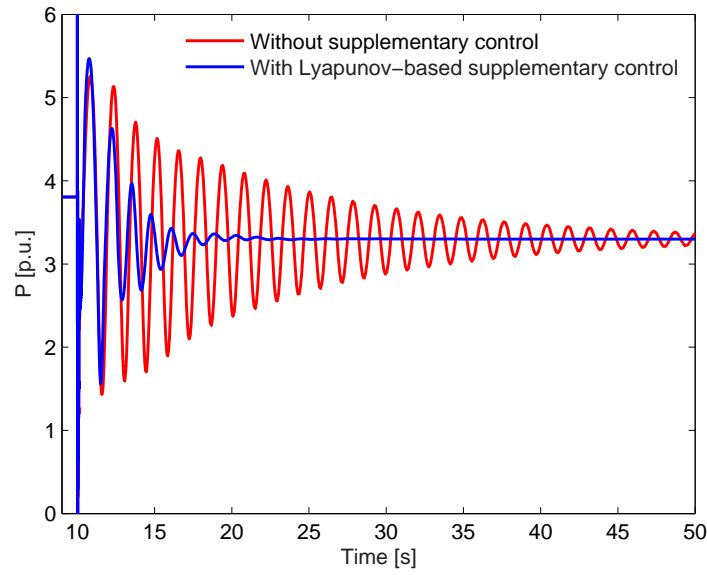


Figure 5.14: Active power flow from area 1 to area 2 with and without the proposed supplementary control law for the series compensator

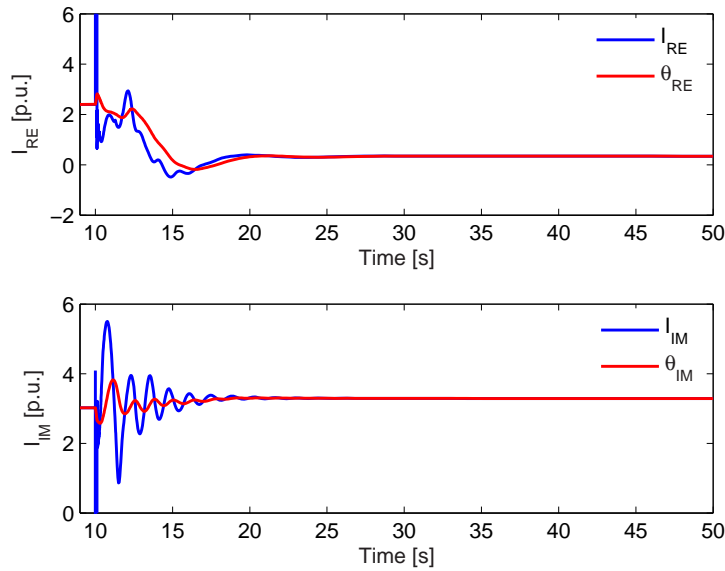


Figure 5.15: Real and imaginary part of line  $8A - 8B$  current and adaptive estimate of respective equilibrium points

## Chapter 6

---

# Two-leg three-phase inverter control for STATCOM and SSSC applications

---

### Summary

*Several converter topologies for FACTS applications have been proposed in the recent literature, even if those based upon voltage source inverters (VSI) seem to be more attractive due to their intrinsic capability to rapidly respond to network changes such as perturbations subsequent to a fault and their property of being immune to resonance problem. In the chapter a new topology for inverter based FACTS devices is proposed. This configuration, employing two-leg three-phase inverters is employed for both series and parallel connected reactive power compensators. The converter utilises a modular topology for allowing a satisfaction of electronic components rating. A control strategy based on variable structure control technique with sliding mode is employed to track appropriate reference quantities.*

*Using a DC-DC chopper for coupling the DC side of the proposed inverter with a storage device like a superconducting coil, results in a topology useful for SMES-based FACTS devices which can be easily employed for practical tracking of stabilising reference control signals obtained in the previous chapter.*

*Design and control, as well as good tracking performances are verified through*

*numerical simulations.*

## 6.1 Introduction

Several power converter topologies have been proposed for the implementation of FACTS devices, such as those based on voltage-source converters [134] and current-source converters [135]. Among voltage-source converters line-frequency switching has been preferred to pulse-width modulation (PWM) due to the past unavailability of high switching frequency power devices with high power handling capabilities. In order to achieve lower harmonic distortion multi-pulse converter are employed, such as the 24 and 48 pulses converters [136, 60, 137]. Magnetic interfaces constituted by complex zig-zag phase shifting transformers are required for interfacing multi-pulse inverters with transmission network in order to counteract low order harmonics. With the use of multilevel converters [138] the necessity of complex coupling transformers could be avoided, at the expense of a greater complexity in control. Comprehensive circuit-level comparisons along with advantages and drawbacks of several common arrangements for high-power converters are presented in [134] and [139].

Several improvements in power semiconductor devices have been reported recently. Insulated gate-commutated thyristors (IGCT) [140, 141] have been proposed and are already commercially available for high power operations with switching frequency in the kHz range. Emitter turn-off thyristor (ETO) promises to be a viable technology for very high power and high frequency PWM operation [142, 143, 144]. These progresses are making PWM operation a competitive and effective alternative to line-frequency commutated control structure which are currently employed [145].

Power converters can be regarded as Variable Structure Systems due to their switching operation. Sliding mode control for this type of system has gained widespread attention in the relevant literature due to its simplicity and intrinsic robustness against disturbances [146, 147]. Sliding mode control is thus an effective alternative to classical PWM techniques, provided that sufficiently high switching frequency devices are available. A viable solution to the problem of high frequency switching of high current levels is the employment of a number of parallel connected converters, controlled in such a way as to guarantee a balanced current sharing among them. In the paper, a converter based on the parallel con-

nection of basic building blocks constituted by two-leg three-phase converter, for both parallel and series compensation, is described. This arrangement can provide an alternative topology for STATCOM and SSSC devices. While the STATCOM based on the proposed converter is employed for stabilizing voltage at the point of common coupling with the network, the SSSC is employed for both capacitive and inductive compensation of a transmission line. Both problems can be rearranged into the problem of tracking a reference reactive power. This problem is thereafter translated into the task of tracking a reference voltage which is effectively achieved with a sliding mode controller, which also tackle the problem of balanced current sharing among the parallel connected converters.

The paper is structured as follows: converter configuration and its application for STATCOM operation is presented in Section II, along with mathematical derivations of both references quantities and control action. Series connection for SSSC operation is described in section III. In Section IV results of numerical simulations are reported, showing good tracking performances along with simplicity in design and control. The Conclusion is presented in section V.

## 6.2 Converter Topology, STATCOM Operation and Control

The topology of the proposed converter is illustrated in Fig. 6.1, as well as its shunt connection with the transmission network through a  $\Delta$ -Y transformer\*. The converter is constituted by the parallel connection of  $n$  two-leg three-phase inverters.  $LC$  filters are connected between each inverter output and the coupling transformer, in order to contribute to the smoothing of output voltages. The basic building block has been proposed as a component minimized topology for variable-speed induction motor drives [149, 150] and as a coupled rectifier/inverter system [151]. A three-level NPC variant has also been proposed for active filtering application [152].

Assuming a balanced three-phase operation, the converter output voltage  $\bar{V}_{ab}$  is given by:

$$\bar{V}_{ab} = \bar{V}_{a'} - jx_t \bar{I}_{a'} \quad (6.1)$$

where  $\bar{V}_{a'}$  is the transmission network phase  $a$  p.u. voltage at the point of common coupling,  $\bar{I}_{a'}$  is the STATCOM phase  $a$  p.u. current and  $x_t$  the coupling

---

\*Y-Y connection is equally possible and has been analysed in [148]

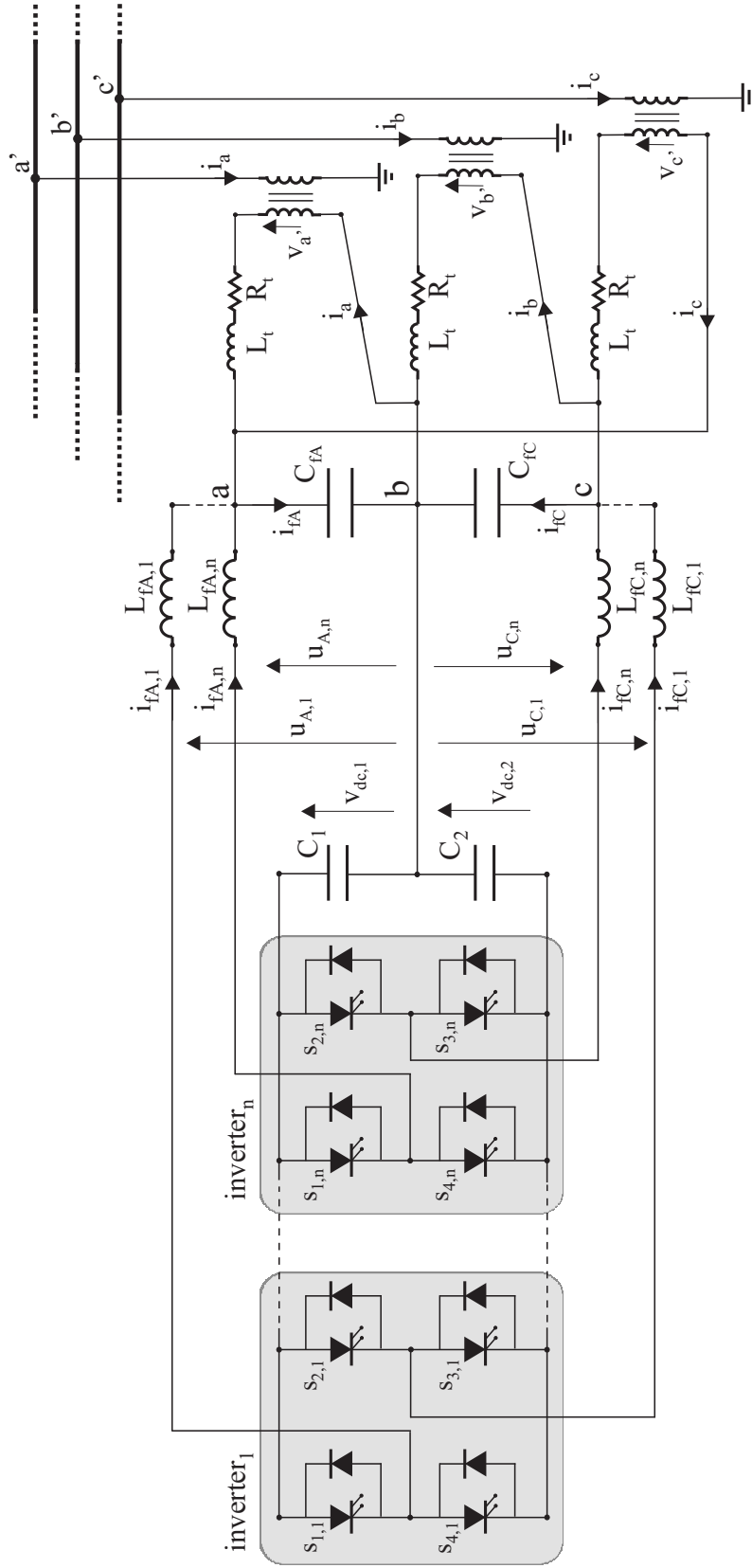


Figure 6.1: Proposed converter topology and parallel connection with the transmission network



transformer leakage reactance. Leakage resistance has been neglected for the sake of simplicity. Voltages  $\bar{V}_{ca}$  and  $\bar{V}_{bc}$  can be derived analogously, and are equal to  $\bar{V}_{ab}$  phase shifted by  $2/3\pi$  and  $4/3\pi$  rad. respectively, as illustrated by the phasor diagram in Fig. 6.2.

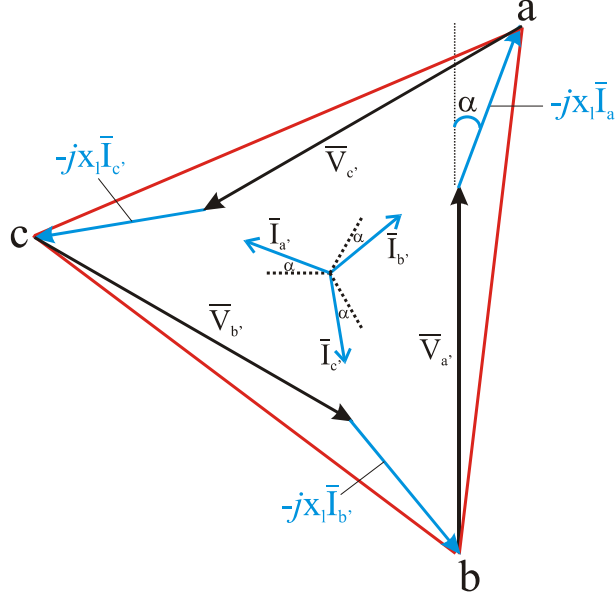


Figure 6.2: Phasor diagram illustrating STATCOM operation in capacitive compensation mode

For the STATCOM to operate as a capacitive compensator the currents  $I_{a',b',c'}$  drawn from the network should lead bus voltages  $\bar{V}_{a',b',c'}$  by  $\pi/2$  rad, while the currents should lag  $\pi/2$  rad behind the voltages when inductive compensation is required. Assuming as a reference the phase of  $\bar{V}_{a'}$  the STATCOM reference phase current is then:

$$\bar{I}_a^{\text{ref}} = I_a^{\text{ref}} e^{j(\pi/2 - \alpha)} \quad (6.2)$$

A phase displacement by an angle  $\alpha$  is necessary for the STATCOM to draw sufficient active power as to compensate for losses in semiconductor devices and coupling transformer, thus maintaining DC voltage at a specified level. The magnitude of reference current, as well as angle  $\alpha$  can be derived by the reference values of active and reactive power as:

$$I_a^{\text{ref}} = I^{\text{ref}} = \frac{\sqrt{P_{\text{ref}}^2 + Q_{\text{ref}}^2}}{V_{a',b',c'}} \quad (6.3)$$

$$\alpha = \frac{\pi}{2} - \tan^{-1} \frac{Q_{\text{ref}}}{P_{\text{ref}}} \quad (6.4)$$

Active and reactive power reference can either be fixed or dynamically adjusted as to regulate some network quantities. The most common STATCOM operation is voltage regulation at the point of common coupling. With this aim in mind, two simple PI regulators, as reported in Fig. 6.3, are adopted in the paper. The difference between network voltage magnitude and a reference is passed through a PI controller which determines the amount of reactive power compensation required. A regulation droop is usually present in practical arrangements and can be easily added. Another PI regulator maintains DC voltage at a specified level, by determining the amount of active power necessary for converter losses compensation. More complex control schemes, which could further enhance system dynamic behaviour, are equally possible but, since the main focus is on the tracking capabilities of the proposed converter and control, only the simplest are presented.

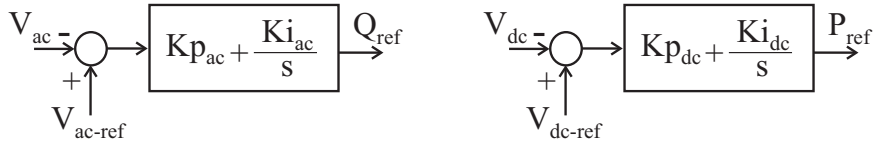


Figure 6.3: Ac and Dc control systems

Reference values for magnitude and phase of converter output voltage are then:

$$|\bar{V}_{ab}^{\text{ref}}| = \sqrt{(V_{a'} + x_t I_a^{\text{ref}} \cos \alpha)^2 + (x_t I_a^{\text{ref}} \sin \alpha)^2} \quad (6.5)$$

$$\angle \bar{V}_{ab}^{\text{ref}} = \angle \bar{V}_{a'} - \tan^{-1} \frac{x_t I_a^{\text{ref}} \sin \alpha}{V_{a'} + x_t I_a^{\text{ref}} \cos \alpha} \quad (6.6)$$

$\bar{V}_{ca}$  and  $\bar{V}_{bc}$  can be derived by phase shifting  $\bar{V}_{ab}$  by  $2/3\pi$  and  $4/3\pi$  rad, respectively. In practical application a Phase-Locked Loop (PLL) is necessary to synchronise with network voltage.

Time domain converter equations are presented in the following.

### 6.2.1 Converter equations

Voltages on ac filter capacitances are:

$$\begin{aligned} \frac{dv_{ab}}{dt} &= \frac{1}{C_{fA}} i_{fA} \\ \frac{dv_{cb}}{dt} &= \frac{1}{C_{fC}} i_{fC} \end{aligned} \quad (6.7)$$

where:

$$\begin{aligned} i_{fA} &= \sum_{k=1}^n i_{fA,k} + i_a - i_c \\ i_{fC} &= \sum_{k=1}^n i_{fC,k} + i_c - i_b \end{aligned} \quad (6.8)$$

Current in filter inductances are given by:

$$\begin{aligned} \frac{di_{fA,k}}{dt} &= \frac{1}{L_{fA,k}} (u_{A,k} - v_{ab}) \\ \frac{di_{fC,k}}{dt} &= \frac{1}{L_{fC,k}} (u_{C,k} - v_{cb}) \quad k \in \{1, \dots, n\} \end{aligned} \quad (6.9)$$

The control inputs  $u_{A,k}, u_{C,k}$  to  $LC$  filters are given by:

$$\begin{aligned} u_{A,k} &= s_{1,k}v_{dc,1} - s_{4,k}v_{dc,2} \\ u_{C,k} &= s_{2,k}v_{dc,1} - s_{3,k}v_{dc,2} \end{aligned} \quad (6.10)$$

where:

$$s_{i,k} = \begin{cases} 1 & \text{if the } i\text{-th switch is on} \\ 0 & \text{if the } i\text{-th switch is off} \end{cases} \quad i \in \{1, \dots, 4\} \quad (6.11)$$

Currents in the primary of the coupling transformer are:

$$\begin{aligned} \frac{di_a}{dt} &= \frac{1}{L_t} (-R_t i_a - v_{ab} + v_{a'}) \\ \frac{di_b}{dt} &= \frac{1}{L_t} (-R_t i_b + v_{cb} + v_{b'}) \\ \frac{di_c}{dt} &= \frac{1}{L_t} (-R_t i_c + v_{ab} - v_{cb} + v_{c'}) \end{aligned} \quad (6.12)$$

Equations (6.7)-(6.12) can be easily rearranged in the state-space form as:

$$\begin{aligned} \dot{\mathbf{x}} &= \mathbf{Ax} + \mathbf{Bu} + \mathbf{Dd} \\ \mathbf{y} &= \mathbf{Cx} \end{aligned} \quad (6.13)$$

where the state variables  $\mathbf{x}$ , the controllable and uncontrollable inputs  $\mathbf{u}, \mathbf{d}$ , respectively, are given by:

$$\begin{aligned} \mathbf{x} &= [v_{ab}, v_{cb}, i_{fA,n}, \dots, i_{fA,1}, i_{fC,n}, \dots, i_{fC,1}, i_a, i_b, i_c]^\top \\ \mathbf{u} &= [u_{A,n}, \dots, u_{A,1}, u_{C,n}, \dots, u_{C,1}]^\top \\ \mathbf{d} &= [v_{a'}, v_{b'}, v_{c'}]^\top \end{aligned} \quad (6.14)$$

and the output  $\mathbf{y}$  is:

$$\mathbf{y} = [v_{ab}, v_{cb}]^\top \quad (6.15)$$

### 6.2.2 Variable Structure Control

Due to the switching action of power devices, power converters naturally belong to the class of variable structure systems, whose structure changes according to some control law. Variable structure control (VSC) is a feedback control action widely employed for this kind of systems. VSC have been proposed for a variety of mechanical and electrical systems, also including power converters [153], power systems [154] and electrical drives [155]. The design of a VSC for a given system entails the choice of a switching control law with the aim of forcing system's state trajectory towards a properly designed sliding surface in the state space, described by  $\Sigma(\mathbf{x}, t) = \mathbf{0}$ . Once the sliding surface is reached, the VS controller must preserve the motion of system's trajectory on it, giving rise to the so-called sliding mode. Control objectives should be taken into account for an appropriate design of the sliding surface. In the present case, the goals of the controller can be itemized as:

1. Regulation of output voltages  $v_{ab}, v_{cb}$
2. Balanced current sharing among parallel connected inverters

Keeping these aims in mind, the following sliding surface is proposed, utilizing the circular chain control strategy from [156]:

$$\Sigma(\mathbf{x}, t) = [\sigma_{A,1}, \dots, \sigma_{A,n}, \sigma_{C,1}, \dots, \sigma_{C,n}]^T = \mathbf{0} \quad (6.16)$$

where:

$$\begin{aligned} \sigma_{A,h} &= (v_{ab} - v_{ab}^{\text{ref}}) + \alpha \left( \frac{dv_{ab}}{dt} - \frac{dv_{ab}^{\text{ref}}}{dt} \right) + \\ &\quad \beta (i_{fA,h} - i_{fA,k}) \\ \sigma_{C,h} &= (v_{cb} - v_{cb}^{\text{ref}}) + \alpha \left( \frac{dv_{cb}}{dt} - \frac{dv_{cb}^{\text{ref}}}{dt} \right) + \\ &\quad \beta (i_{fC,h} - i_{fC,k}) \end{aligned} \quad (6.17)$$

with :

$$\begin{aligned} k &= n, & \text{if } h &= 1 \\ k &= h - 1, & \text{if } h &= 2, \dots, n \end{aligned}$$

The first two terms on the rhs of (6.17) account for output voltage regulation, while the third for balanced current sharing among parallel connected converters. The derivative term is added recognizing that the relative degree (i.e. the order of the derivative of the output  $\mathbf{y}$  required for the input  $\mathbf{u}$  to appear explicitly

[146]) is two [157]. Once the sliding surface is hit at  $t = t_0$ , the sliding mode occurs if and only if:

$$\dot{\Sigma}(\mathbf{x}, t) = \frac{\partial \Sigma}{\partial \mathbf{x}} \cdot \dot{\mathbf{x}} + \frac{\partial \Sigma}{\partial t} = \mathbf{0}, \quad \forall t > t_0 \quad (6.18)$$

The equivalent control  $\mathbf{u}_{\text{eq}}$  given by:

$$\mathbf{u}_{\text{eq}} = - \left( \frac{\partial \Sigma}{\partial \mathbf{x}} \cdot \mathbf{B} \right)^{-1} \cdot \left[ \frac{\partial \Sigma}{\partial \mathbf{x}} \cdot (\mathbf{A}\mathbf{x} + \mathbf{D}\mathbf{d}) + \frac{\partial \Sigma}{\partial t} \right] \quad (6.19)$$

assuming  $\det \left[ \left( \frac{\partial \Sigma}{\partial \mathbf{x}} \right) \cdot \mathbf{B} \right] \neq 0$ , describes an equivalent smooth feedback control that forces state trajectory of system (6.13) to stay on  $\Sigma(\mathbf{x}, t) = \mathbf{0}$ . Direct application of Proposition 1 in [158] to the present case demonstrates that a sliding mode exists if and only if  $\forall \mathbf{x} \in \{\mathbf{x} : \Sigma = \mathbf{0}\}$  each component  $u_{k,\text{eq}}$  of the equivalent control  $\mathbf{u}_{\text{eq}}$  satisfies:

$$-v_{dc,2} < u_{k,\text{eq}} < v_{dc,1} \quad (6.20)$$

This condition is fulfilled provided that voltages on dc capacitors are sufficiently high.

A reaching condition, sufficient for the trajectory of system's state to reach the sliding surface is:

$$\left( \frac{d\Sigma}{dt} \right)^{\top} \cdot \Sigma < 0 \quad (6.21)$$

Condition (6.21) guarantees that the time derivative of the quadratic function:

$$\mathcal{V} = 1/2 \Sigma^{\top} \cdot \Sigma \quad (6.22)$$

is negative definite, thus (6.22) qualifies as a Lyapunov function, demonstrating asymptotic stability of the state  $\Sigma = \mathbf{0}$ . In single input control problem actual control is derived as to fulfill condition (6.21). Since system (6.13) is a multi-input system,  $2n$  actual controls would appear in a coupled manner in (6.22) thus making impossible to derive appropriate control actions. A linear time-invariant transformation:

$$\hat{\Sigma} = \Omega \cdot \Sigma \quad (6.23)$$

with  $\Omega$  a nonsingular matrix, is chosen in order to transform the coupled multi-input control problem into  $2n$  decoupled single input problems [147]. Motion on the sliding surface is not altered by transformation (6.23) since the equivalent

control can be easily derived to be the same as (6.19). Furthermore, since  $\Omega$  is nonsingular,  $\Sigma = \mathbf{0} \Leftrightarrow \hat{\Sigma} = \mathbf{0}$ . The candidate Lyapunov function is now:

$$\hat{\mathcal{V}} = 1/2 \hat{\Sigma}^\top \cdot \hat{\Sigma} \quad (6.24)$$

whose time derivative is:

$$\frac{d\hat{\mathcal{V}}}{dt} = \hat{\Sigma}^\top \cdot \Omega \cdot \left[ \frac{\partial \Sigma}{\partial \mathbf{x}} \cdot (\mathbf{Ax} + \mathbf{Bu} + \mathbf{Dd}) + \frac{\partial \Sigma}{\partial t} \right] \quad (6.25)$$

If  $\Omega$  is chosen such that:

$$\Omega \cdot \frac{\partial \Sigma}{\partial \mathbf{x}} \cdot \mathbf{B} = \mathbf{I} \iff \Omega = \left( \frac{\partial \Sigma}{\partial \mathbf{x}} \cdot \mathbf{B} \right)^{-1} \quad (6.26)$$

where  $\mathbf{I}$  is the identity matrix, then the time derivative of the function  $\hat{\mathcal{V}}$  is:

$$\frac{d\hat{\mathcal{V}}}{dt} = \hat{\Sigma}^\top \cdot \Omega \cdot \left[ \frac{\partial \Sigma}{\partial \mathbf{x}} \cdot (\mathbf{Ax} + \mathbf{Dd}) + \frac{\partial \Sigma}{\partial t} \right] + \hat{\Sigma}^\top \cdot \mathbf{u} \quad (6.27)$$

Expression for  $\Omega$  in the present case is given in Appendix B.

A negative definite term is added to (6.27) if the control inputs are chosen as:

$$u_{A,i}, u_{C,i} = \begin{cases} u^+ = v_{dc,1} & \text{if } \hat{\sigma}_i < 0 \\ u^- = -v_{dc,2} & \text{if } \hat{\sigma}_i > 0 \end{cases} \quad (6.28)$$

Again, if dc voltages are sufficiently high, the reaching condition is satisfied, allowing sliding surface to be reached in finite time. Direct application of (6.28) would require an infinite switching frequency. In practical realisation an hysteresis band  $HB$  is considered in order to provide a finite and sufficiently low switching frequency.

### 6.3 Converter Topology, SSSC Operation and Control

The series connected converter is reported in Fig. 6.4. Apart from network connection, the converter and the filtering interface are the same as those already described for the STATCOM, thus their functions and equations will not be repeated here. The role of a series compensator is to provide a capacitive compensation for long transmission lines. As for STATCOM, besides the main objective, supplementary controls could be added to provide additional capabilities such as current, power flow control and damping of power oscillations. Although capacitive compensation is the most common operation of the SSSC, inductive compensation could be required in some circumstances, as well.

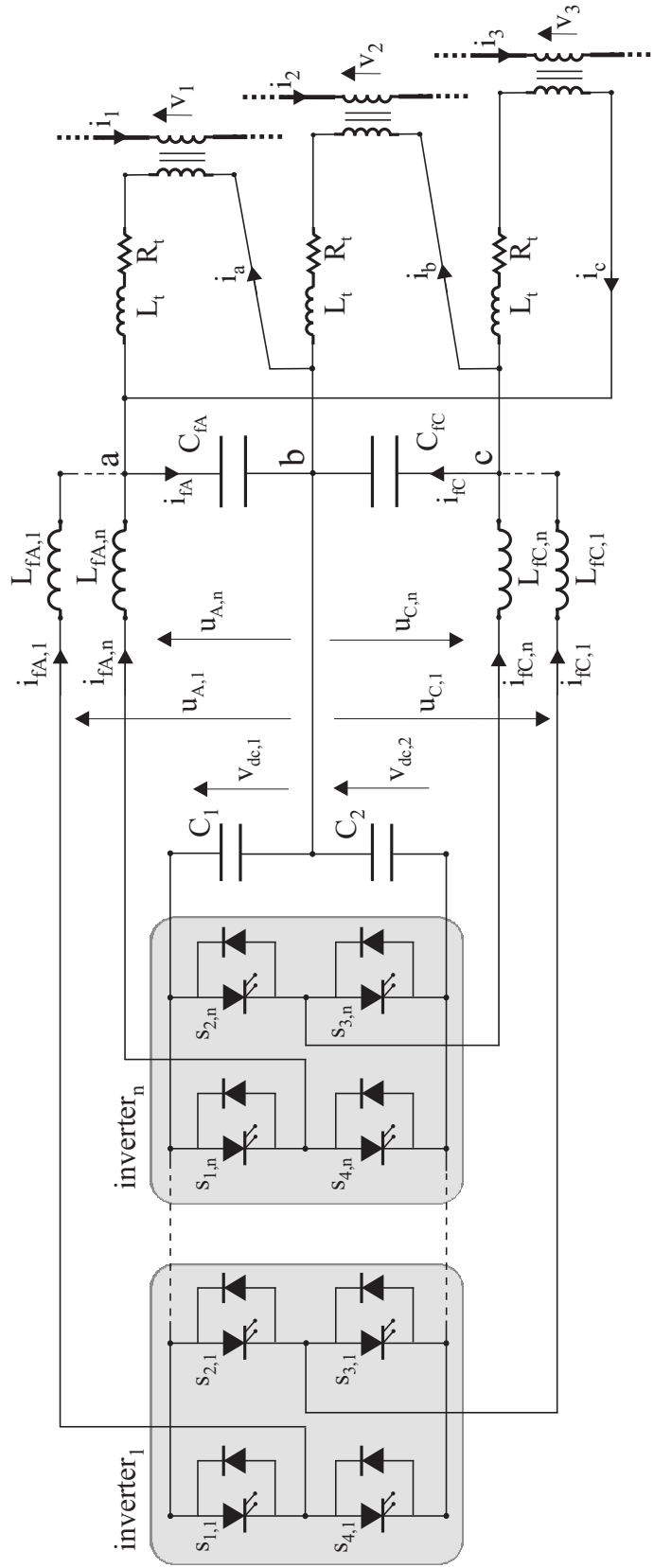


Figure 6.4: Proposed converter topology and series connection with the transmission network

Phasor diagram reported in Fig. 6.5 illustrates the principle of capacitive compensation of SSSC, which injects three-phase voltages  $\pi/2$  rad lagging line currents. Again, an angle  $\alpha \neq 0$  is required for active power to flow into the converter in order to compensate for losses.

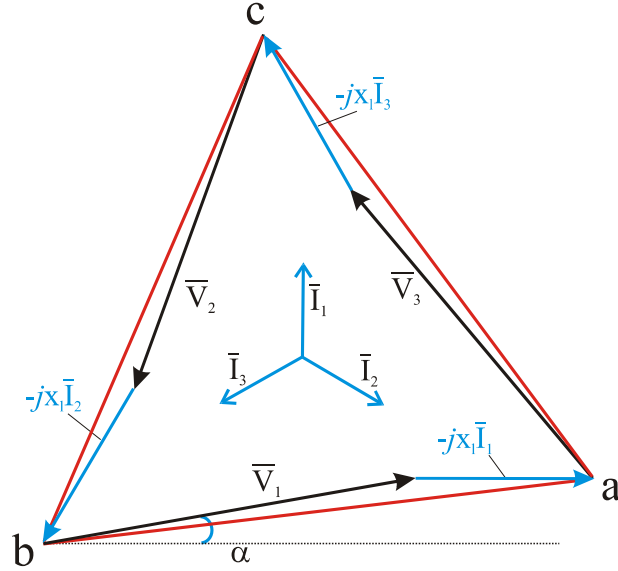


Figure 6.5: Phasor diagram illustrating SSSC operation in capacitive compensation mode

The following relationships, assuming balanced three-phase capacitive operation, are easily derived:

$$\bar{V}_{ab} = \bar{V}_1 - jx_t \bar{I}_a, \quad \bar{I}_a = \bar{I}_1 \quad (6.29)$$

Injected series voltage is:

$$\bar{V}_1 = -jx_{\text{comp}} |\bar{I}_1| e^{j(\angle \bar{I}_1 + \alpha)} \quad (6.30)$$

where  $x_{\text{comp}}$  is the desired compensator equivalent reactance. Magnitude and phase of converter output reference voltage are:

$$|\bar{V}_{ab}^{\text{ref}}| = |\bar{I}_1| \cdot \sqrt{(x_{\text{comp}} \cos \alpha + x_t)^2 + (x_{\text{comp}} \sin \alpha)^2} \quad (6.31)$$

$$\angle \bar{V}_{ab}^{\text{ref}} = \angle \bar{I}_1 - \tan^{-1} \frac{x_t + x_{\text{comp}} \cos \alpha}{x_{\text{comp}} \sin \alpha} \quad (6.32)$$

Again,  $\bar{V}_{ca}$  and  $\bar{V}_{bc}$  can be derived by phase shifting  $\bar{V}_{ab}$  by  $2/3\pi$  and  $4/3\pi$  rad, respectively.



## 6.4 Numerical Simulations

Numerical simulations for both compensators are reported in the following.

### 6.4.1 STATCOM

The test system reported in Fig. 6.6, adapted from [60], is employed for STATCOM simulation. It consists of a three-phase 230kV ideal generator which feeds a load area through a transmission line and a step-down transformer. Three loads are switched sequentially, in order to provide different operating conditions. The proposed STATCOM is shunt connected to bus  $B_2$  through a coupling transformer. Network data are reported in Fig. 6.6 while converter and controller data are given in Appendix C. The converter utilized in numerical simulations is constituted by three parallel connected inverters.

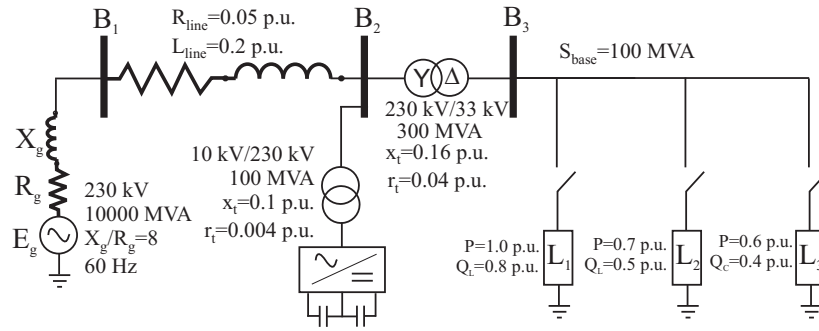


Figure 6.6: 230kV test system for STATCOM simulation

Load  $L_1$  is connected from the beginning of simulation. At  $t = 0.5$ s a second inductive load  $L_2$  is connected, while load  $L_3$  which has a capacitive component is switched on at  $t = 0.75$ s. At  $t = 1$ s loads  $L_1$  and  $L_2$  are both disconnected, leaving only the capacitive load, resulting in inductive operation of the STATCOM, as shown in Fig. 6.7 where both measured reactive power absorbed by the converter and its reference are shown.

The magnitude of voltage at the regulated bus  $B_2$  and the magnitude of the current absorbed by the STATCOM are plotted in Fig. 6.8. Dc capacitor voltages and the angle  $\alpha$  are shown in Fig. 6.9.

Phase  $a$  voltage and current at STATCOM output at the passage from capacitive (voltage lagging) to inductive (voltage leading) mode of operation are reported in Fig. 6.10.

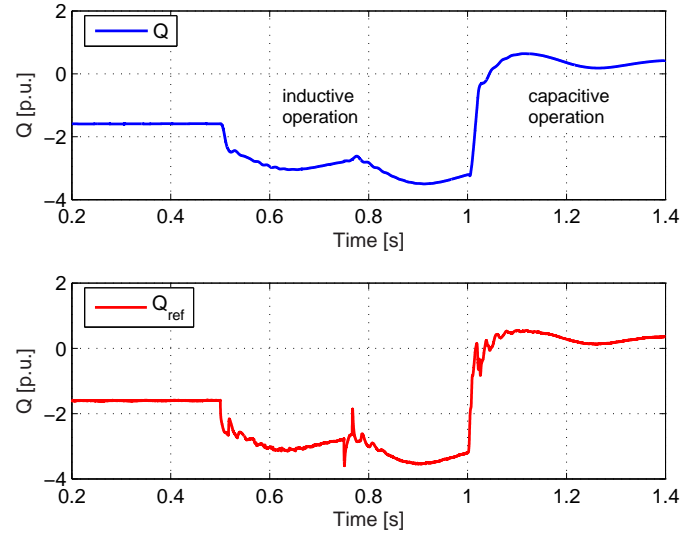


Figure 6.7: Actual (top) and reference (bottom) reactive power absorbed by the STATCOM

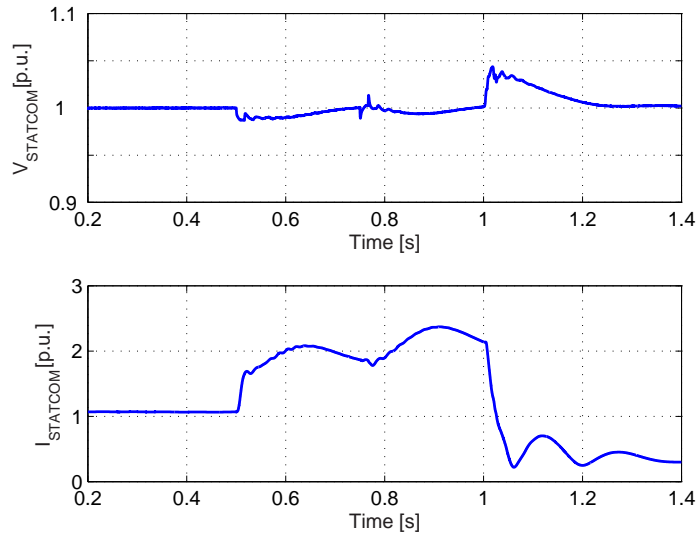
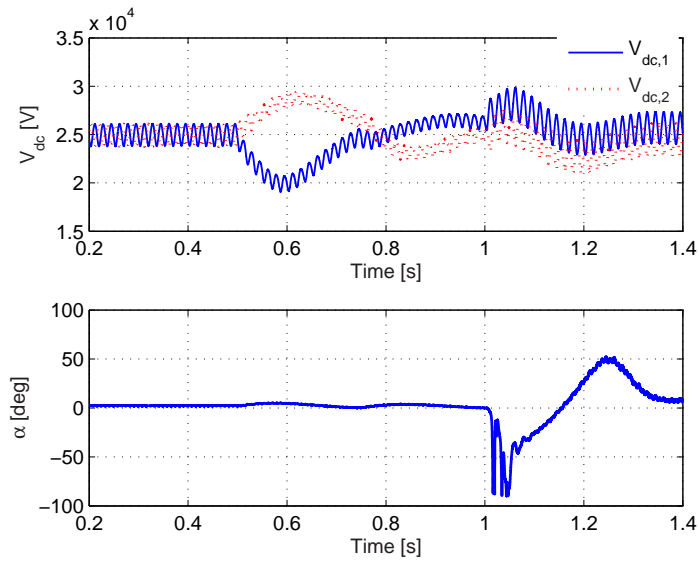
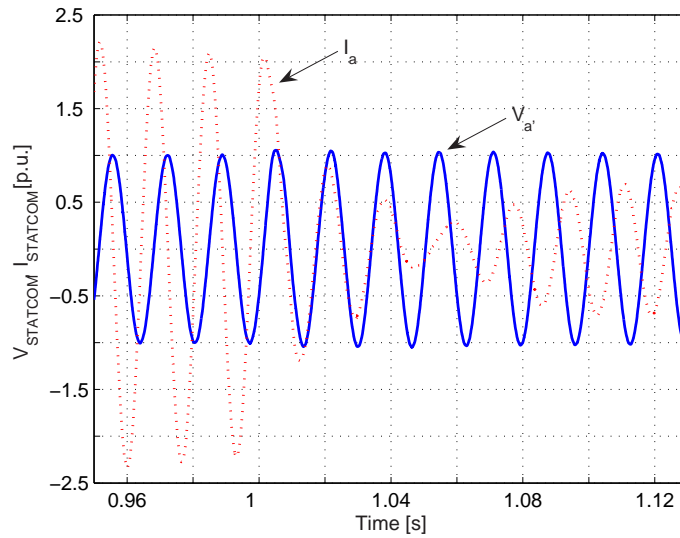


Figure 6.8: Magnitude of voltage (top) and current (bottom) at STATCOM output

RMS values of phase *a* output current of the three converters are reported in Fig. 6.11. Despite different values for filter inductances, the current sharing is good. A higher number of parallel connected inverters could be easily added to

Figure 6.9: Dc capacitors voltages (top) and angle  $\alpha$  (bottom)Figure 6.10: Phase  $a$  STATCOM voltage and current

lower the current through each of them.

Voltage across filter capacitance  $v_{ab}$  and its reference  $v_{ab}^{\text{ref}}$  are reported in Fig. 6.12. Good tracking performances are obtained, resulting in low distortion of output voltage, as demonstrated by a THD value well below 0.1% as shown in Fig. 6.13. Sliding mode control results in a variable switching frequency. By

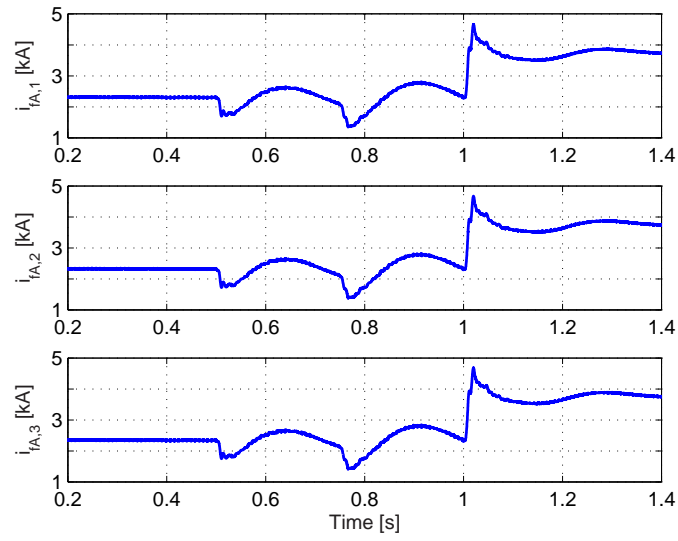


Figure 6.11: Current RMS in filter inductances

means of a running window the number of commutations in a period has been evaluated and its maximum has been found to result in a maximum switching frequency as low as 1250Hz.

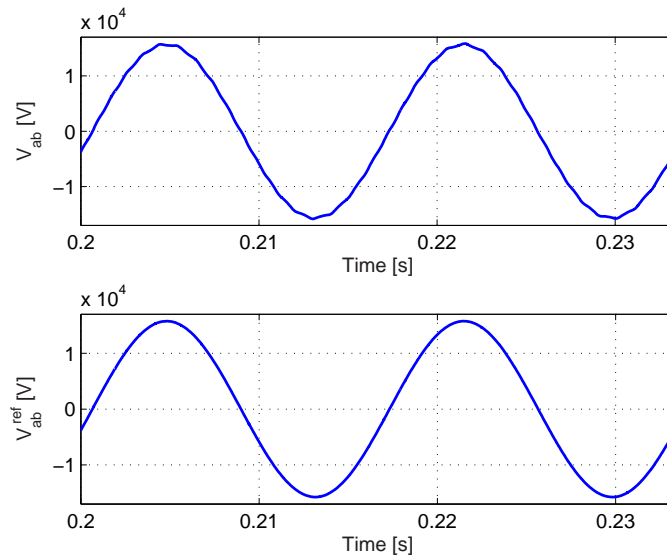
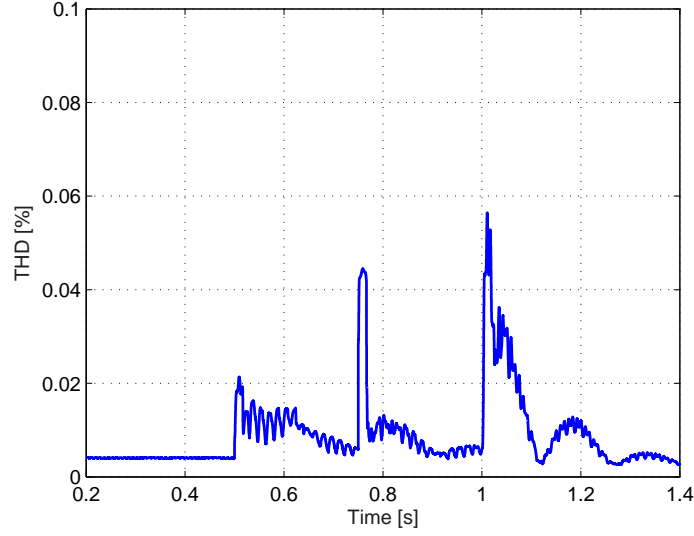


Figure 6.12:  $v_{ab}$  (top) and  $v_{ab}^{ref}$  (bottom)

Figure 6.13: Total Harmonic Distortion of bus  $B_2$  voltage

### 6.4.2 SSSC

The test system used in SSSC simulations is reported in Fig. 6.14 [60]. Different operating conditions are tested by switching on and off three loads and correspondingly changing the reference SSSC reactance. Load  $L_1$  is connected from the beginning of the simulation while inductive load  $L_2$  and capacitive load  $L_3$  are switched on at  $t = 0.25s$  and  $t = 0.5s$ , respectively. At  $t = 0.75s$  loads  $L_1$  and  $L_2$  are both switched off while compensator goes into inductive compensation.

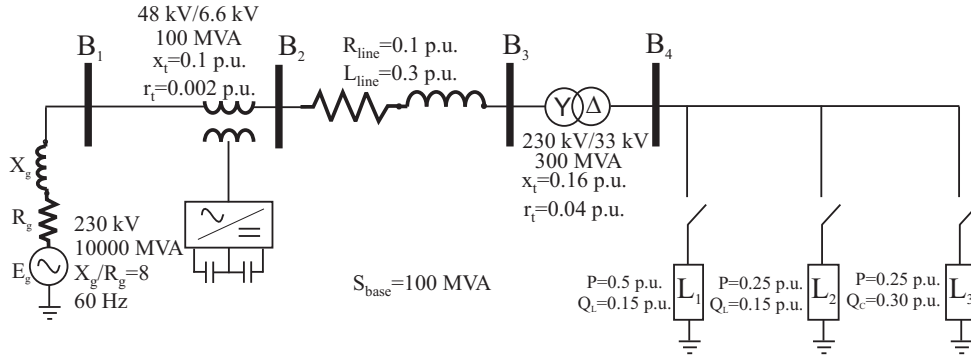


Figure 6.14: 230kV test system for SSSC simulation

Figure 6.15 shows equivalent reference reactance and the active and reactive power absorbed by the compensator. Magnitude of injected voltage and cur-

rent through SSSC are reported in Fig. 6.16, while Fig. 6.17 shows dc voltages and angle  $\alpha$ . Phase 1 voltage and current of the SSSC, following the removal of inductive loads, thus determining the passage from capacitive to inductive compensation, is reported in Fig. 6.18. RMS values of phase 1 output current of the three converters are reported in Fig. 6.19. As for STATCOM good tracking performances are obtained with respect to output voltages with a switching frequency lower than 1250Hz, which result in a THD level well below 0.1%.

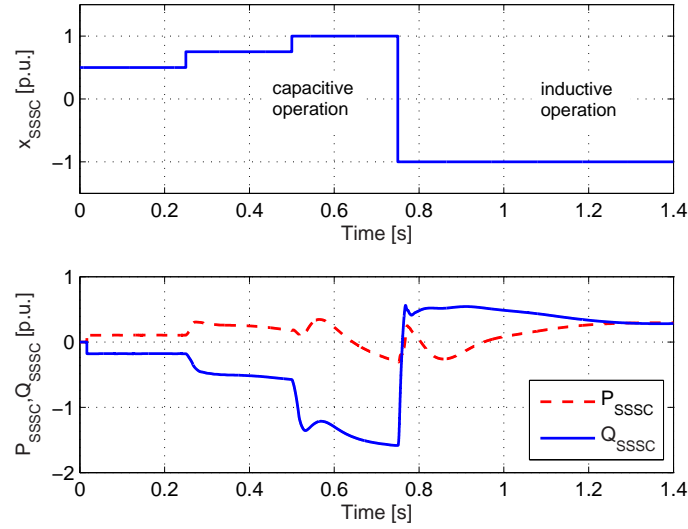


Figure 6.15: SSSC equivalent reactance (top). Active and reactive power absorbed by SSSC (bottom)

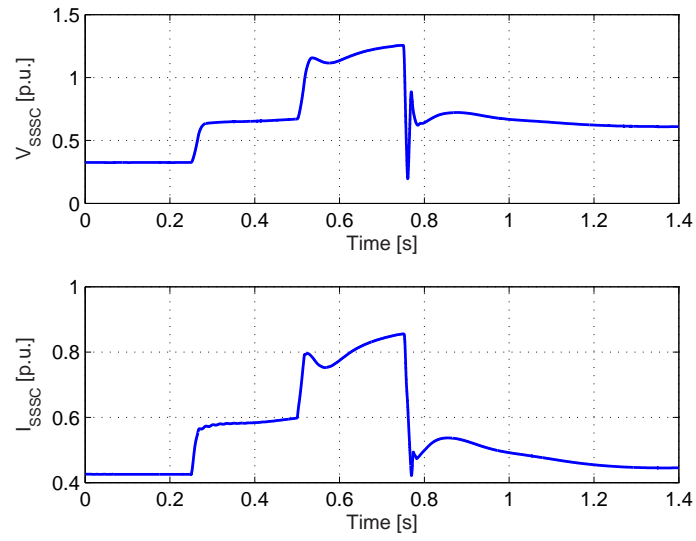


Figure 6.16: Magnitude of injected voltage (top) and current through SSSC (bottom)

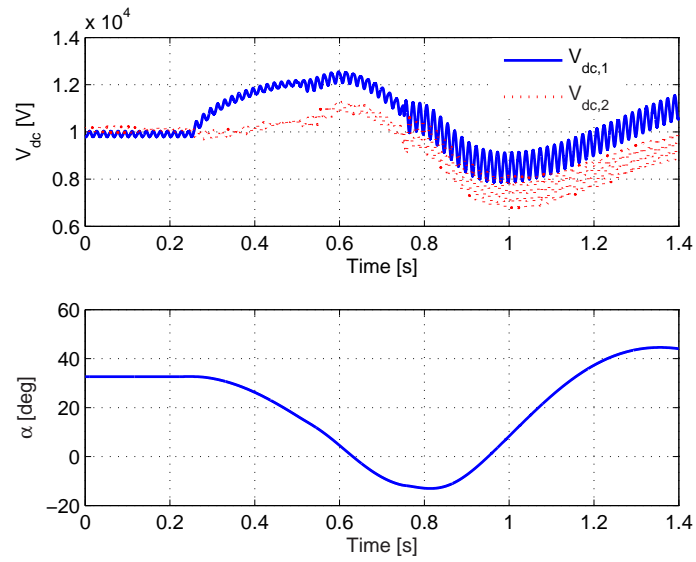


Figure 6.17: Dc capacitors voltages (top) and angle  $\alpha$  (bottom)

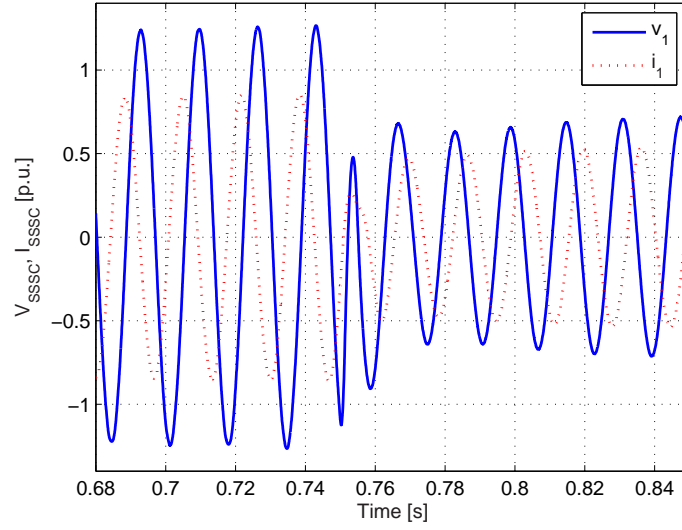


Figure 6.18: Phase 1 SSSC voltage and current

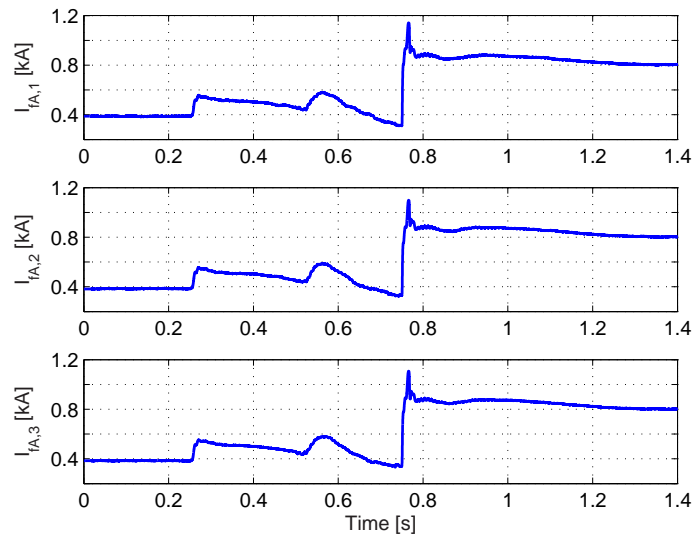


Figure 6.19: Current RMS in filter inductances



## 6.5 Converter control for active power exchange

A suitable controlled FACTS device can exchange active power if some sort of energy source or storage system is available. Several devices capable of storing electromagnetic, mechanical or chemical energy, ranging from ultra and hyper-capacitors, batteries and flywheel were proposed in literature for power applications [62]. However, Superconducting Magnetic Energy Storage (SMES) devices appear as the most viable and cost effective solution for high power applications.

A SMES system contains an inductor (the SMES coil) whose superconducting properties are maintained at very low temperatures by a cryogenic system. Energy in a SMES coil whose inductance is  $L_{SMES}$ , is given by:

$$E = \frac{1}{2} L_{SMES} I_{SMES}^2 \quad (6.33)$$

This energy is stored in the magnetic field produced by the current  $I_{SMES}$  flowing, with zero resistance, in the coil.

Although the costs of the superconducting coil and its associated refrigeration system are still very high, the main cost of a complete SMES system is due to the power electronic interface with AC network. The cost of the DC-AC converter is avoided if the SMES coil is connected to an already existing FACTS device, thus making this solution attractive also from an economical viewpoint [62].

DC current flows in the SMES coil, which is either charged or discharged depending upon the sign of the applied voltage. If zero voltage is applied to the coil the SMES is in stand-by mode, maintaining constant DC current.

The proposed power conditioning system for SMES-based FACTS devices is given in Fig. 6.20. A DC-DC chopper allows the exchange of power between the inverter and the superconducting coil. It maintains the proper voltage across the coil terminals, applying the capacitor voltage during the charging mode and reversing this voltage during the discharging mode. It also provides a free-wheeling path to the coil current when no power exchange is needed. The basic chopper topology is presented in Fig. 6.21, while the equivalent circuits during charging and discharging modes are given in Figs. 6.22, 6.23, respectively [159, 160].

The evolution of coil current is governed by the following differential equation:

$$\begin{aligned} L_{SMES} \frac{di_{SMES}}{dt} &= u_{ch} v_C \quad \text{Charging} \\ L_{SMES} \frac{di_{SMES}}{dt} &= -\bar{u}_{dis} v_C \quad \text{Discharging} \end{aligned} \quad (6.34)$$

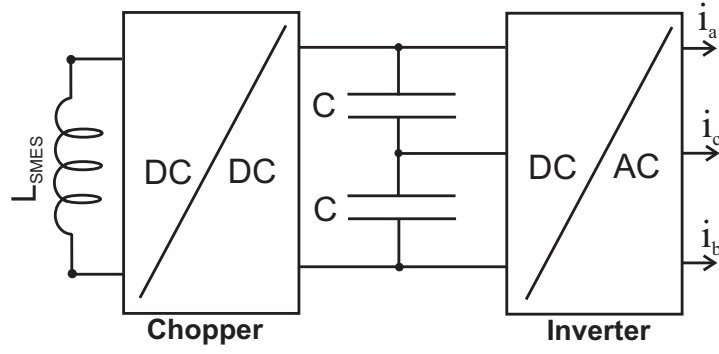


Figure 6.20: Proposed power conditioning system for SMES-based FACTS devices

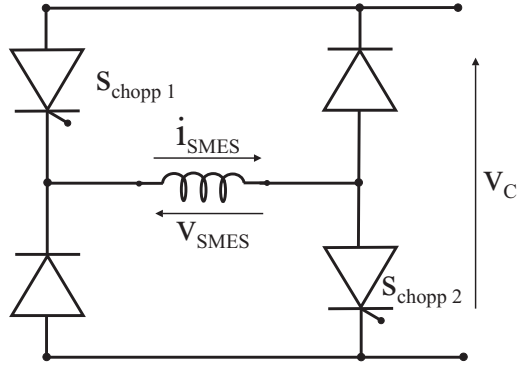


Figure 6.21: SMES DC-DC chopper

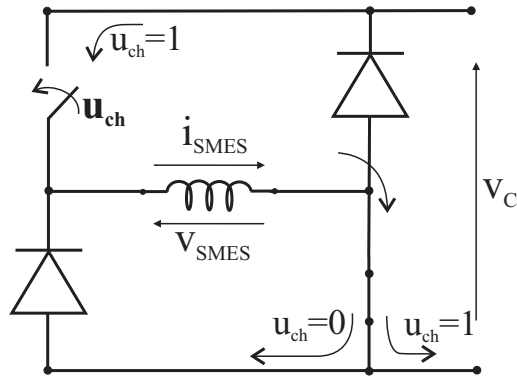


Figure 6.22: SMES DC-DC chopper in charging mode

where  $v_C = v_{Ca} - v_{Cb}$ ,  $u_{ch}$  and  $u_{dis}$  are boolean variables governing the state of the two switches in the chopper,  $\bar{u}_{dis}$  stands for the complementary of  $u_{dis}$ .

The switching signals during both charging and discharging modes are sum-

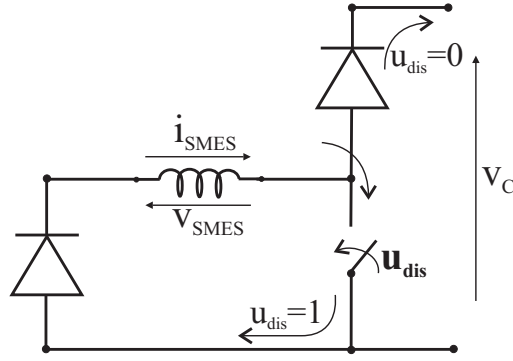


Figure 6.23: SMES DC-DC chopper in discharging mode

marized in Tables 6.1 and 6.2, respectively.

$s_{chop1}$	$s_{chop2}$	$u_{ch}$	$V_{SMES}$
0	1	0	0
1	1	1	$V_C$

Table 6.1: Chopper switching signals during charging mode

$s_{chop1}$	$s_{chop2}$	$u_{dis}$	$V_{SMES}$
0	0	0	$-V_C$
0	1	1	0

Table 6.2: Chopper switching signals during discharging mode

The following simple sliding surface is proposed for chopper control during transients when active power exchange is required:

$$S_{chopper} = s_{chopper}(v_{DC,ref} - v_{DC}) \quad (6.35)$$

where  $v_{DC} = v_{DC,1} + v_{DC,2}$ , therefore acting to restore the reference DC voltage. If  $S_{chopper} > 0$  then  $v_{DC} < v_{DC,ref}$  and the chopper enters into discharging mode, with coils discharging to recover DC voltage. If  $S_{chopper} < 0$  then  $v_{DC} > v_{DC,ref}$  and the chopper enters into charging mode drawing current from DC side to charge SMES coil and decrease DC voltage.

Results of numerical simulations are reported in Figs. 6.24-6.27 with respect to the series connected compensator used for oscillation damping in the previous

chapter. Results for shunt connected compensator are analogous and are not reported for the sake of brevity.

Figures 6.24 and 6.25 reports real and imaginary parts of injected series voltages, respectively, as well as their reference values as obtained in the previous chapter. The fault happens at 0.1 s, and the first 10 seconds of simulation are shown. Figure 6.26 shows SMES coil current and the applied voltage, while Fig. 6.27 shows DC capacitor voltages. Again good tracking performances are obtained.

The chosen value for  $L_{SMES}$  is 5 H, resulting in a stored energy, at the rated current value of 6000 A lower than 100 MJ. A 100 MJ SMES demonstration is being built at Florida State University [161] for research and educational purposes.

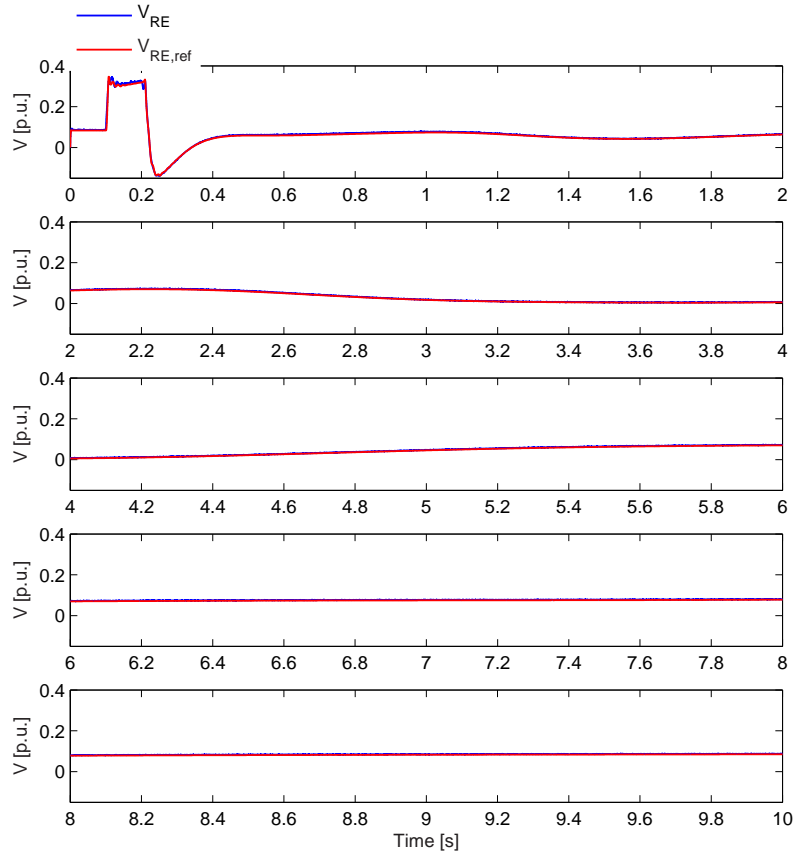
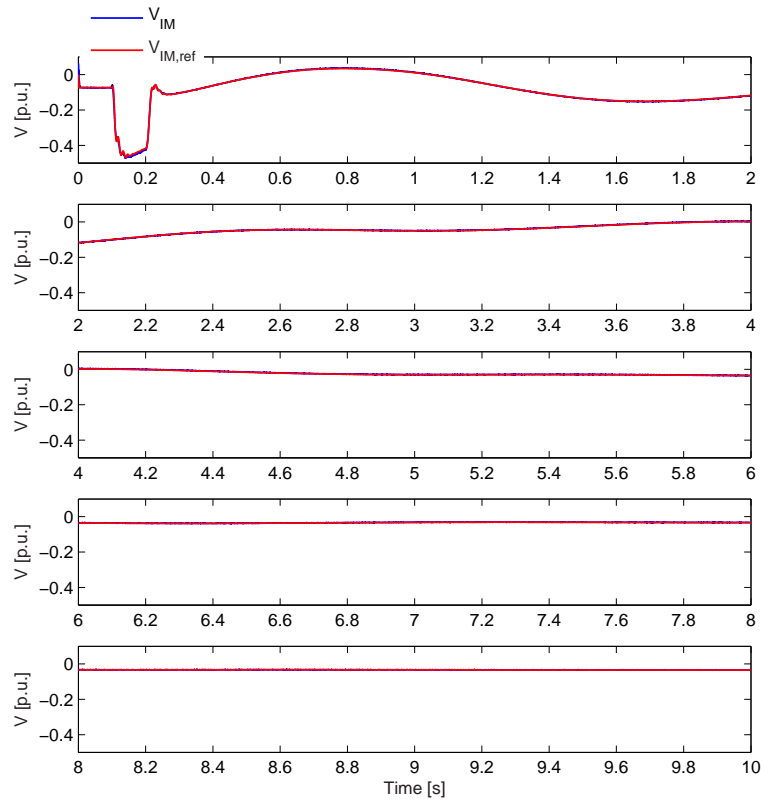


Figure 6.24:  $V_{RE}$  and  $V_{RE,rm}$

Figure 6.25:  $V_{IM}$  and  $V_{IM,rm}$ 

## 6.6 Conclusion

In the chapter a converter constituted by the parallel operation of basic building blocks is utilised for both series and parallel reactive power compensation, thus proposing an alternative topology for FACTS devices. Each building block is the most basic two-leg three-phase inverter constituted by four switches and a split capacitor. The compensation problem is translated into the task of tracking reference three-phase voltages at converter output. Recognizing the variable structure nature of the converter, the tracking problem is tackled by means of a sliding controller, which also provide a solution to the problem of a balanced current sharing among the two-leg parallel connected inverters. Numerical simulations are reported both for a STATCOM and a SSSC based on the proposed converter, showing simplicity both in control and converter topology, as well as effective tracking performance of the sliding controller.

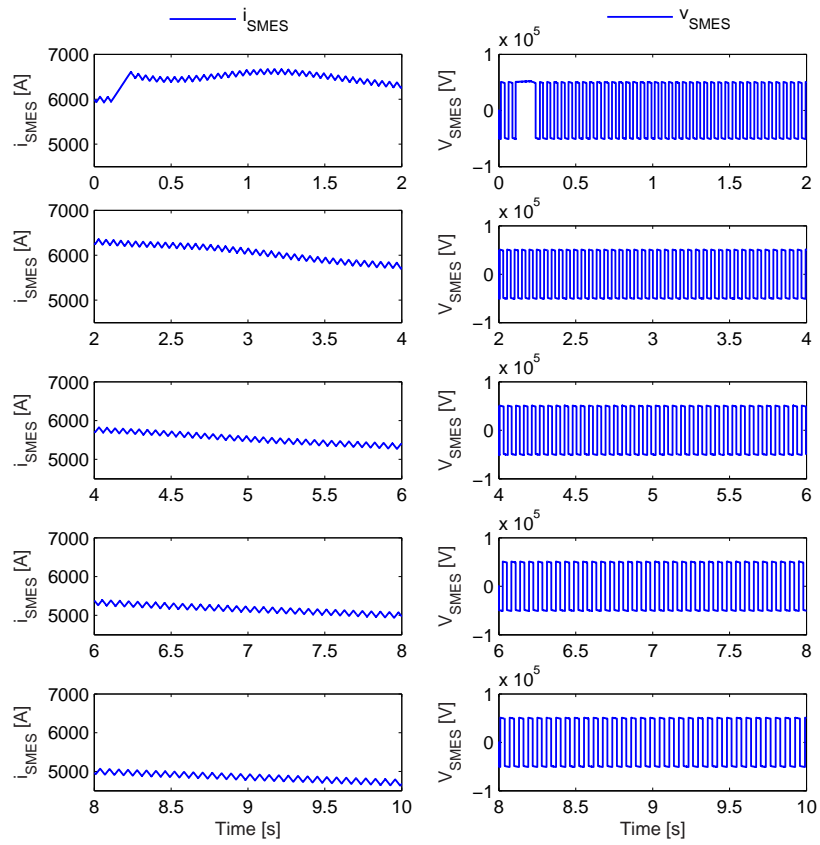


Figure 6.26:  $i_{SMES}$  (left) and  $v_{SMES}$  (right)

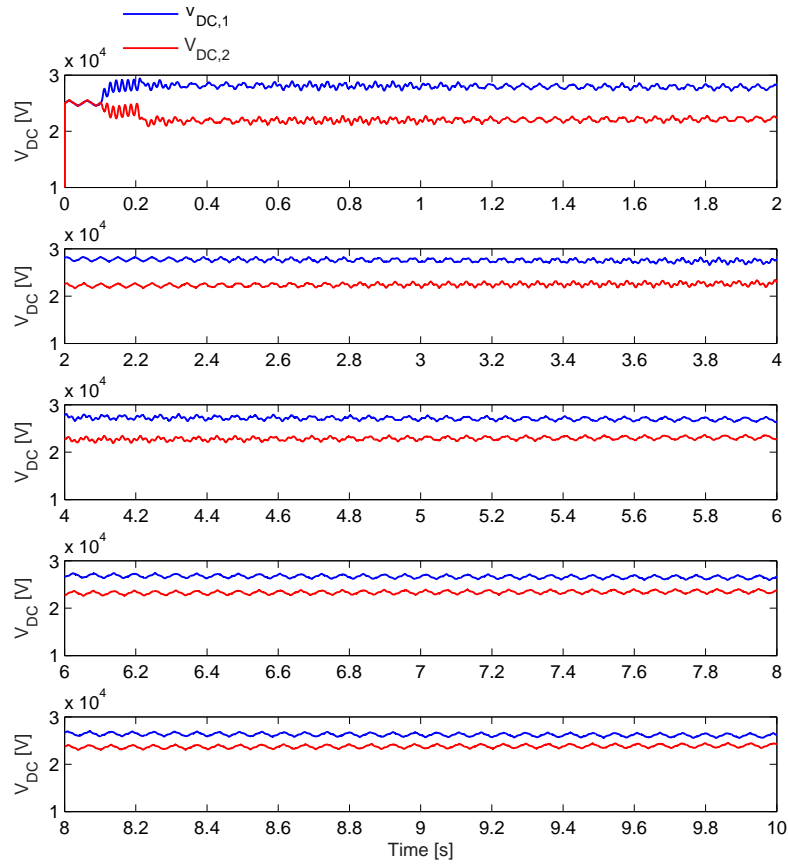


Figure 6.27: DC capacitor voltages





---

# Bibliography

---

- [1] IEEE-Task-Force, “Proposed terms and definition for power system stability,” *IEEE Trans. Power App. Syst.*, vol. 101, pp. 1894–1897, July 1982. [cited at p. 6]
- [2] P. Kundur, J. Paserba, V. Ajjarapu, G. Andersson, A. Bose, C. Canizares, N. Hatziargyriou, D. Hill, A. Stankovic, C. Taylor, T. V. Cutsem, and V. Vittal, “Definition and classification of power system stability,” *IEEE Trans. Power Syst.*, vol. 19, no. 2, pp. 1387–1401, May 2004. [cited at p. 6, 8, 14, 17]
- [3] J. Thorp, C. Seyel, M. Parashar, and A. Phadke, “The large scale electric power system as a distributed continuum,” *IEEE Power Engineering Review*, pp. 49–50, Jan. 1998. [cited at p. 6]
- [4] J. Thorp, C. Seyel, and A. Phadke, “Electromechanical wave propagation in large electrical power systems,” *IEEE Trans. Circuits Syst. I*, pp. 614–622, June 1998. [cited at p. 6]
- [5] M. Parashar, J. Thorp, and C. Seyel, “Continuum modeling of electromechanical dynamics in largescale power systems,” *IEEE Trans. Circuits Syst. I*, pp. 1848–1858, Sept. 2004. [cited at p. 6]
- [6] A. Griffo and D. Lauria, “Optimal reclosure time for improving power-system dynamic behaviour,” *IEE Proceedings Generation, Transmission and Distribution*, vol. 152, no. 6, pp. 939–944, Nov. 2005. [cited at p. 6]
- [7] I. A. Hiskens and M. A. Pai, “Trajectory sensitivity analysis of hybrid systems,” *IEEE Trans. Circuits Syst. I*, vol. 19, no. 2, pp. 204–220, Feb. 2000. [cited at p. 7]

- [8] I. A. Hiskens and P. J. Sokolowski, "Systematic modeling and symbolically assisted simulation of power systems," *IEEE Trans. Power Syst.*, vol. 19, no. 2, pp. 229–234, May 2001. [cited at p. 7]
- [9] I. A. Hiskens and M. A. Pai, "Hybrid systems view of power system modelling," in *Proceedings of the IEEE International Symposium on Circuits and Systems*, no. 2, Geneva, Switzerland, May 2000, pp. 228–231. [cited at p. 7]
- [10] Y. Zou, M. H. Yin, and H. D. Chiang, "Theoretical foundation of the controlling UEP method for direct transient-stability analysis of network-preserving power system models," *IEEE Trans. Circuits Syst.*, vol. 50, no. 10, pp. 1324–1336, Oct. 2003. [cited at p. 7]
- [11] H. Khalil, *Nonlinear Systems, 3rd edition*. Prentice Hall, 2001. [cited at p. 8, 9, 56, 79]
- [12] J. J. Slotine, *Applied Nonlinear Control*. New York: Prentice Hall, 1990. [cited at p. 8, 11, 78]
- [13] S. Sastry, *Nonlinear Systems*. New York: Springer Verlag, 2004. [cited at p. 8, 11, 78, 80, 89]
- [14] A. M. Lyapunov, *The general problem of motion stability*. in Russian-1892: Reprinted in Ann. Math. Study n. 17, 1949, Princeton University Press. [cited at p. 9, 78]
- [15] P. Kundur, *Power system stability and control*. New York: McGraw-Hill Inc., 1994. [cited at p. 14, 17, 20, 25, 32, 33, 36, 45, 46, 52, 65, 70, 97, 151]
- [16] G. Andersson, *Dynamics and Control of Electric Power Systems*. Zurich, Switzerland: EEH - Power Systems Laboratory ETH, 2004. [cited at p. 14]
- [17] V. Knazkins, "Stability of power systems with large amounts of distributed generation," Ph.D. dissertation, KTH Institution for Elektrotekniska System, Stockholm, Sweden, Oct. 2004. [cited at p. 14]
- [18] J. G. Slootweg, H. Polinder, and W. L. Kling, "Dynamic modelling of a wind turbine with doubly fed induction generator," in *IEEE PES Summer Meeting*, July 2001. [cited at p. 16]

- [19] K. Sedghisigarchi and A. Feliachi, "Control of grid-connected fuel cell power plant for transient stability enhancement," in *IEEE PES Winter Meeting*, vol. 1, Jan. 2002, pp. 383–388. [cited at p. 16]
- [20] J. V. Milanovic and T. M. David, "Stability of distribution networks with embedded generators and induction motors," in *IEEE PES Winter Meeting*, vol. 2, 2002, pp. 1023–1028. [cited at p. 16]
- [21] B. C. Pal, "Robust damping of inter-area oscillations in power systems with superconducting magnetic energy storage devices," Ph.D. dissertation, Imperial College, London, United Kingdom, June 1999. [cited at p. 17]
- [22] G. Rogers, *Power system oscillations*. Boston, MA: Kluwer Academic Publisher, 2000. [cited at p. 17, 30, 36]
- [23] F. R. Schleif and J. H. White, "Damping for Northwest-Southwest tie line oscillations- an analogous study," *IEEE Trans. Power App. Syst.*, vol. 85, no. 12, pp. 1234–1247, Dec. 1966. [cited at p. 17]
- [24] N. Martins, A. A. Barbosa, J. C. R. Ferraz, M. G. dos Santos, B. Bergamo, C. S. Yung, V. R. Oliveira, and N. J. P. Macedo, "Retuning stabilizers for the north-south brazilian interconnection," in *Proc. IEEE PES Summer Meeting*, vol. 1, July 1999, pp. 58–67. [cited at p. 17]
- [25] A. Fischer and I. Erlich, "Impact of long-distance power transits on the dynamic security of large interconnected power systems," in *Proc. 2001 IEEE Power Tech. Conf.*, vol. 2, Sept. 2001, p. 6. [cited at p. 17]
- [26] V. Venkatasubramanian and Y. Li, "Analysis of 1996 western american electric blackouts," in *Bulk power systems dynamics and control*, VI, Aug. 2004, pp. 685–721. [cited at p. 18, 19]
- [27] M. A. Pai, *Power system stability by Lyapunov's direct method*. North Holland Publishing, 1981. [cited at p. 19, 80, 82]
- [28] ———, *Energy functions analysis for power system stability*. Kluwer Academic Press, 1989. [cited at p. 19, 80, 82]
- [29] T. V. Cutsem and C. Vournas, *Voltage Stability of Electric Power Systems*. Norwell, MA: Kluwer, 1998. [cited at p. 19, 56]

- [30] T. VanCutsem, “Voltage instability: phenomena, countermeasures, and analysis methods,” *Proc. IEEE*, vol. 88, no. 2, pp. 208–227, Feb. 2000.  
[cited at p. 19]
- [31] IEEE Subsynchronous Resonance Working Group, “Second benchmark model for computer simulation of subsynchronous resonance,” *IEEE Trans. Power App. Syst.*, vol. 104, pp. 1057–1066, 1985. [cited at p. 20, 66]
- [32] A. E. Fitzgerald, C. Kingsley, and S. D. Umans, *Electric Machinery*, 6th ed. New York: McGraw Hill, 2003. [cited at p. 21]
- [33] Machowski and Bialek, *Power system stability*, 1st ed. New York: John Wiley, 2000. [cited at p. 23]
- [34] P. Anderson and A. Fouad, *Power System Control and Stability*. IEEE Press, 1994. [cited at p. 23]
- [35] I. P. W. G. on Prime Mover and E. S. M. for System Dynamic Performance Studies, “Dynamic models for fossil fueled steam units in power system studies,” *IEEE Trans. Power Syst.*, vol. 6, no. 2, pp. 753–761, May 1991. [cited at p. 28]
- [36] ———, “Hydraulic turbine and turbine control models for system dynamic studies,” *IEEE Trans. Power Syst.*, vol. 7, no. 1, pp. 167–179, Feb. 1992.  
[cited at p. 28]
- [37] X. Xu, R. Mathur, J. Jiang, G. Rogers, and P. Kundur, “Modeling of generators and their controls in power system simulations using singular perturbations,” *IEEE Trans. Power Systems*, vol. 13, no. 1, pp. 109–114, Feb. 1998. [cited at p. 28, 151]
- [38] *Guide for identification, testing and evaluation of the dynamic performance of excitation control systems*, IEEE Excitation Systems Subcommittee of the Power Generation Committee of the IEEE Power Engineering Society Std. 421.2-1990, 1990. [cited at p. 29]
- [39] *IEEE Recommended Practice for Excitation System Models for Power System Stability Studies*, Energy Development and Power Generation Committee of the IEEE Power Engineering Society Std. 421.5-2005, 2005.  
[cited at p. 29]

- [40] P. Kundur, M. Klein, G. J. Rogers, and M. S. Zywno, "Application of power system stabilizers for enhancement of overall system stability," *IEEE Trans. Power Syst.*, vol. 4, no. 2, pp. 614–626, May 1989. [cited at p. 30]
- [41] J. H. Chow, G. E. Boukarim, and A. Murdoch, "Power system stabilizers as undergraduate control design projects," *IEEE Trans. Power Syst.*, vol. 19, no. 1, pp. 144–151, Feb. 2004. [cited at p. 30]
- [42] I. Kamwa, R. Grondin, and G. Trudel, "IEEE PSS2B versus PSS4B: the limits of performance of modern power system stabilizers," *IEEE Trans. Power Syst.*, vol. 20, no. 2, pp. 903–915, May 2005. [cited at p. 30]
- [43] A. R. Bergen and V. Vittal, *Power System Analysis*, 2nd ed. Upper Saddle River, NJ: Prentice Hall, 2004. [cited at p. 31]
- [44] W. W. Price, K. A. Wirgau, A. Murdoch, J. V. Mitsche, E. Vaahedi, and M. A. El-Kady, "Load modeling for power flow and transient stability computer studies," *IEEE Trans. Power Syst.*, vol. 3, no. 1, pp. 180–187, Feb. 1988. [cited at p. 31]
- [45] IEEE Task Force on load representation for dynamic performance. System dynamic performance subcommittee. Power system engineering committee, "Standard load models for power flow and dynamic performance simulation," *IEEE Trans. Power Syst.*, vol. 10, no. 3, pp. 1302–1313, Aug. 1995. [cited at p. 31]
- [46] D. Karlsson and D. Hill, "Modelling and identification of nonlinear dynamic loads in power systems," *IEEE Trans. Power Systems*, vol. 9, no. 1, pp. 157–166, Feb. 1994. [cited at p. 32, 65]
- [47] E. Allen and M. Ilic, "Interaction of transmission network and load phasor dynamics in electric power systems," *IEEE Trans. Circuits and Systems-I*, vol. 47, no. 11, pp. 1613–1620, Nov. 2000. [cited at p. 32, 52]
- [48] M. K. Pal, "Voltage stability: analysis needs, modelling requirement and modelling adequacy," *IEEE Trans. Power Syst.*, vol. 7, no. 1, pp. 243–249, Feb. 1992. [cited at p. 32]
- [49] V. Vittal, "Consequence and impact of electric utility industry restructuring on transient stability and small-signal stability analysis," *Proc. IEEE*, vol. 88, no. 2, pp. 196–207, Feb. 2000. [cited at p. 36]

- [50] E. Acha, C. R. Fuerte-Esquivel, H. Ambriz-Perez, and C. Angeles-Camacho, *FACTS: Modelling and simulation in power networks*. Chichester, U.K.: Wiley, 2004. [cited at p. 36]
- [51] V. K. Sood, *HVDC and FACTS controllers. Applications of static converters in power systems*. Boston, MA: Kluwer Academic Publisher, 2004. [cited at p. 36]
- [52] P. Moore and P. Ashmole, “Flexible AC Transmission Systems,” *Power Engineering Journal*, vol. 9, no. 6, pp. 282–286, Dec. 1995. [cited at p. 36]
- [53] N. Mohan, T. M. Undeland, and W. P. Robbins, *Power electronics. Converters, applications and design*, 3rd ed. USA: John Wiley and Sons, Inc., 2003. [cited at p. 37]
- [54] L. Gyugyi, “Power electronics in electric utilities: static VAR compensators,” *Proc. IEEE*, vol. 76, no. 4, pp. 483–494, Apr. 1988. [cited at p. 37, 41]
- [55] K. K. Sen, “STATCOM-STATIC COMPensator: Theory, modeling and applications,” *IEEE Trans. Power Delivery*, vol. 2, pp. 1177–1183, Feb. 1999. [cited at p. 37]
- [56] ———, “SSSC-static synchronous series compensator: Theory, modeling and applications,” *IEEE Trans. Power Delivery*, vol. 13, no. 1, pp. 241–246, Jan. 1998. [cited at p. 37, 69]
- [57] K. K. Sen and E. J. Stacey, “UPFC-unified power flow controller: Theory, modeling and applications,” *IEEE Trans. Power Delivery*, vol. 13, no. 4, pp. 1453–1460, Oct. 1998. [cited at p. 37]
- [58] L. Chen, Y. Liu, A. B. Arsoy, P. F. Ribeiro, M. Steurer, and M. R. Iravani, “Detailed modeling of Superconducting Magnetic Energy Storage (SMES) system,” *IEEE Trans. Power Delivery*, vol. 21, no. 2, pp. 699–710, Apr. 2006. [cited at p. 37]
- [59] L. Gyugyi, C. D. Schauder, and K. K. Sen, “Static synchronous compensator: a solid-state approach to the series compensation of transmission lines,” *IEEE Trans. Power Delivery*, vol. 12, no. 1, pp. 406–417, Jan. 1997. [cited at p. 41]

- [60] M. S. El-Moursi and A. M. Sharaf, "Novel controllers for the 48-pulse VSC STATCOM and SSSC for voltage regulation and reactive power compensation," *IEEE Trans. Power Syst.*, vol. 20, no. 4, pp. 1985–1997, Nov. 2005. [cited at p. 41, 104, 115, 119]
- [61] A. B. Arsoy, Y. Liu, P. F. Ribeiro, and F. Wang, "STATCOM-SMES: static-synchronous compensators and superconducting magnetic energy storage systems in controlling power system dynamics," *IEEE Industry Applications Magazine*, vol. 9, no. 2, pp. 21–28, Mar. 2003. [cited at p. 41, 48, 49]
- [62] P. F. Ribeiro, B. K. Johnson, M. L. Crow, A. Arsoy, and Y. L. and, "Energy storage systems for advanced power applications," *Proc. IEEE*, vol. 89, no. 12, pp. 1744–1756, Dec. 2001. [cited at p. 41, 49, 123]
- [63] B. T. Ooi, M. Kazerani, R. Marceau, Z. Wolanski, F. D. Galiana, D. McGillis, and G. Joos, "Mid-point siting of FACTS devices in transmission lines," *IEEE Trans. Power Delivery*, vol. 12, no. 4, pp. 1717–1722, Oct. 1997. [cited at p. 42]
- [64] F. A. L. Jowder, "Influence of mode of operation of the SSSC on the small disturbance and transient stability of radial power system," *IEEE Trans. Power Syst.*, vol. 20, no. 2, pp. 935–942, May 2005. [cited at p. 45]
- [65] A. Xue, F. F. Wu, Y. Ni, Q. Lu, and S. Mei, "Power system transient stability assessment based on quadratic approximation of stability region," *Elect. Power Syst. Research*, vol. 76, no. 9-10, pp. 709–715, June 2006. [cited at p. 45]
- [66] ———, "Power system transient stability assessment based on quadratic approximation of stability region," in *IEEE/PES Transmission and Distribution Conference and Exhibition: Asia and Pacific*, June 2005, p. 6pp. [cited at p. 45]
- [67] A. Griffo and D. Lauria, "Some considerations on power system stability improvement by FACTS devices," in *Proceeding of International Symposium on Power Electronics, Electrical Drives, Automation and Motion, SPEEDAM*, Taormina, Italy, May 2006, pp. 809–813. [cited at p. 45]
- [68] B. C. Pal, A. H. Coonick, and D. C. Macdonald, "Robust damping controller design in power systems with superconducting magnetic energy stor-

- age devices,” *IEEE Trans. Power Syst.*, vol. 15, no. 1, pp. 320–325, Feb. 2000. [cited at p. 49]
- [69] B. C. Pal, A. H. Coonick, and B. J. Cory, “Robust damping of inter-area oscillations in power systems with superconducting magnetic energy storage devices,” *IEE Proc. Generation Transmission and Distribution*, vol. 146, no. 6, pp. 633–639, Nov. 1999. [cited at p. 49]
- [70] H. Chiang, C. Chu, and G. Cauley, “Direct stability analysis of electric power systems using energy functions: theory, applications, and perspective,” *Proc. IEEE*, vol. 83, no. 11, pp. 1497–1529, Nov. 1995. [cited at p. 52, 80]
- [71] E. Allen, J. Chapman, and M. Ilic, “Effects of torsional dynamics on nonlinear generator control,” *IEEE Trans. Control Systems Technology*, vol. 4, no. 2, pp. 125–140, 1996. [cited at p. 52]
- [72] V. Venkatasubramanian, H. Schattler, and J. Zaborszky, “Dynamics of large constrained nonlinear systems - a taxonomy theory,” *IEEE Proc.*, vol. 83, no. 11, pp. 1530–1561, 1995. [cited at p. 52]
- [73] V. Venkatasubramanian, “Tools for dynamic analysis of the general large power system using time-varying phasors,” *International Journal of Electric Power and Energy Systems*, pp. 365–376, Dec 1994. [cited at p. 52, 54]
- [74] V. Venkatasubramanian, H. Schattler, and J. Zaborszky, “Fast time-varying phasor analysis in the balanced large electric power system,” *IEEE Trans. on Automatic Control*, vol. 40, no. 11, pp. 1975–1982, Nov 1995. [cited at p. 52]
- [75] ———, “Time-delay differential-algebraic phasor formulation of the large power system dynamics,” in *Proc. IEEE International Symposium on Circuits and Systems, ISCAS 1994*, vol. 6, June 1994, pp. 49–52. [cited at p. 52]
- [76] M. Ilic and J. Zaborszky, *Dynamics and Control of Large Electric Power Systems*. New York: Wiley, 2000. [cited at p. 52, 55]
- [77] E. Allen, N. LaWhite, Y. Yoon, J. Chapman, and M. Ilic, “Interactive object-oriented simulation of interconnected power systems using SIMULINK,” *IEEE Trans. on Education*, vol. 44, no. 1, pp. 87–95, Feb. 2001. [cited at p. 52]



- [78] R. Shintaku and K. Strunz, "Branch companion modeling for diverse simulation of electromagnetic and electromechanical transients," in *Proceedings of the 6th International Conference on Power System Transients IPST05*, June 2005. [cited at p. 52]
- [79] I. Hiskens and J. Milanovic, "Load modelling in studies of power system damping," *IEEE Trans. Power Systems*, vol. 10, no. 4, pp. 1781–1788, Nov. 1995. [cited at p. 53, 65]
- [80] V. A. Caliskan, G. C. Verghese, and A. M. Stankovic', "Multifrequency averaging of dc/dc converters," *IEEE Trans. Power Electron.*, vol. 14, no. 1, pp. 124–133, Jan. 1999. [cited at p. 53]
- [81] A. M. Stankovic', S. R. Sanders, and T. Aydin, "Dynamic phasors in analysis of unbalanced polyphase ac machines," *IEEE Trans. Energy Conversion*, vol. 17, no. 1, pp. 107–113, Mar. 2002. [cited at p. 53]
- [82] A. M. Stankovic', B. C. Lesieutre, and T. Aydin, "Modeling and analysis of single-phase induction machines with dynamic phasors," *IEEE Trans. Power Syst.*, vol. 14, no. 1, pp. 9–14, Feb. 1999. [cited at p. 53]
- [83] A. M. Stankovic' and T. Aydin, "Analysis of asymmetrical faults in power systems using dynamic phasors," *IEEE Trans. Power Syst.*, vol. 15, no. 3, pp. 1062–1068, Aug. 2000. [cited at p. 53]
- [84] P. Mattavelli, A. M. Stankovic', and G. C. Verghese, "Ssr analysis with dynamic phasor model of thyristor-controlled series capacitor," *IEEE Trans. Power Syst.*, vol. 14, no. 1, pp. 200–208, Feb. 1999. [cited at p. 53]
- [85] P. C. Stefanov and A. Stankovic', "Modeling of upfc operation under unbalanced conditions with dynamic phasors," *IEEE Trans. Power Syst.*, vol. 17, no. 2, pp. 395–403, May 2002. [cited at p. 53]
- [86] P. Mattavelli, G. C. Verghese, and A. M. Stankovic', "Phasor dynamics of thyristor-controlled series capacitor systems," *IEEE Trans. Power Syst.*, vol. 12, no. 3, pp. 1259–1267, Aug. 1997. [cited at p. 53]
- [87] A. Stankovic, H. Lev-Ari, and M. Perisic', "Analysis and implementation of model-based linear estimation of dynamic phasors," *IEEE Trans. Power Syst.*, vol. 19, no. 4, pp. 1903–1910, Nov. 2004. [cited at p. 53]

- [88] T. Demiray and G. Andersson, “Simulation of power systems dynamics using dynamic phasor models,” in *Proceedings of X SEPOPE*, Florianopolis, Brasil, May 2006, p. 8. [cited at p. 53]
- [89] ———, “Comparison of the efficiency of dynamic phasor models derived from abc and dq0 reference frame in power system dynamic simulations,” in *7th IEE Conference on Advances in Power System Control, Operation and Management*, Hong Kong, Oct. 2006, p. 8. [cited at p. 53]
- [90] V. Saksena, J. O’Reilly, and P. Kokotovic, “Singular perturbations and time-scale methods in control theory: survey 1976-1983,” *Automatica*, vol. 20, pp. 273–293, May 1984. [cited at p. 57]
- [91] C. Guo and A. Laub, “On the iterative solution of a class of nonsymmetric algebraic riccati equations,” *SIAM J. Matrix Anal. Appl.*, vol. 22, no. 2, pp. 376–391, 2000. [cited at p. 57]
- [92] J. Arrillaga and C. P. Arnold, *Computer Analysis of Power Systems*. New York: John Wiley and Sons, 1990. [cited at p. 60]
- [93] H. Dommel, “Digital computer solutions of electromagnetic transients in single and multiple networks,” *IEEE Trans. Power App. Syst.*, vol. 88, no. 4, pp. 388–399, Apr. 1969. [cited at p. 60]
- [94] T. T. Inc., *SimPowerSystems User’s Guide*. The Mathworks, Inc., 2005. [cited at p. 60]
- [95] M. Pai, P. Sauer, and B. Lesieutre, “Static and dynamic nonlinear loads and structural stability in power systems,” *IEEE Proc.*, vol. 83, pp. 1562–1571, Nov. 1995. [cited at p. 65]
- [96] I. Perez-Arriaga, G. Verghese, and F. Schweppe, “Selective modal analysis with applications to electric power systems, part 1: heuristic introduction,” *IEEE Trans. Power Appar. and Systems*, vol. PAS-101, no. 9, pp. 3117–3125, 1982. [cited at p. 66]
- [97] L. Shampine and M. Reichelt, “The MATLAB ODE suite,” *SIAM J. Sci. Comp.*, vol. 18, no. 1, pp. 1–22, Jan. 1997. [cited at p. 66]

- [98] F. A. R. A. Jowder and B.-T. Ooi, "Series compensation of radial power system by a combination of sssc and dielectric capacitors," *IEEE Trans. Power Delivery*, vol. 20, no. 1, pp. 458–465, Jan. 2001. [cited at p. 69]
- [99] L. A. S. Pilotto, A. Bianco, W. F. Long, and A. A. Edris, "Impact of TCSC control methodologies on subsynchronous oscillations," *IEEE Trans. Power Delivery*, vol. 18, no. 1, pp. 243–252, Jan. 2003. [cited at p. 69]
- [100] M. Ribbens-Pavella and F. J. Evans, "Direct methods for studying dynamics of large-scale electric power systems - a survey," *Automatica*, vol. 21, no. 1, pp. 1–21, 1985. [cited at p. 80]
- [101] H. D. Chiang, F. F. Wu, and P. P. Varaiya, "Foundation of direct methods for power system transient stability analysis," *IEEE Trans. Circuits Syst.*, vol. 34, pp. 160–173, Feb. 1987. [cited at p. 80]
- [102] H. D. Chiang, M. W. Hirsch, and F. F. Wu, "Stability region of nonlinear autonomous dynamical systems," *IEEE Trans. Automat. Contr.*, vol. 33, pp. 16–27, Jan. 1988. [cited at p. 81]
- [103] H. D. Chiang and J. Thorp, "The closest unstable equilibrium point method for power system dynamic security assessment," *IEEE Trans. Circuits Syst.*, vol. 36, no. 7, pp. 1187–1200, Sept. 1989. [cited at p. 81]
- [104] H. D. Chiang and C.-C. Chu, "Theoretical foundation of the bcu method for direct stability analysis of network-reduction power system models with small transfer conductances," *IEEE Trans. Circuits Syst.*, vol. 42, no. 5, pp. 252–265, May 1995. [cited at p. 81]
- [105] Y. Zou, M.-H. Yin, and H. D. Chiang, "Theoretical foundation of the controlling uep method for direct transient-stability analysis of network-preserving power system models," *IEEE Trans. Circuits Syst. I*, vol. 50, no. 10, pp. 1324–1336, Oct. 2003. [cited at p. 81]
- [106] N. A. Tsolas, A. Arapostathis, and P. P. Varaiya, "A structure preserving energy function for power system transient stability analysis," *IEEE Trans. Circuits Syst.*, vol. 32, no. 10, pp. 1041–1049, Oct. 1985. [cited at p. 82]
- [107] R. J. Davy and I. A. Hiskens, "Lyapunov functions for multimachine power systems with dynamic loads," *IEEE Trans. Circuits Syst. I*, vol. 44, no. 9, pp. 796–812, Sept. 1997. [cited at p. 82]

- [108] C. L. DeMarco and C. A. Canizares, “A vector energy function approach for security analysis of ac/dc systems,” *IEEE Trans. Power Syst.*, vol. 7, pp. 1001–1011, Aug. 1992. [cited at p. 82]
- [109] V. Azbe, U. Gabrijel, D. Povh, and R. Mihalic, “The energy function of a general multimachine system with unified power flow controller,” *IEEE Trans. Power Syst.*, vol. 20, no. 3, pp. 1478–1485, Aug. 2005. [cited at p. 82]
- [110] M. Ghandhari, G. Andersson, and I. A. Hiskens, “Control Lyapunov functions for controllable series devices,” *IEEE Trans. on Power Systems*, vol. 16, pp. 689–694, Nov. 2001. [cited at p. 82, 89]
- [111] N. Narasimhamurthi, “On the existence of energy function for power systems with transmission losses,” *IEEE Trans. Circuits Syst.*, vol. 31, no. 2, pp. 199–203, Feb. 1984. [cited at p. 84]
- [112] H. D. Chiang, “Study of the existence of energy functions for power systems with losses,” *IEEE Trans. Circuits Syst.*, vol. 36, no. 11, pp. 1423–1429, Nov. 1989. [cited at p. 84]
- [113] R. Ortega, M. Galaz, A. Astolfi, Y. Sun, and T. Shen, “Transient stabilization of multimachine power systems with nontrivial transfer conductances,” *IEEE Trans. Automat. Contr.*, vol. 50, no. 1, pp. 60–75, Jan. 2005. [cited at p. 84]
- [114] H. M. Rodrigues, L. F. C. Alberto, and N. G. Bretas, “On the invariance principle: generalizations and applications to synchronization,” *IEEE Trans. Circuits Syst. I*, vol. 47, no. 5, pp. 730–739, May 2000. [cited at p. 84]
- [115] N. G. Bretas and L. F. C. Alberto, “Lyapunov function for power systems with transfer conductances: extension of the invariance principle,” *IEEE Trans. Power Syst.*, vol. 18, no. 2, pp. 769–777, May 2003. [cited at p. 84, 86]
- [116] A. Griffo and D. Lauria, “Sulle funzioni di controllo di Lyapunov per il miglioramento del comportamento dinamico dei sistemi elettrici,” in *atti del 101 Convegno Nazionale AEIT*, Capri, Italy, Sept. 2006, p. 11pp. [cited at p. 86]
- [117] R. Sepulchre, M. Jankovic, and P. Kokotovic, *Constructive Nonlinear Control*. Springer-Verlag, 1997. [Online]. Available: <http://www>.

- [montefiore.ulg.ac.be/services/stochastic/pubs/1997/SJK97a](http://montefiore.ulg.ac.be/services/stochastic/pubs/1997/SJK97a) [cited at p. 89, 90]
- [118] P. Kokotovic and M. Arcak, “Constructive nonlinear control: a historical perspective,” *Automatica*, vol. 37, no. 5, pp. 637–662, May 2001. [cited at p. 89]
- [119] E. D. Sontag, *Mathematical Control Theory: Deterministic Finite Dimensional Systems*, 2nd ed. New York, NJ: Springer, 1998. [Online]. Available: <http://www.math.rutgers.edu/~sontag/mct.html> [cited at p. 89, 90, 91]
- [120] A. S. Bazanella, P. V. Kokotovic, and A. S. Silva, “A dynamic extension for LgV controllers,” *IEEE Trans. Automat. Contr.*, vol. 44, no. 3, pp. 588–592, Mar. 1999. [cited at p. 89, 97]
- [121] M. Galaz, R. Ortega, A. S. Bazanella, and A. M. Stankovic, “An energy-shaping approach to the design of excitation control of synchronous generators,” *Automatica*, vol. 39, no. 1, pp. 111–119, Jan. 2003. [cited at p. 89]
- [122] J. Machowski, S. Robak, J. W. Bialek, J. R. Bumby, and N. Abi-Samra, “Decentralized stability-enhancing control of synchronous generator,” *IEEE Trans. Power Syst.*, vol. 15, no. 4, pp. 1336–1344, Nov. 2000. [cited at p. 89]
- [123] M. Ghandhari, G. Andersson, M. Pavella, and D. Ernst, “A control strategy for controllable series capacitor in electric power systems,” *Automatica*, vol. 37, no. 10, pp. 1575–1583, Oct. 2001. [cited at p. 89]
- [124] M. Januszewski, J. Machowski, and J. W. Bialek, “Application of the direct lyapunov method to improve damping of power swings by control of upfc,” *IEE Proc. Gener. Transm. Distrib.*, vol. 151, no. 2, pp. 252–260, 2004. [cited at p. 89]
- [125] J. Machowski and D. Nelles, “Optimal modulation controller for superconducting magnetic energy storage,” *Intern. Journ. Elect. Power Energy Syst.*, vol. 16, no. 5, 1994. [cited at p. 89]
- [126] A. Griffo and D. Lauria, “Superconducting magnetic energy storage control strategy for power system stability improvement,” *International Journal of*

- Emerging Electric Power Systems*, vol. 4, no. 1, p. 20, 1172 2005. [Online]. Available: <http://www.bepress.com/ijeeps/vol4/iss1/art1172> [cited at p. 89]
- [127] J. F. Gronquist, W. A. Sethares, F. L. Alvarado, and R. H. Lasseter, “Power oscillation damping control strategies for facts devices using locally measurable quantities,” *IEEE Trans. Power Syst.*, vol. 10, no. 3, pp. 1598–1605, Aug. 1995. [cited at p. 89]
- [128] M. Ghandhari, “Control lyapunov functions: A control strategy for damping of power oscillations in large power systems,” Ph.D. dissertation, KTH, Department of Electric Power Engineering, Stockholm, Sweden, Nov. 2000. [Online]. Available: <http://www.diva-portal.org/kth/abstract.xsql?dbid=3039> [cited at p. 89]
- [129] M. Noroozian, M. Ghandhari, G. Andersson, J. Gronquist, and I. Hiskens, “A robust control strategy for shunt and series reactive compensators to damp electromechanical oscillations,” *IEEE Trans. Power Delivery*, vol. 16, no. 4, pp. 812–817, Mar. 2001. [cited at p. 89]
- [130] A. Bacciotti, “Stability Analysis Based on Direct Lyapunov’s Method,” in *Proc. of Summer school on mathematical control theory*, vol. 13, Sept. 2001, pp. 318–363. [Online]. Available: [http://users.ictp.it/~pub\\_off/lectures/lns008/Bacciotti/Bacciotti.ps.gz](http://users.ictp.it/~pub_off/lectures/lns008/Bacciotti/Bacciotti.ps.gz) [cited at p. 90]
- [131] J. W. Curtis and R. W. Beard, “Satisficing: a new approach to constructive nonlinear control,” *IEEE Trans. Automat. Contr.*, vol. 49, no. 7, pp. 1090–1102, Jul. 2004. [cited at p. 91]
- [132] A. S. Bazanella, P. V. Kokotovic, and A. S. E. Silva, “On the control of dynamic systems with unknown operating point,” *International Journal of Control*, vol. 73, no. 7, pp. 600–605, 2000. [cited at p. 97]
- [133] A. Trofino, A. S. Bazanella, and A. Fischman, “Designing robust controllers with operating point tracking,” in *IFAC Conference on System Structure and Control*, June 1998. [Online]. Available: [http://www.das.ufsc.br/~trofino/pub/tbf98\\_ifacSSCnantes.ps.gz](http://www.das.ufsc.br/~trofino/pub/tbf98_ifacSSCnantes.ps.gz) [cited at p. 97]
- [134] D. Soto and T. C. Green, “A comparison of high-power converter topologies for the implementation of FACTS controllers,” *IEEE Trans. Ind. Electron.*, vol. 49, no. 5, pp. 1072–1080, Oct. 2002. [cited at p. 104]

- [135] Y. Ye, M. Kazerani, and V. H. Quintana, "Current-source converter based STATCOM: modeling and control," *IEEE Trans. Power Delivery*, vol. 20, no. 2, pp. 795–800, Apr. 2005. [cited at p. 104]
- [136] A. H. Norouzi and A. M. Sharaf, "Two control schemes to enhance the dynamic performance of the STATCOM and SSSC," *IEEE Trans. Power Delivery*, vol. 20, no. 1, pp. 435–442, Jan. 2005. [cited at p. 104]
- [137] M. S. El-Moursi and A. M. Sharaf, "Novel reactive power controllers for the STATCOM and SSSC," *Electr. Power Syst. Res.*, vol. 76, no. 4, pp. 228–241, Jan. 2006. [cited at p. 104]
- [138] J. Rodriguez, J. S. Lai, and F. Z. Peng, "Multilevel inverters: a survey of topologies, controls, and applications," *IEEE Trans. Ind. Electron.*, vol. 49, no. 4, pp. 724–738, Aug. 2002. [cited at p. 104]
- [139] C. K. Lee, J. S. K. Leung, S. Y. R. Hui, and H. S.-H. Chung, "Circuit-level comparison of STATCOM technologies," *IEEE Trans. Power Electron.*, vol. 18, no. 4, pp. 1084–1092, July 2003. [cited at p. 104]
- [140] P. K. Steimer, H. E. Grüning, J. Werninger, E. Carroll, S. Klaka, and S. Linder, "IGCT: a new emerging technology for high power, low cost inverter," in *Thirty-second Ind. Applic. Soc. Annual Meeting*, no. 2, New Orleans, LA, USA, Oct. 1997, pp. 1592–1599. [cited at p. 104]
- [141] P. K. Steimer, O. Apeldoorn, and E. Carroll, "IGCT devices - applications and future opportunities," in *IEEE PES Summer Meeting*, no. 2, Seattle, WA, USA, July 2000, pp. 1223–1228. [cited at p. 104]
- [142] Y. Li, A. Q. Huang, and K. Motto, "Analysis of the snubberless operation of the Emitter Turn-Off Thyristor (ETO)," *IEEE Trans. Power Electron.*, vol. 18, no. 1, pp. 30–37, Jan. 2003. [cited at p. 104]
- [143] B. Zhang, A. Q. Huang, Y. Liu, and S. Atcitty, "Performance of the new generation emitter turn-off (ETO) thyristor," in *37th IAS Annual Meeting*, no. 1, 2002, pp. 559–563. [cited at p. 104]
- [144] B. Zhang, A. Q. Huang, Y. Liu, B. Chen, and S. Atcitty, "SPETO: A superior power switch for high power, high frequency, low cost converters," in *39th IAS Annual Meeting*, no. 3, Oct. 2004, pp. 1940–1946. [cited at p. 104]

- [145] B. Mwinyiwiwa and Z. W. B. T. Ooi, “High power switch mode linear amplifiers for flexible ac transmission system,” *IEEE Trans. Power Delivery*, vol. 11, no. 4, pp. 1993–1998, Oct. 1996. [cited at p. 104]
- [146] J. Y. Hung, W. Gao, and J. C. Hung, “Variable structure control: a survey,” *IEEE Trans. Ind. Electron.*, vol. 40, no. 1, pp. 2–22, Feb. 1993. [cited at p. 104, 111]
- [147] R. A. DeCarlo, S. H. Zak, and G. P. Matthews, “Variable structure control of nonlinear multivariable systems: a tutorial,” *Proc. IEEE*, vol. 76, no. 3, pp. 212–232, Mar. 1988. [cited at p. 104, 111]
- [148] A. Griffo and D. Lauria, “Advanced series and parallel converters for power system stability improvement,” in *Proceeding of International Symposium on Power Electronics, Electrical Drives, Automation and Motion, SPEEDAM*, Taormina, Italy, May 2006, pp. 803–808. [cited at p. 105]
- [149] F. Blaabjerg, S. Freysson, H. H. Hansen, and S. Hansen, “A new optimized space-vector modulation strategy for a component-minimized voltage source inverter,” *IEEE Trans. Power Electron.*, vol. 12, no. 4, pp. 704–714, July 1997. [cited at p. 105]
- [150] E. Ledezma, B. McGrath, A. Munoz, and T. A. Lipo, “Dual AC-drive system with a reduced switch count,” *IEEE Trans. Ind. Applicat.*, vol. 37, no. 5, pp. 1325–1333, Sept. 2001. [cited at p. 105]
- [151] G. T. Kim and T. A. Lipo, “VSI-PWM rectifier-inverter system with a reduced switch count,” *IEEE Trans. Ind. Applicat.*, vol. 32, no. 6, pp. 1331–1337, Nov. 1996. [cited at p. 105]
- [152] B. R. Lin and T. C. Wei, “A novel NPC inverter for harmonics elimination and reactive power compensation,” *IEEE Trans. Power Delivery*, vol. 19, no. 3, pp. 1449–1456, July 2004. [cited at p. 105]
- [153] V. I. Utkin, J. Guldner, and J. Shi, *Sliding mode control in electromechanical systems*. London, UK: Taylor & Francis, 1999. [cited at p. 110]
- [154] A. G. Loukianov, J. M. Canedo, V. I. Utkin, and J. Cabrera-Vázquez, “Discontinuous controller for power systems: Sliding-mode block control



- approach,” *IEEE Trans. Ind. Electron.*, vol. 51, no. 2, pp. 340–353, Apr. 2004. [cited at p. 110]
- [155] V. I. Utkin, “Sliding mode control design principles and applications to electric drives,” *IEEE Trans. Ind. Electron.*, vol. 40, no. 1, pp. 23–36, Feb. 1993. [cited at p. 110]
- [156] R. Ramos, D. Biel, F. Guinjoan, and E. Fossas, “Design considerations in sliding-mode controlled parallel-connected inverters,” in *Proceedings of IEEE ISCAS*, no. 4, 2002, pp. 357–360. [cited at p. 110]
- [157] M. Carpita and M. Marchesoni, “Experimental study of a power conditioning system using sliding mode control,” *IEEE Trans. Power Electron.*, vol. 11, no. 5, pp. 731–742, Sept. 1996. [cited at p. 111]
- [158] H. Sira-Ramirez, “Sliding motions in bilinear switched networks,” *IEEE Trans. Circuits Syst.*, vol. 34, no. 8, pp. 919–933, Aug. 1987. [cited at p. 111]
- [159] H. Zhang, Y. Kang, P. Zhu, X. Kong, P. Liu, and J. Chen, “Theoretical analysis and experimental results on smes in dynamic simulation test of power system,” in *Proc. of IEEE Conf. Elect. Machines and Drives*, 2001, pp. 736–741. [cited at p. 123]
- [160] B. M. Han and G. G. Karady, “New combined power-conditioning system for superconducting magnetic energy storage,” *Electric Power System Research*, vol. 37, pp. 79–85, 1996. [cited at p. 123]
- [161] C. A. Luongo, T. Baldwin, P. Ribeiro, and C. M. Weber, “A 100 MJ SMES demonstration at FSU-CAPS,” *IEEE Trans. Appl. Superconduct.*, vol. 13, no. 2, pp. 1800–1805, June 2003. [cited at p. 126]



# Appendices



## Appendix A

---

### Test systems' data

---

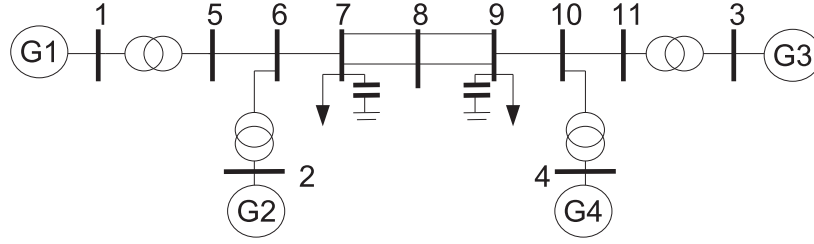


Figure A.1: Two-area test system

Parameters of the SMIB system (4.28)-(4.30) are:

$$\omega = 2\pi f = 2\pi 60, M = \frac{3.5}{60\pi}, D = 0.01, P_m = 0.9[p.u.]$$

$$E = 1.123[p.u.], V = 0.995[p.u.], l = 0.95[p.u.], r = 0.065[p.u.]$$

Parameters of synchronous generators, thyristor exciter and PSS of the four-machine test system in Fig. A.1 are the same as [15]. Loads are:

$$\begin{aligned} P_7 &= 9.384[p.u.] & P_9 &= 18.211[p.u.] \\ Q_7 &= 0.971[p.u.] & Q_9 &= 1.033[p.u.] \end{aligned}$$

Turbine and governor model is reported in Fig. (2.3), data are [37]:

$$T_{G1} = 0, T_{G2} = 0.1, T_{G3} = 0.25, T_{G4} = 0.42, T_{G5} = 4.25, T_{G6} = 0.72$$

$$K_1 = 15, K_2 = 0.25, K_3 = 0.25, K_4 = 0.5$$

$$R_{max} = 1.1, R_{min} = -0.5, P_{max} = 1, P_{min} = 0$$



## Appendix B

---

# Derivation of expression for matrix $\Omega$ in eq. (6.27)

---

Matrix  $\Omega$  in (6.23) is given by (6.26):

$$\Omega = \left( \frac{\partial \Sigma}{\partial \mathbf{x}} \cdot \mathbf{B} \right)^{-1} \quad (\text{B.1})$$

where:

$$\frac{\partial \Sigma}{\partial \mathbf{x}} \cdot \mathbf{B} = [\Gamma_1, \Gamma_2] \quad (\text{B.2})$$

and:

$$\Gamma_1 = \begin{bmatrix} \frac{1}{L_{fA,n}} \frac{\partial \sigma_{A,1}}{\partial i_{fA,n}} & \cdots & \frac{1}{L_{fA,1}} \frac{\partial \sigma_{A,1}}{\partial i_{fA,1}} \\ \vdots & \ddots & \vdots \\ \frac{1}{L_{fA,n}} \frac{\partial \sigma_{A,n}}{\partial i_{fA,n}} & \cdots & \frac{1}{L_{fA,1}} \frac{\partial \sigma_{A,n}}{\partial i_{fA,1}} \\ \frac{1}{L_{fA,n}} \frac{\partial \sigma_{C,1}}{\partial i_{fA,n}} & \cdots & \frac{1}{L_{fA,1}} \frac{\partial \sigma_{C,1}}{\partial i_{fA,1}} \\ \vdots & \ddots & \vdots \\ \frac{1}{L_{fA,n}} \frac{\partial \sigma_{C,n}}{\partial i_{fA,n}} & \cdots & \frac{1}{L_{fA,1}} \frac{\partial \sigma_{C,n}}{\partial i_{fA,1}} \end{bmatrix} \quad (\text{B.3})$$

$$\Gamma_2 = \begin{bmatrix} \frac{1}{L_{fC,n}} \frac{\partial \sigma_{A,1}}{\partial i_{fC,n}} & \cdots & \frac{1}{L_{fC,1}} \frac{\partial \sigma_{A,1}}{\partial i_{fC,1}} \\ \vdots & \ddots & \vdots \\ \frac{1}{L_{fC,n}} \frac{\partial \sigma_{A,n}}{\partial i_{fC,n}} & \cdots & \frac{1}{L_{fC,1}} \frac{\partial \sigma_{A,n}}{\partial i_{fC,1}} \\ \frac{1}{L_{fC,n}} \frac{\partial \sigma_{C,1}}{\partial i_{fC,n}} & \cdots & \frac{1}{L_{fC,1}} \frac{\partial \sigma_{C,1}}{\partial i_{fC,1}} \\ \vdots & \ddots & \vdots \\ \frac{1}{L_{fC,n}} \frac{\partial \sigma_{C,n}}{\partial i_{fC,n}} & \cdots & \frac{1}{L_{fC,1}} \frac{\partial \sigma_{C,n}}{\partial i_{fC,1}} \end{bmatrix} \quad (\text{B.4})$$

It results:

$$\begin{aligned} \frac{\partial \sigma_{A,j}}{\partial i_{fA,k}} &= \begin{cases} \frac{\alpha}{C_{fA}} & \text{if } k \neq j, k \neq j-1 \\ \frac{\alpha}{C_{fA}} + \beta & \text{if } k = j \\ \frac{\alpha}{C_{fA}} - \beta & \text{if } k = j-1 \end{cases} \\ \frac{\partial \sigma_{A,j}}{\partial i_{fC,k}} &= 0 \end{aligned} \quad (\text{B.5})$$

and analogously:

$$\begin{aligned} \frac{\partial \sigma_{C,j}}{\partial i_{fC,k}} &= \begin{cases} \frac{\alpha}{C_{fC}} & \text{if } k \neq j, k \neq j-1 \\ \frac{\alpha}{C_{fC}} + \beta & \text{if } k = j \\ \frac{\alpha}{C_{fC}} - \beta & \text{if } k = j-1 \end{cases} \\ \frac{\partial \sigma_{C,j}}{\partial i_{fA,k}} &= 0 \end{aligned} \quad (\text{B.6})$$



## Appendix C

---

# FACTS circuits and controllers data

---

### STATCOM data

STATCOM converter data used in simulations of Chapter 6 are given in Tab. C.1, while STATCOM controllers data are reported in Tab. C.2 and C.3.

Table C.1: STATCOM circuit data

$C_1, C_2$	20 mF	$L_{fA,1}, L_{fC,1}$	5.0 mH
$C_{fA}$	2.55 mF	$L_{fA,2}, L_{fC,2}$	4.5 mH
$C_{fC}$	2.55 mF	$L_{fA,3}, L_{fC,3}$	4.0 mH

Table C.2: STATCOM PI controller's data

$K_{i,ac}$	500	$K_{i,dc}$	25
$K_{i,dc}$	5	$K_{i,dc}$	0.25

Table C.3: STATCOM sliding mode controller's data

$\alpha$	$2.0 \cdot 10^{-4}$	HB	5
$\beta$	0.3		

**SSSC data**

SSSC converter data are given in Tab. C.4, while SSSC controllers data are reported in Tab. C.5 and C.6.

Table C.4: SSSC circuit data

$C_1, C_2$	10 mF	$L_{fA,1}, L_{fC,1}$	10 mH
$C_{fA}$	1 mF	$L_{fA,2}, L_{fC,2}$	11 mH
$C_{fC}$	1 mF	$L_{fA,3}, L_{fC,3}$	12 mH

Table C.5: SSSC PI controller's data

$K_{i,dc}$	50	$K_{i,dc}$	0.05
------------	----	------------	------

Table C.6: SSSC sliding mode controller's data

$\alpha$	$2.0 \cdot 10^{-3}$	HB	1.5
$\beta$	1		

---

# List of Symbols and Abbreviations

---

Abbreviation	Description	Definition
AVR	Automatic Voltage Regulator	page 28
CLF	Control Lyapunov Function	page 90
DAE	Differential Algebraic Equation	page 7
DPL	Distributed Parameter Line	page 60
FACTS	Flexible AC Transmission Systems	page 36
GTO	Gate Turn-Off Thyristor	page 37
IGBT	Insulated Gate Bipolar Transistor	page 37
IGCT	Insulated Gate Commutated Thyristor	page 37
PSS	Power System Stabilizer	page 28
SMES	Superconducting Magnetic Energy Storage	page 37
SSSC	Static Synchronous Series Compensator	page 37
SSR	SubSynchronous Resonance	page 20
STATCOM	STATic COMpensator	page 37
TCSC	Thyristor Controlled Series Compensator	page 37
TGR	Transient Gain Reduction	page 30
UPFC	Unified Power Flow Controller	page 37
VSI	Voltage Source Inverter	page 40

---

# List of Figures

---

1.1	Phase plane portrait of the system in example 1 . . . . .	12
1.2	Phase plane portrait of the system in example 2 . . . . .	14
1.3	A schematic drawing illustrating time-scale of dynamical phenomena in power systems . . . . .	15
2.1	Schematic diagram of a three-phase synchronous machine . . . . .	22
2.2	Transformation for interfacing machine reference with network reference	27
2.3	Turbine and governor . . . . .	29
2.4	Thyristor exciter . . . . .	29
2.5	PSS . . . . .	30
2.6	SMIB . . . . .	33
3.1	A simple two buses power system representing a generator connected to a stiff bus through a lossless transmission line . . . . .	38
3.2	Power-angle relationship for the SMIB system in Fig. 3.1 . . . . .	38
3.3	Basic structure and equivalent circuit of a STATCOM . . . . .	40
3.4	Operating modes, waveforms and phasor diagram illustrating STAT- COM operation . . . . .	41
3.5	Midpoint compensation of a transmission line . . . . .	42
3.6	Power-angle relationship for midpoint compensated line . . . . .	43
3.7	Basic structure of an SSSC . . . . .	44
3.8	A series compensated transmission line . . . . .	44
3.9	Phasor diagram of the series compensated transmission line in Fig. 3.8	45
3.10	Power-angle relationship for series compensated transmission line, with constant reactance and constant quadrature voltage mode of operation	46

3.11 Single Machine power system coupled to an infinite bus, with series and parallel connected compensators. . . . .	47
3.12 Stability region and quadratic approximation of its boundary as effected by shunt compensation . . . . .	47
3.13 Stability region and quadratic approximation of its boundary as effected by capacitive series compensation . . . . .	48
4.1 II circuit . . . . .	56
4.2 Three-phase abc to rectangular transformation . . . . .	58
4.3 Framework for Re-Im/abc coupled simulations: the component is modelled in three-phase abc framework . . . . .	59
4.4 Framework for Re-Im/abc coupled simulations: the component is modelled in rectangular Re-Im framework . . . . .	60
4.5 Transmission line models comparison: 10 Hz modulation of generator's magnitude . . . . .	61
4.6 Transmission line models comparison: 10 Hz phase modulation . . . . .	62
4.7 SMIB power system . . . . .	62
4.8 Projection on $\delta - I_{RE} - I_{IM}$ axes of the phase portrait of SMIB system	63
4.9 Projection on $I_{RE} - I_{IM}$ axes of the phase portrait of SMIB system .	64
4.10 Projection on (a): $\delta - I_{RE}$ , (b): $\delta - I_{IM}$ axes of the phase portrait of SMIB system . . . . .	64
4.11 Projection on $\delta - \omega$ axes of the phase portrait of SMIB system . . . . .	65
4.12 Angle oscillations of machines 1 $\div$ 3 versus machine 4 . . . . .	67
4.13 Speed deviation of generators . . . . .	67
4.14 Active power flow on tie lines 7 – 8 . . . . .	68
4.15 Voltage at bus 8 . . . . .	68
4.16 (a): Eigenvalues of the linearised system about the stable equilibrium point. (b): A zoomed area of the eigenvalues with modulus less than 10	69
4.17 IEEE second benchmark model for subsynchronous resonance with a SSSC . . . . .	70
4.18 Four masses mechanical subsystem . . . . .	70
4.19 Equivalent SSSC reactance PI power flow controller . . . . .	70
4.20 Eigenvalues of system with algebraic model. $K = 0.05$ . . . . .	72
4.21 Eigenvalues of system with algebraic model. $K = 0.05$ . . . . .	72
4.22 Eigenvalues of system with algebraic model. $K = 0.05 \div 20$ . . . . .	73
4.23 Eigenvalues of system with dynamic model. $K = 0.05 \div 20$ . . . . .	73

4.24	Eigenvalues of system with dynamic model. $K = 0.05 \div 20$ . . . . .	74
4.25	Active power flow . . . . .	74
4.26	Torque between HP-LP (top panel) and LP-GEN (bottom panel) shaft sections. On the right an expanded region is reported to better show oscillations in the subsynchronous range . . . . .	75
5.1	Lyapunov function for SMIB power system . . . . .	82
5.2	A one-dimensional graphical illustration of the level sets involved in the statement of the extended invariance principle. . . . .	85
5.3	Two cross sections of the proposed extended Lyapunov function of the SMIB test case . . . . .	88
5.4	A one-dimensional graphical illustration of the effect of a control input which adds a negative definite term to the time derivative of the Lyapunov function, on the level sets involved in the statement of the extended invariance principle. . . . .	92
5.5	$\mathcal{V}$ with and without control . . . . .	94
5.6	$\dot{\mathcal{V}}$ with and without the proposed control . . . . .	95
5.7	$E'_q, \Delta\omega, \delta$ phase-plane section of the SMIB system with and without the proposed control . . . . .	95
5.8	$I_{re}, I_{im}$ phase-plane section of the SMIB system with and without control . . . . .	96
5.9	Active power flow over line 1. Comparison between PI controller and the Lyapunov based controller . . . . .	97
5.10	Rotor angles of machines $1 \div 3$ with respect to machine 4, with and without the proposed supplementary control law for the shunt compensator . . . . .	100
5.11	Active power flow from area 1 to area 2 with and without the proposed supplementary control law for the shunt compensator . . . . .	100
5.12	Real and Imaginary part of bus 8 voltage (blue line) and adaptive estimate of respective equilibrium point (red line) . . . . .	101
5.13	Rotor angles of machines $1 \div 3$ with respect to machine 4, with and without the proposed supplementary control law for the series compensator . . . . .	101
5.14	Active power flow from area 1 to area 2 with and without the proposed supplementary control law for the series compensator . . . . .	102

5.15 Real and imaginary part of line 8A–8B current and adaptive estimate of respective equilibrium points . . . . .	102
6.1 Proposed converter topology and parallel connection with the transmission network . . . . .	106
6.2 Phasor diagram illustrating STATCOM operation in capacitive compensation mode . . . . .	107
6.3 Ac and Dc control systems . . . . .	108
6.4 Proposed converter topology and series connection with the transmission network . . . . .	113
6.5 Phasor diagram illustrating SSSC operation in capacitive compensation mode . . . . .	114
6.6 230kV test system for STATCOM simulation . . . . .	115
6.7 Actual (top) and reference (bottom) reactive power absorbed by the STATCOM . . . . .	116
6.8 Magnitude of voltage (top) and current (bottom) at STATCOM output	116
6.9 Dc capacitors voltages (top) and angle $\alpha$ (bottom) . . . . .	117
6.10 Phase $a$ STATCOM voltage and current . . . . .	117
6.11 Current RMS in filter inductances . . . . .	118
6.12 $v_{ab}$ (top) and $v_{ab}^{\text{ref}}$ (bottom) . . . . .	118
6.13 Total Harmonic Distortion of bus $B_2$ voltage . . . . .	119
6.14 230kV test system for SSSC simulation . . . . .	119
6.15 SSSC equivalent reactance (top). Active and reactive power absorbed by SSSC (bottom) . . . . .	120
6.16 Magnitude of injected voltage (top) and current through SSSC (bottom)	121
6.17 Dc capacitors voltages (top) and angle $\alpha$ (bottom) . . . . .	121
6.18 Phase 1 SSSC voltage and current . . . . .	122
6.19 Current RMS in filter inductances . . . . .	122
6.20 Proposed power conditioning system for SMES-based FACTS devices	124
6.21 SMES DC-DC chopper . . . . .	124
6.22 SMES DC-DC chopper in charging mode . . . . .	124
6.23 SMES DC-DC chopper in discharging mode . . . . .	125
6.24 $V_{RE}$ and $V_{RE,\text{rm}}$ . . . . .	126
6.25 $V_{IM}$ and $V_{IM,\text{rm}}$ . . . . .	127
6.26 $i_{SMES}$ (left) and $v_{SMES}$ (right) . . . . .	128
6.27 DC capacitor voltages . . . . .	129

A.1 Two-area test system . . . . .	151
------------------------------------	-----



---

# List of Tables

---

4.1	Local and interarea modes . . . . .	69
6.1	Chopper switching signals during charging mode . . . . .	125
6.2	Chopper switching signals during discharging mode . . . . .	125
C.1	STATCOM circuit data . . . . .	155
C.2	STATCOM PI controller's data . . . . .	155
C.3	STATCOM sliding mode controller's data . . . . .	155
C.4	SSSC circuit data . . . . .	156
C.5	SSSC PI controller's data . . . . .	156
C.6	SSSC sliding mode controller's data . . . . .	156